ABSTRACT

Title of dissertation: WING KINEMATICS, DEFORMATIONS, AND AERODYNAMICS OF DRAGONFLIES IN FREE FLIGHT

Nathan Shumway
Doctor of Philosophy, 2019

Dissertation directed by: Assistant Professor Stuart Laurence
Department of Aerospace Engineering

The development of Micro Aerial Vehicles (MAVs) has led researchers to study insects in order to better understand aerodynamic mechanisms and wing kinematics that achieve high performance flight at small scales. Dragonflies in particular are a good candidate for study, as their size is comparable to the target size of MAVs and they are able remain stable while flying in highly variable conditions. To better understand undisturbed steady flight and gust response of dragonflies, experiments were conducted to measure detailed wing kinematics and deformations in free flight both through a quiescent environment and when encountering a lateral gust. A custom testing environment was developed in which dragonflies would fly through an enclosed area with high-speed cameras capturing both their body motion and that of markers placed on their wings. Due to the nature of the setup and how the dragonflies were released, they would frequently fly while inverted rather than upright and a comparison between upright and inverted flight is included in this work. During inverted flight the tested specimens flew in such a way that their

wings had a similar orientation in the global reference frame to that of the wings in the upright flights. The two primary kinematic variables that were changed to produce this result were the wing pitch angle and the body elevation angle. In addition, the dragonflies modulated the amount of time spent in the downstroke versus the upstroke so that in either case their wings spent more time moving down in the global frame. When dragonflies encountered a lateral gust, they increased the pitching of their windward wings, using left-right asymmetric kinematics to maintain a straight flight path through the disturbance.

From these experimental data, models were developed for both the wing kinematics and the wing deformations, and these were incorporated into flapping wing simulations using the OVERTURNS computational fluid dynamics (CFD) code. Two sets of such CFD simulations were run: one of rigid wings and the other of deforming wings. For both rigid and deforming wings, the interaction between the fore- and hindwing increased the force production on both wings when compared to fore- and hindwings in isolation. The largest differences between isolated and tandem wings were seen for the hindwing as it passed through the wake of the forewing. The wing deformations slightly decreased the total force production, compared to the rigid wings, by reducing the amount of flow separation on the bottom of the wing during the upstroke. The impact of the camber deformation, during the body-relative downstroke, was dependent on the specific wing kinematics. Though the total force produced decreased, the wing deformations substantially increased the efficiency for both wings.

WING KINEMATICS, DEFORMATIONS, AND AERODYNAMICS OF DRAGONFLIES IN FREE FLIGHT

by

Nathan Shumway

Dissertation submitted to the Faculty of the Graduate School of the
University of Maryland, College Park in partial fulfillment
of the requirements for the degree of
Doctor of Philosophy
2019

Advisory Committee:
Professor Stuart Laurence, Chair/Advisor
Professor James Baeder
Professor Anya Jones
Professor Inderjit Chopra
Professor James Duncan, Dean's Representative

Acknowledgments

The work that has been done over the last four years on this research (and the two years before that working on hypersonic boundary layer transition) has been supported by many hands and much encouragement. Before getting into the details of everything that was done, I want to acknowledge the help and support that I've received. As many people have supported me and this research project, and encouraged me through my time in graduate school the list is long and I hope I don't miss anyone, but to start I want to share a quick story.

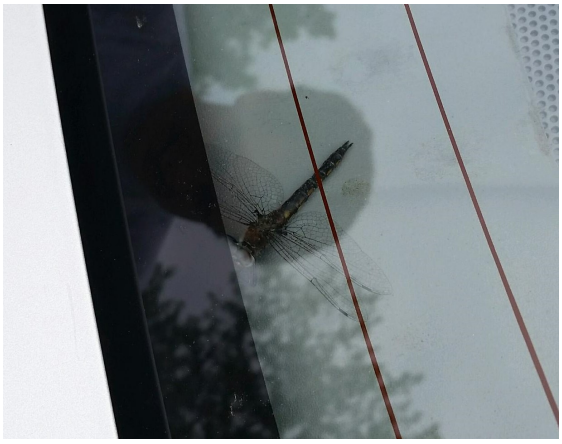

When we (myself and Mateusz Gabryszuk working on the project under the supervision of Stuart Laurence) began our initial experimental campaign during the summer of 2015, we were particularly interested in a species of dragonfly known as the Common Baskettail. These dragonflies are typically out from mid April until the end of June, which are three months with iffy weather in the area around the University of Maryland. During the first week in June the high temperatures were in the low 60s, which, as I'll mention again later, meant that dragonflies were not typically out flying. Nonetheless we went out to the park every day that week in an attempt to catch any dragonflies that were out. Near the end of that week, as I was driving into campus, I heard a small thump and then a buzzing sound. Glancing into my rear-

view mirror I saw that a dragonfly had flown into my car and was trying to fly out through my back windshield. When I finally got to park and jump out of the car to examine the dragonfly with Mateusz, we realized that this dragonfly was a Common Baskettail, exactly the species we were looking for. That dragonfly, pictured above, was the only dragonfly that we managed to catch during the whole week and we were able to capture video of it fluttering its wings. As a Christian, I believe that there is a God who created and governs the whole universe, and whenever I remember this story (which is fairly often) I'm reminded that my success is due to His grace and generosity for which I will never be sufficiently grateful.

As I mentioned, this work was conducted by myself and Mateusz Gabryszuk. It is hard to overstate how critical Mateusz's participation was for the success of this research. He ran two summers worth of testing with me, and during the first summer having two people was necessary in order to run tests. He also did the majority of the work designing and building the test section that was used during our 2016 tests. He also helped in the early development of the marker tracking software that was crucial to this research, along with writing the code we used to extract bulk wing kinematics.

Throughout this research I've been supported by the mentoring, advice, and instruction from several different people. I should probably start with my adviser, Stuart Laurence, who has supported me over the past six years. Though I haven't always been as receptive of his advice as I should have been, I appreciate the work he has put in to help me mature as an engineer and a researcher. Imraan Faraque was also an important mentor for me during our two years of running experiments

with dragonflies. He was willing to make time for us as we had plenty of questions about how to run tests and work with insects. The rest of my committee members, particularly James Baeder and Anya Jones, have been encouraging and ready to offer advice and take time to listen to me when I needed to sound out some of my ideas. I was taught to use OVERTURNS by Camli Badrya and Dylan Jude primarily, but James Lankford, Yong Su Jung, and Bumseok Lee also helped me think through the modifications that needed to be made to OVERTURNS and gave me ideas when I was debugging the code. Joe Chung helped with OVERTURNS simulations by allowing me to borrow extra computer time that he wasn't using when it became clear that I needed more computer hours than I'd had available. We also benefited from the generosity of Sean Humbert, Anya Jones, and Philippe Bardet as they allowed us to borrow cameras for our experiments. Anthony Leonardo gave us additional advice on dragonfly behavior as we were designing our setup for testing in the summer of 2016 and the Oxford Animal Flight group provided calibration software for us to use for calibrating our camera setup. The computing resources that were used to run all of the simulations that are presented herein were made available by the University of Maryland (http://hpcc.umd.edu). And last, but not least of the people who provided direct support for the research, Lucie Ugarte helped us by doing data extraction work during her free time and Tom Whalen provided the optimization function used throughout our data processing.

I should also take a moment to acknowledge the funding support that we have received for this research and that I have received to allow me to continue to work on this project. The research project was supported by the Army Research Laboratory's

Micro Autonomous Systems and Technology CTA. In addition to the funding for this specific research project, I received support from a National Defense Science and Engineering Graduate Fellowship and a Ann G. Wylie Dissertation Fellowship.

Over the last six years I've benefited from discussions and advice from other students when analyzing my results. Field Manar was particularly helpful when I needed help understanding the growth of the leading edge vortex that is seen in my simulation results. I've always appreciated from getting feedback from my fellow members of the High Speed Aerodynamics and Propulsion Laboratory. Will, Cam, Rich, Tom, Alvin, Mateusz, Andrew, Laura, Graeme, and Sean, you've all made life working in our office a lot of fun. I've also really learned from my discussions with my fellow students in the Separated and Transient Aerodynamics Laboratory. I really appreciate how you guys welcomed me in, even though I was working in a different research group. And I'm thankful the support and companionship of my fellows on the Graduate Student Advisory Committee, who worked with me to organize fun and informative activities for the graduate students in our department.

Beyond the confines of the university, I'm thankful for the support of my parents and my wife as I've pursued my degree. I've benefited from their support and encouragement, even when I don't feel like I'm doing anything to deserve it. And to my many friends from InterVarsity and Solid Rock Church, thanks for being there to have fun and serve together, being a part of these two communities has enriched my time at the University of Maryland in ways I never expected.

Table of Contents

List of Tables

List of Figures

Chapter 1: Introduction

The advent of small electronics has created opportunities to build smaller unmanned vehicles that have the potential to conduct a variety of missions in confined spaces and urban environments. As the power systems for such micro aerial vehicles (MAVs) must also be small, the vehicle must be highly efficient and able to reject disturbances with minimal energy use. These requirements, along with the need for maneuverability, has spurred research into low Reynolds number aerodynamics with many researchers looking to birds or insects for inspiration [1].

1.1 Micro Aerial Vehicles

The definition of a micro aerial vehicle, a vehicle with a maximum dimension of less than 15 cm and take off weight less than 100 g [2], was established as DARPA set out its "MAV-project" in an attempt to kick-start the development of such vehicles. Since then there have been many designs that have been developed and tested, primarily with a surveillance mission in mind. There are several major challenges to building vehicles at this scale: the low operating Reynolds number reduces the performance of both fixed and rotary wing platforms; small power systems lack the energy to compensate for the loss of efficiency; and the stringent weight requirement

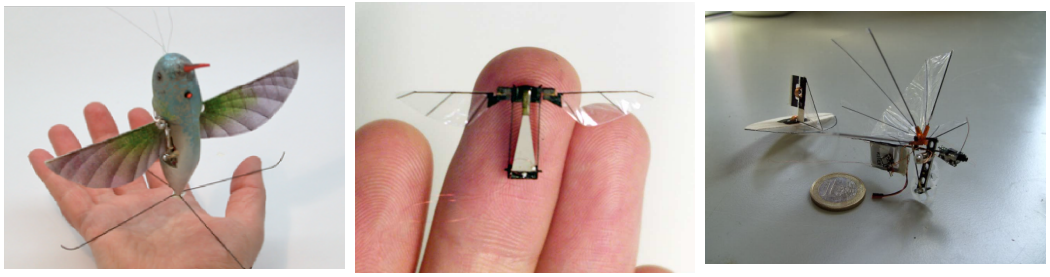

(a) (b) (c)

Figure 1.1: Examples of flapping wing micro aerial vehicles. (a) Aerovironment Nano Hummingbird from [4], (b) Harvard RoboBee from [5], (c) Delft University of Technology Delft Fly from [6].

means the vehicles are not capable of carrying a variety of payloads at once [3]. As flapping wings may provide a more efficient solution for generating lift and thrust to these type of vehicles, engineers have developed several vehicles based on designs found in nature.

The Nano Hummingbird, developed by Aerovironment and seen in figure 1.1, demonstrated the capabilities of flapping wing MAVs. This vehicle was the first to demonstrate that mechanically actuated flapping wings could be used to hold a vehicle in a controlled hover. Though the final product did not meet all of the originial design requirements, the Nano Hummingbird demonstrated the feasibility of a flapping wing vehicle for surveillance missions [4].

Since then two widely publicized university-developed flapping-wing vehicles have emerged: the Harvard RoboBee [7] and the Delft Fly from Delft University of Technology [6] both of which are pictured in figure 1.1. The RoboBee uses two bee-like wings on opposite sides of its body to generate lift, whereas the Delft Fly

has two pairs of conjoined wings that take advantage of vortices produced by wings when they clap together or fling apart [8]. These vehicles demonstrate that flapping wings are a feasible lift and propulsion generation mechanism for a MAV, but further improvements in efficiency are necessary for flapping-wing designs to compete with rotary wing vehicles. Through the study of birds and insects, it may be possible to improve the design and control of flapping wings and obtain the efficiency and stability improvements that can make these designs more practical.

1.2 Insect Gust Response

As micro aerial vehicles move closer to deployable prototypes and production models, it is important that they be able to remain stable when encountering various disturbances. Experiments with a flapping wing model have indicated that flapping wings may inherently reject some scales of disturbances, depending on the flapping frequency [9]. Seeking low energy methods for gust rejection, several researchers have looked at the response of insects to a lateral gust and three of those studies are highlighted here. Though none of these studies focus on dragonflies, the different species highlighted here have some similarity in their responses which may indicate how dragonflies mitigate the effects of disturbances.

Previous work at the University of Maryland [10] has focused on the gust response of bumble bees and stalk eyed flies, both of which are significantly smaller than dragonflies. By hitting the insects with a jet of air while they were in flight, the researchers were able to measure the wing kinematics and body motion that the

insects employed to compensate for the disturbance. Both insects used left-right asymmetric stroke amplitudes to recover after encountering the disturbance, and the stalk-eye flies also employed asymmetric wing pitching.

Two studies have analyzed the disturbance response of larger insects. One study focused on the wing kinematics of a locust in sideslip (or yawed relative to the incoming flow). Though this study used tethered insect, the conditions are similar to a sustained lateral disturbance [11], whereas the second study, observing butterflies entering a crossflow, is more comparable to encountering a finite duration lateral wind gust [12]. In both cases the insects responded using asymmetric wing kinematics, though the specific wing that exhibited an increase in flapping amplitude differed between the two. In all three of these studies left-right asymmetries in wing kinematics have been the response to encountering a lateral disturbance, regardless of insect size or configuration.

1.3 Low Reynolds Number Aerodynamics

The analysis of unsteady, low Reynolds number (Re) flows ($Re \leq O(10^5)$ [13]) associated with flapping wings involves different flow features and scaling parameters than high Reynolds number flight [14, 15]. The flapping of insect wings includes a high effective angle of attack (defined as the angle between the wing and the fluid velocity in a wing fixed frame) throughout most of the wingstroke and constant acceleration of the wing throughout the stroke. This presents a challenge for aerodynamic design and analysis, as most aerodynamic theory is based either on steady

conditions or a small effective angle of attack [16]. Research on unsteady wing motion at high angle of attack has shown that the flow around the wing is dominated by vortex structures. One such vortex begins at the leading edge and can grow to cover a significant portion of the wing; this vortex is known as the leading edge vortex (LEV) [15]. The general shape of the LEV on a surging wing is shown using flow visualization in figure 1.2. Research focused on this vortex has shown that it can be stable on a rotating wing, though it sheds in cases where the wing is oscillating or if there is a freestream present [14, 13]. Since flapping is a reciprocating rotational motion of the wings, vortices are consistently being formed as the wing accelerates and shed as the wing decelerates and reverses direction. This is in contrast to pure rotation, where a stable vortex can persist [17], and a surging wing, where an initial leading edge vortex sheds and gives way to stalled flow (with the possibility of some additional vortex sheding immediately after the LEV is shed) [18]. Nonetheless, the work that has been done on the unsteady aerodynamics of surging and rotating wings can be useful in understanding the important flow features in flapping wing flight.

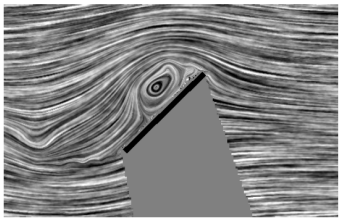

Figure 1.2: Flow visualization of a LEV on a surging wing from [19].

Research on surging and rotating wings has indicated that the leading edge vortex provides significant lift enhancement for a wing. These vortex structures are found when wings undergo unsteady motions with a high effective angle of attack and on delta-wing aircraft in steady flight. For unsteady motions, the LEV grows as it is fed by the shear layer coming off the leading edge

of the wing, then at some point it is shed into the wake, which is more commonly seen in surging wings [19], or bursts (where the vortex loses any coherent structure), which happens in the outboard regions of revolving wings [20]. The growth of the LEV is correlated with the normalized local distance traveled for surging, pitching, and rotating wings [18, 21, 22, 23]. The LEV size is also related to the angle of attack of the wing, with wings at higher angle of attack generating larger LEVs [21]. Thus, for flapping insect wings, the leading edge vortex is largest near the wing tip, where the wing velocity and effective angle of attack are highest, and smaller near the wing root. As the vortex grows it convects away from the leading edge, both in the chordwise and wing normal directions [18]. If a LEV grows too large before it sheds away from the wing it will burst which does not result in an immediate decrease in force production, but the force on the wing does not continue to grow after this point [24]. As the leading edge vortex provides significant lift enhancement, it is an important feature to analyze when studying insect flight.

1.4 The Study of Dragonflies

Of all the insects that use flapping wings as their primary means of locomotion, dragonflies are of interest for three particular reasons. First, insects with the same body configuration, and some of the same wing features, as present-day dragonflies have been in existence for almost 300 million years in a variety of different environments [25]. Second, dragonflies span a large range of scales (body lengths varying from $\sim$ 12 mm to $\sim$ 100 mm just in the area around the University of Maryland)

that corresponds to the desired size range for MAVs. Third, dragonflies are highly accomplished flyers: having been observed flying at speeds approaching 10 m/s and can produce forces in excess of five times their body weight [26, 27]. These three factors indicate that the dragonfly is a proven aerial platform, more capable than current MAVs of similar size. Thus, a better understanding of how dragonflies fly may provide insight leading to improvements in micro aerial vehicle design and control.

In order to better understand dragonfly flight, researchers have focused on measuring the wing kinematics of dragonflies in various flight conditions. There are two general approaches that researchers have taken to better understand the wing kinematics of dragonflies. The first is observing dragonflies in their natural environment. One of the most comprehensive of such studies was conducted by Rüppell [28], who analyzed videos of 20 species of Odonata (an order comprising both dragonflies and damselflies) from two different continents. The major findings pertaining to dragonflies were:

- Wingbeat frequency varies with species size, with larger dragonflies having lower wingbeat frequencies
- Stroke amplitude increases with increased acceleration
- The forewing-hindwing phase relationship is correlated with the acceleration of the dragonfly, with smaller phase differences being associated with higher accelerations

A later study by May [26] focused on flapping frequencies, flight velocities, and

accelerations to determine the power required by dragonflies in flight. The flight velocities observed were generally between 0 and 2 m/s with accelerations approaching 20 m/s^2. These field studies provide valuable insight into normal dragonfly flight behavior that can be used to validate the results garnered from studies using different techniques or in artificial environments.

The second approach to measuring wing kinematics of dragonflies is observing them in a controlled environment. This has several advantages over studies of dragonflies in nature, as wind conditions are known and measurements can be much more accurate and detailed; however, the artificial conditions can lead to abnormal behavior [29]. Nonetheless, much has been learned about the details of dragonfly wing kinematics through such experiments. One important parameter that has been analyzed in controlled tests is the orientation of the wing stroke plane. This plane is generally defined by the root to tip vector at the top and bottom of the wingstroke. Studies of free flying dragonflies have shown that the orientation of the stroke plane is relatively constant when measured with respect to the body axis [30, 31]. Because experiments in a controlled environment allow for more detailed measurements, several studies have also been able to report wing pitch data [30, 32, 33, 34], which are essential for estimating the aerodynamic performance of dragonflies. Since dragonfly wings deform during flight, most studies report wing pitch at particular spanwise locations or multiple spanwise locations. Looking across these four studies it becomes clear that the pitching amplitude is highest at the wingtip and lower near the wing root. They also show that the average pitch angle has significantly less variation along the span than the pitching amplitude; the average pitch is also more

consistent across different studies than the pitching amplitude.

In addition to studies focused purely on the wing motion, researchers have used both experiments and simulations to better understand the aerodynamics of dragonfly flight. Smoke visualizations of the airflow around tethered dragonflies in a wind tunnel showed vortex structures that correlated with significant increases in the force produced [27]. Further work to identify the flow topology around a dragonfly in forward flight, again using smoke visualization, identified a large leading-edge vortex that forms over the forewings during the downstroke [35]. This vortex was further studied using stereo particle image velocimetry, with results indicating that the vortex diameter and circulation increase from root to tip [36]. This general vortex structure has also been identified in computational fluid dynamics (CFD) simulations of dragonfly flight [34, 37, 38, 39].

Dragonfly wings are also characterized by significant corrugation, seen in figure 1.3; though the large scale flow structures dominate the force production for dragonflies [36], researchers have also analyzed the impact of this corrugation on the aerodynamics. Experimental studies with two dimensional wing profiles mimicking the cross section of a dragonfly wing have shown that the valleys created by the corrugation are filled by vortices. The wing profiles created by the filled corrugations exhibit a similar performance to a flat plate [40]. CFD simulations of corrugated airfoils have found that the corrugations can produce an increase in instantaneous lift, but that there was little effect on the average lift or drag [41]. Studies of the structural properties of insect wings have indicated that the corrugation produces the stiffness required for a flapping, high aspect-ratio wing without

the need for heavy structures [42]. This indicates that the corrugation primarily provides a structural benefit with a minimal aerodynamic cost.

One kinematic parameter governing dragonfly flight that has been the focus of several experimental and computational studies is the phase difference between the fore- and hindwing. Experiments with mechanical flappers approximating dragonfly wings have shown that proper phasing can reduce the swirl in the wake, and thereby increase the efficiency of the motion [43]. Experiments with tandem plunging wings found similar benefits to thrust production and propulsive efficiency [44]. Two-dimensional simulations of tandem dragonfly wings determined that the manner in which dragonflies shift the phase difference between their wings is consistent with a shift between high force production and high efficiency flight [45]. Three-dimensional simulations of dragonfly wings using hovering kinematics found that tandem wings produce less lift than two wings in isolation; this trend held true at a variety of advance ratios [37, 39]. In contrast, further CFD simulations of a dragonfly undergoing unsteady maneuvers shortly after takeoff indicated that there is an increase in force production for the tandem wings over a combination of the isolated wings [34, 38]. As a result of these apparently opposite findings, a recent review of the dragonfly flight literature noted that the exact consequences of the wing-wing interaction are controversial [36], but it is worth pointing out that the studies done thus far have not been of a consistent set of kinematics or a common flight condition. Though the questions surrounding the benefits of the wing-wing interaction of dragonflies will not be conclusively answered without a more exhaustive study of many different wing kinematics and flight conditions, the addition of simulations

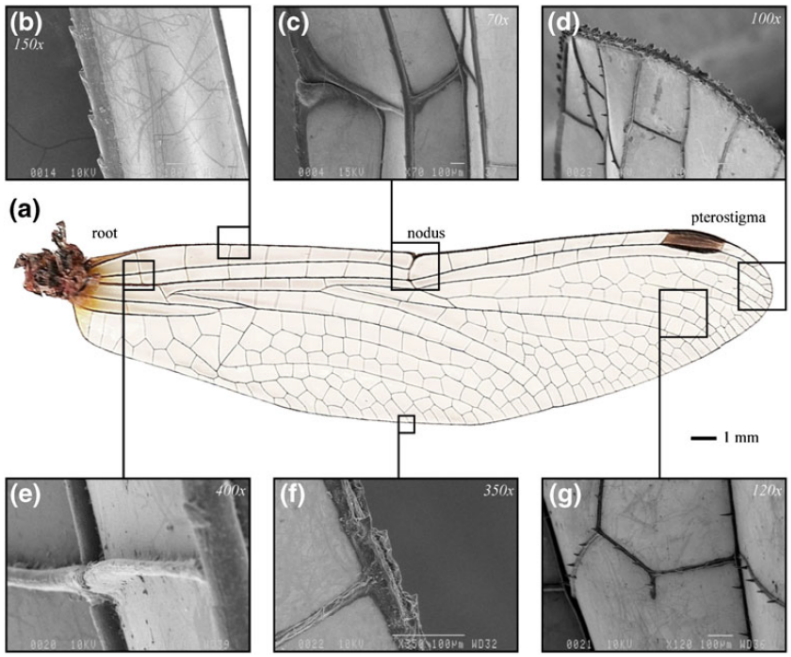

Figure 1.3: A dragonfly forewing with detailed views (b)-(g) of the indicated sections showing several different types of vein joints and the corrugation along the leading edge of the wing. Taken from Jongerius and Lentink [46].

based around steady straight flight should shed further light on the subject.

To add to the already complex nature of dragonfly wing motion and the resulting aerodynamics, it must be noted that dragonfly wings have a complex structure and are highly deformable. This has lead researchers to inspect the details of the micro-structures within dragonfly wings through detailed scans [47] and finite element analysis [46]. There are two primary components to the dragonfly wing, veins that provide the primary structure of the wing and membranes that stretch between the veins [36]. The veins give the shape to the wing, producing corrugation along the leading edge (figure 1.3 (c) and (d)) and near the wing root. There are also two specific features of the wing that should be noted: the nodus and the pterostigma.

The nodus joins two sections of the leading edge structure and acts as a hinge, allowing the wing to twist when rotating before the upstroke [25]. The pterostigma is a section of thicker veins and wing membrane near the wing tip, which increases the moment of inertia of the wing [46]. Several studies analyzing the details of the dragonfly wing structure have shown that there are a variety of different types of joint between wing veins that are more adept at bending in one direction than the other [48]. This indicates that the joint types and micro-structure of the wing may be controls on wing deformation [46, 47]. Measurements of the deformation of dragonfly wings while in flight have indicated that the wings are generally cambered during the downstroke and twisted during the upstroke [33, 49]. This is consistent with structural analyses, which have indicated that the deformation during the downstroke would be much lower in magnitude than that during the upstroke [46] and that the wing is much more likely to twist than bend [50].

1.5 Wing Flexibility

The effect of wing flexibility on the aerodynamic forces and flow features of wings operating at low Reynolds numbers has been a particular subject of interest for the micro aerial vehicle community. At the MAV scales, the frequencies of the relevant fluid phenomena and the natural frequencies of the structure can be very close to each other [51], meaning that there is significant potential for coupled fluid-structure interactions. Beyond the potential for interactions, insects and bats have wing structures that are highly flexible and deform during flight. In the case of insects,

there is no active deformation control within the wing, so the wing deformation is a result of balancing structural, inertial, and aerodynamic forces. Because of the weight reduction flexible structures could provide, researchers have studied both mechanical models and insect wings to better understand how flexibility changes the performance and flow features around the wing.

Experiments and simulations of flexible wings undergoing a variety of motions have been conducted to study the aerodynamic impact of flexibility. Experiments with an accelerating flexible plate found that chordwise flexibility led to an induced camber, which resulted in higher lift coefficients than a rigid plate undergoing the same motions [23]. Additional experiments have examined the impact of chordwise and spanwise flexibility on a heaving wing [51]. Spanwise flexibility enhanced the lift coefficient of the wing when oscillating at high Strouhal number while chordwise flexibility increased thrust and efficiency. In addition to the thrust enhancement, vibrations of flexible wings promote reattachment and lead to higher performance at high angles of attack. Though these motions are only loosely related to the motion of a flapping wing, these results provide insight into how flexible structures interact with low Reynolds number unsteady flows.

Studies of flexible flapping wings, either simulating or directly studying insect wings, have shown mixed results. Experiments on a mechanical flapper with a stiff leading edge spar attached to a flexible wing demonstrated that increasing material stiffness resulted in increased lift production when flapped in a horizontal stroke plane [52]. Since insect wings generally, and dragonfly wings in particular, involve specific patterns of deformation research has been done to determine the

impact of twist and camber on flapping wings. Simulations and experiments of wings with a variety of twist angles have found that wing twist significantly reduces the amount of flow separation and can increase the efficiency of the wing [53, 54]. Research on the impact of camber has been less conclusive. Simulations of a plunging wing did not indicate that there was any significant change in thrust production or propulsive efficiency with the addition of camber [55], but simulations of a rigid fruit fly wing with varying amounts of camber found that wings with positive camber produce higher lift to drag ratios than flat wings [56]. Experiments of a flapping wing with camber showed a tradeoff between the bound circulation of the wing and the circulation of the LEV [57]. These significantly different results highlight the difficulty of determining the impact of wing deformations, as benefits are frequently seen for particular geometries and particular motions, but are difficult to generalize [1].

The flexibility of insect wings is governed by the pattern of venation in the wings. For most insects, the leading edge veins are much thicker, and therefore stiffer, than the veins in the rest of the wing. The wings are thus much stiffer in the spanwise direction than they are in the chordwise direction [58]. Experiments with the wings of a hawkmoth indicated that the wing deformation is primarily a result of inertial forces, though unsteady high-lift structures like the leading edge vortex may increase the significance of aerodynamic forces [59]. Simulations using coupled fluid-dynamics and structural-dynamics solvers have shown that the flexibility of large insect wings can improve the efficiency and force generation [60, 61]. These findings are further confirmed by CFD simulations of deforming locust wings, using mea-

sured wing deformations. The simulations showed that aerodynamic performance of a rigid wing is lower than that of a wing following the measured deformations [62]. This research on insect wing deformations indicates that deformations provide aerodynamic benefits for insect flight.

1.6 Research Objectives

The present study focuses on steady dragonfly flight, with two primary objectives. The first is to determine the impact of dragonfly wing deformations on the forces and flow features produced during flight. Since the specific deformations of locust and hawkmoth wings have been found to improve flight performance, this goal focuses on improving our understanding of how dragonfly wing deformations in particular can lead to these benefits. In order to compare both rigid and deforming wings undergoing the same base motion, simulations are run using bulk kinematics and deformations measured during experiments with free-flying dragonflies. Half of the simulations use only the bulk kinematics and are compared with simulations using the same kinematics with the measured deformations. These simulations are also used to shed light on how the interaction between the fore- and hindwing changes the forces and flow features on each wing.

The second goal of this research is to determine how dragonflies respond to a lateral wind gust, with the aim of providing insight that can lead to improved control of MAVs in uncontrolled environments. Through experiments with free flying dragonflies, in which some dragonflies flew through a lateral gust and others

did not, the wing kinematic differences between gust encounters and undisturbed flights are determined. Though this analysis is based on a small number of flights, it provides insight into the key kinematic variables that dragonflies manipulate when encountering a disturbance.

The work that was conducted to achieve these two goals is detailed in the following four chapters. In chapter 2 the experimental setup, analysis software, kinematic and deformation models, and computational fluid dynamics solver are presented; chapter 3 contains the results of the experiments with free flying dragonflies. The results from the CFD simulations are detailed and discussed in chapter 4, and chapter 5 contains the key conclusions from this research.

Chapter 2: Methods

This research was broken into two phases: first, experiments were conducted to determine the bulk wing kinematics and wing deformations of dragonflies in free flight; second, numerical simulations were run - with both rigid and deforming wings - to determine the aerodynamic features of dragonfly flight. Since the experiments were performed on free-flying dragonflies, and the equipment and expertise to mount sensors on the dragonflies were not available, no direct measurements of dragonfly motion or airflow were possible. The sole measurement system used in the experiments was multiple-camera photogrammetry, with an array of 4-5 high-speed cameras recording backlit videos of the dragonfly in each test. In order to determine body motion and wing kinematics from the videos, several MATLAB programs were developed for extracting position data from the videos. Once the position data were extracted, models were developed for the wing kinematics and deformations. In addition, the CFD solver required modification to enable the simulation of both rigid and deforming wing kinematics based on the experimental data. Since the models incorporated into the CFD solver are based on the experimental data, they will be further justified when the wing motion is presented in chapter 3.

2.1 Experimental Methods

Dragonflies were captured at the Lake Artemesia Natural Area with permission from park authorities. Though we captured and tested several different species over two summers (2015 and 2016), the data presented here are solely from tests of the species *Pachydiplax longipennis*, commonly known as the Blue Dasher. This species was chosen for its moderate size, which was small enough to fit into our testing environment, and clear wings, allowing artificial markers placed on the wings to be easily tracked. In order to immobilize the dragonflies prior to marking, they were placed in a refrigerator for 35-45 minutes. A fine tipped permanent marker was used to place 20-40 markers on each wing of the immobilized dragonflies. The artificial markers had diameters of 500-750 μm. Six to eight markers were applied to the leading edge of each wing, two markers to the wing tip, at least eight markers to the trailing edge, and the remainder to the interior of the wing. The exact number of markers varied according to the wing area available, and the total mass of the markers was verified to be less than 2% of the overall wing mass. An example of a marked dragonfly wing, as recorded in a free-flight test, is shown in figure 2.1.

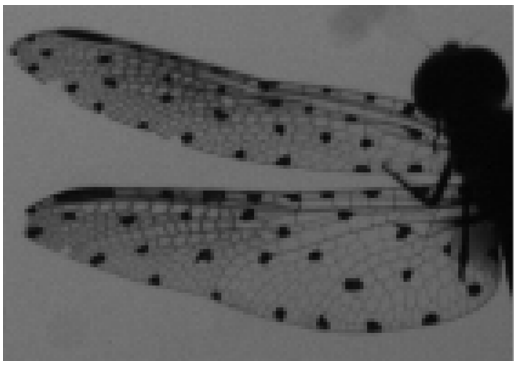

Figure 2.1: An example of a marked wing from taken from a test video.

Dragonflies were tested within three hours of capture, and each specimen was tested no more than five times in order to avoid depleting its energy stores. Individ-

ual dragonflies were cycled through testing, so after each test that specimen would be recaptured and stored in a cooler before their next test. Since the tests were conducted inside of the Autonomous Vehicle Laboratory at the University of Maryland, the temperature during the tests was 5-10° C colder than the environment in which the dragonflies were captured. This temperature difference affected some of the kinematic variables and contributed to the difficulty of getting dragonflies to fly. Once the dragonflies had completed their tests they were released back into the park where they had been captured.

2.1.1 Testing Environment

During the summer of 2015, a variety of different test section designs were trialled to determine the optimal setup. The objective was to develop a testing environment in which dragonflies would repeatedly fly the same flight path and could be forced to encounter a lateral wind gust. At the beginning of the project, it was decided to utilize an existing low speed wind tunnel for these tests. Early experiments, however, indicated that dragonflies would not exhibit normal flight behavior when placed in the wind tunnel, which necessitated experimenting with various other configurations. In testing it was observed that dragonflies would fly out of a tube into a larger enclosure when sufficiently agitated. Based on this observation, we experimented with several different tube geometries and found that, for the species of dragonfly used in this research, a 12 inch long tube with a 4 inch diameter was sufficient. This length gave enough space to position the dragonfly where it could

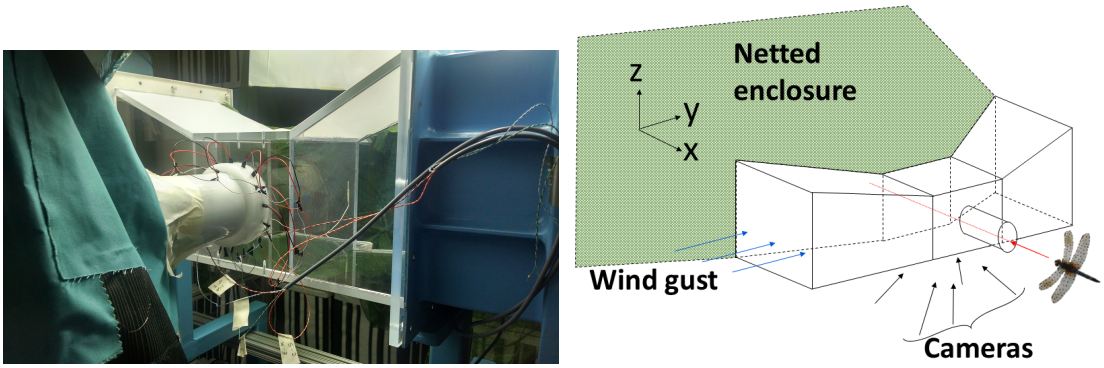

Figure 2.2: Photograph (left) and diagram (right) of the test section used for recording the free flight and gust encounters of dragonflies.

easily see the opening, while still providing the dragonfly sufficient distance to be in steady flight when exiting the tube.

Since early observations indicated that dragonflies would preferentially fly into open areas, the testing volume was designed with the staging tube on one side and a large netted enclosure on the opposite side. The testing volume dimensions were constrained by our camera-based measurement system, but needed to be sufficiently large that the dragonflies could maneuver when encountering the lateral gust. In particular, we wished to ensure that the dragonfly was visible and in focus for all of the cameras throughout an ideal flight (straight through the test volume). Based on the required spacing and limited depth of field of the camera, as high-speed videography requires a larger aperture to ensure sufficient lighting with shorter exposure, an 8 inch cube was determined to be a sufficient test volume.

The test section, seen in figure 2.2, was built to interface with the small scale wind tunnel in the Autonomous Vehicle Laboratory at the University of Maryland.

The configuration was such that the dragonflies would fly across the test section of the wind tunnel, which, when operating, provided the lateral gust of approximately 0.3 m/s. The dragonfly would first be placed in a staging tube, which was painted so the only light came from the opening into the test section. In this tube, the dragonfly would hang from a stick until it was agitated and flew out of the tube. Because the dragonflies were hanging off of the stick, in flights where they flew directly across the test section they would not correct their orientation and would fly upside-down. Thus the majority of the straight flights recorded during this experimental campaign are of dragonflies flying while inverted. During the tests with gust encounters, when the wind tunnel was operating, the opening into the netted enclosure was sealed to ensure that the flow in the test section was perpendicular to the desired dragonfly flight path. For these tests a piece of acrylic with a textured inner surface that provided something for the dragonflies to perch on was used to block the opening. In all tests, an array of four or five cameras was situated below the test section to record the dragonfly motion. Over the course of the summer this array consisted of a variety of Phantom cameras. Three different types of V series cameras were used: three to four v711s were used for each test, a v2512 was used when it was available, and a v311 was used when the v2512 or one of the v711s were unavailable. All of the cameras were operating at 7200 frames per second, which requred the v311 to used a reduced resolution (768x584 pixels), but all other cameras were capable of that framerate at full resolution (1280x800 pixels). These cameras were placed as far from one another as the 80/20 frame, and space constraints, would allow.

Accurate photogrammetric measurements also require an angular offset be-

tween the different cameras, making the camera orientation a critical parameter in the setup. The central camera (if there were five cameras in use) was placed directly underneath the test section pointed vertically. The other cameras were placed around the test section with angular offsets of approximately 30° between cameras. The angular offset was constrained both by the space constraints and the limited lighting. Lighting over the test section was provided by an array of 7500 lumen LED flood lights. These lights flickered at 120 Hz, so to maintain a constant average background illumination for the cameras three different sets of lights were plugged into three different outlets, which provided phase offsets of 0°, 120°, and 240°. As the lighting was directed straight down and blocked by various pieces of equipment, the cameras could not be angled more than 30° off of vertical, but the combination of spacing between the cameras and angular offsets provided sufficient visual coverage of the test volume to be able to track the dragonfly body motion. Because of various obstructions and the large variation in the orientation of the wings when flapping, tracking the wing motion was limited to a smaller region of the test volume.

The cameras were calibrated using the bundle adjustment routine provided by the Oxford Animal Flight group [63] to determine their positions and internal parameters. This program uses images of a calibration grid, an array of dots with known spacing, with a bundle adjustment algorithm to solve for the camera positions and orientations relative to the central camera. From this calibration, the location of any feature that is identified in two or more cameras can be determined. After identifying the location of the feature in each camera image plane, a line connecting

the image plane location and the focal point for that camera is extended out through the test volume for each camera. If all cameras are accurately modeled by the pinhole camera model and are accurately calibrated, the lines from all of the cameras will intersect at the feature's location. For real cameras, where the pinhole model is not a perfectly accurate model and there is some error in the calibration, the lines do not intersect. To determine the location of the point when the lines do not intersect, the point of closest approach for all of the lines is determined and the feature location is the average of those points. In order to ensure that the recording captured the dragonfly's exit from the staging tube a triggering system was built. The triggering system for the cameras, which is prominent in the picture in figure 2.2, was a custom-built collection of infrared lasers and receivers which were connected to a microcontroller; this sent a trigger signal to the cameras when the dragonfly crossed the exit plane of the tube.

2.1.2 Processing Tools

In order to determine the flight path of the dragonfly and the motion of the wing markers, MATLAB programs were developed to process the video data obtained during the experiments. The initial step in the processing was to determine the position and orientation of the dragonfly throughout the test. This was accomplished through the use of a geometric model approximating a dragonfly body, as seen in figure 2.3. There are ten parameters governing this model: the x, y, and z position of the dragonfly, encapsulated in the location of the point P_1; heading, elevation,

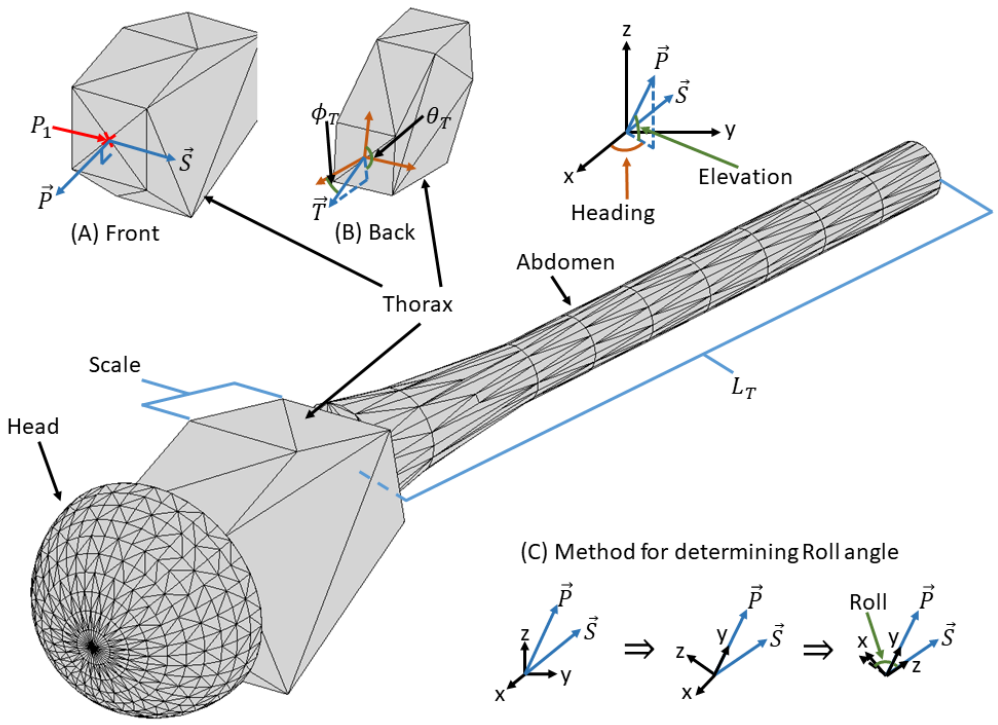

Figure 2.3: Body model used for determining dragonfly position and orientation

and roll angles to determine the orientation of the dragonfly and which are used to construct the $\overrightarrow{P}$ axis, which points in the direction the dragonfly is facing, and $\overrightarrow{S}$ axis which points to the left side of the dragonfly; two parameters, Scale and L_T, to adjust the overall size and abdomen length, respectively; and two angles, ϕ_T and θ_T, to determine the orientation of the abdomen, which is in the direction indicated by $\overrightarrow{T}$, relative to the rest of the dragonfly's body. The Scale parameter is used to determine the size of the thorax and the head as well as the abdomen diameter.

The program required the user to input an initial guess for the position, orientation, and size of the dragonfly in a chosen image in a given sequence, before using Nelder-Mead optimization to determine the best fit of the model to that image. The measure of fit quality used in optimization was calculated by projecting

the body model onto each camera image and determining the overlap between the projection of the model and the dark region corresponding to the dragonfly body. Because the majority of a dragonfly body is axisymmetric and the region around the thorax, which is the only non-axisymmetric part of the body model, contains both the most opaque sections of the wings (except for the pterostigma) and the legs (which further add to the dark region around the thorax) the roll angle was the most difficult parameter to determine accurately. In order to increase the probability of accurately approximating the roll angle, additional weight was given to the region around the thorax when determining the fit quality, but even so, there remained significant error in roll-angle determination. After the optimization was completed for the initial frame, the size parameters were fixed and the optimization function was used to determine the position and orientation of the dragonfly in all subsequent and previous frames.

After determining the flight path of the dragonfly, the next step in the processing of the video data was tracking the motion of the markers on the dragonfly wings. This was done through a semi-automated MATLAB program written specifically for the task. The program required the user to identify the markers in a starting frame, and would then attempt to automatically track the motion of the markers. When the program would lose track of a marker, due to occlusion in multiple cameras, wing-wing overlap, or incorrect identification, the program would pause for the user to manually identify the marker. Because of the positioning of the cameras and the variation in wing orientation, the program would frequently lose track of markers, making the process of marker tracking very time consuming. Once the initial ex-

traction was completed, the marker location data were smoothed using third order spline fits.

To determine the accuracy of the multiple camera system and the processing programs, a single wing was attached to linear and rotational stages and moved through the test volume. The wing was translated in the x-y plane with steps from 0.01 mm to 5 mm and rotated in increments of 1° to 5°. The marker-tracking software was then used to determine the motion of the wing. The results of this series of tests indicated that the multiple camera system could determine the location of a marker to within 0.1 mm, assuming that the marker was correctly identified in all camera views, and could determine the orientation of the wing to within 5°.

2.1.3 Kinematics Extraction

The process for extracting wing kinematics is only summarized here, as it has already been covered in the Master's thesis of Mateusz Gabryszuk's [64]. There are three parameters that are used to describe the wing position and orientation: the stroke plane orientation, the flap angle, and the geometric pitch angle. These parameters are shown in figure 2.4. The stroke plane is determined by calculating the cross product of the vectors pointing from the wing base to the wing tip at the top and bottom of the wingstroke. This gives the normal vector to the stroke plane, i.e., the stroke-plane vector in figure 2.4b, which is then used to determine two angles that describe the stroke-plane orientation. The angles are the angle between the stroke-plane vector and $\overrightarrow{P}$ in the $\overrightarrow{P} - \overrightarrow{S}$ plane, referred to as θ, and the angle

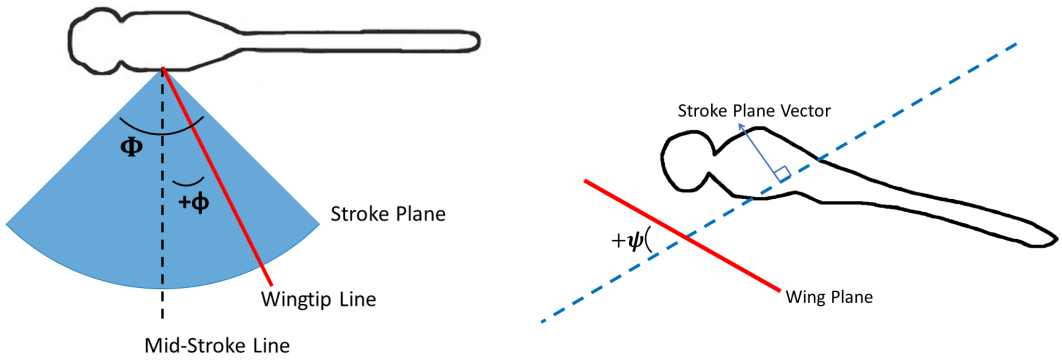

(a) (b)

Figure 2.4: Diagrams of dragonfly wing kinematic variables used to describe the wing motion during free flights.

between the stroke plane vector and the $\overrightarrow{P} - \overrightarrow{S}$ plane, referred to as ρ.

Once the stroke plane has been determined for each half stroke, the flap and geometric pitch angles are calculated. The flap angle is characterized by a flap amplitude, Φ, and offset, Φ_{off}. The flap offset is the angle between the mid-stroke line, i.e., the line connecting the wing base to the wing tip at mid-stroke, and the wing base plane, which is the plane on the body model where the wings attach to the body. The geometric pitch angle is the angle between the wing plane, calculated as the least-squares plane fit to all of the points on the wing, and the stroke plane. The kinematics are all derived in a body reference frame, so the down- and upstroke are not necessarily in the global down and up directions. This is particularly important when analyzing flights where the dragonfly is inverted (where body-relative up and down are opposite the global convention) or is rolled by 90° or more off of the normal upright orientation. The flap angle is used to determine the upstroke-to-downstroke ratio (UDR), that is, the ratio of the duration of the upstroke to the duration of the

downstroke. The UDR was calculated by determining stroke reversal times based on the flap angle and then comparing adjacent up- and downstrokes.

2.1.4 Deformation Extraction

Once the bulk wing kinematics have been determined, the wing deformations can be extracted. Prior experiments have shown that the primary deformations that dragonfly wings undergo are twist and camber [33, 49]. In order to characterize these the function

$$
\begin{gathered}
z = (a_1 + a_2\overline{y})\overline{x} + M(\beta_1, (a_3 + a_4\overline{x}), \overline{y}) + M(\beta_2, (a_5 + a_6\overline{x} + a_7\overline{x}^2), \overline{y}) + a_8 \\
\text{where } M(\beta, A, \overline{y}) = A\Big[\cos(\beta\overline{y}) - \cosh(\beta\overline{y}) + \tfrac{\cos(\beta)+\cosh(\beta)}{\sin(\beta)+\sinh(\beta)}\big(\sinh(\beta\overline{y}) - \sin(\beta\overline{y})\big)\Big], \\
\text{with } \overline{y} = \tfrac{-y+0.5\overline{c}}{1.2\overline{c}}, \overline{x} = \tfrac{x}{b} \\
\text{and } \beta_1 = 1.8751, \beta_2 = 4.6941
\end{gathered}
\tag{2.1}
$$

was introduced. This equation is in a wing coordinate system, where the origin is the wingbase, the x axis is in the spanwise direction from the root to the tip, and the y axis is in the chordwise direction pointing forward. This function has 8 parameters that can be used to fit the function to the points on the wings. There are three distinct parts; a linear portion to characterize the wing twist, and the first two mode shapes of a cantilevered beam to describe the camber in the wing.

There were two steps to fit the function for each frame. First, the reconstructed markers were rotated into a wing fixed reference frame by matching their spanwise and chordwise locations to those in previous frames. Once this rotation was completed MATLAB's built in *fit* function was used to determine the coeffi-

cient values for each frame; once the function had been fit for all of the frames with sufficient markers reconstructed, the coefficients were smoothed using a third order spline fit. Then, to create coefficient files for use in the CFD simulations, a Tukey window function was applied to the coefficients for one wingbeat to force the coefficients to an average value at the down-to-upstroke reversal point. This forced the deformation coefficients to be periodic and continuous, which was necessary for obtaining converged simulation results.

2.2 Computational Methods

In order to study the aerodynamics involved in dragonfly flight, numerical simulations were performed using OVERTURNS CFD solver. OVERTURNS (OVERset Transonic Unsteady Navier-Stokes) solves the compressible, Reynolds-averaged Navier-Stokes equations on structured meshes and has been used and validated, prior to this study, for the simulation of low Reynolds number flapping wing flight; at these conditions it uses low Mach number preconditioning to ensure a stable solution [65]. For the present simulations, a third-order MUSCL (Monotonic Upwind Scheme for Conservation Laws) scheme [66] with Korens limiters was employed to solve the spatial terms and a second-order implicit scheme calculated the time derivatives. For the flow near the wings, body-fitted O-O meshes were created with a Cartesian background grid to solve for the flowfield away from the wings. An example of the meshes used to simulate a tandem wing configuration is shown in figure 2.5. The OVERTURNS code uses an implicit hole-cutting technique developed by

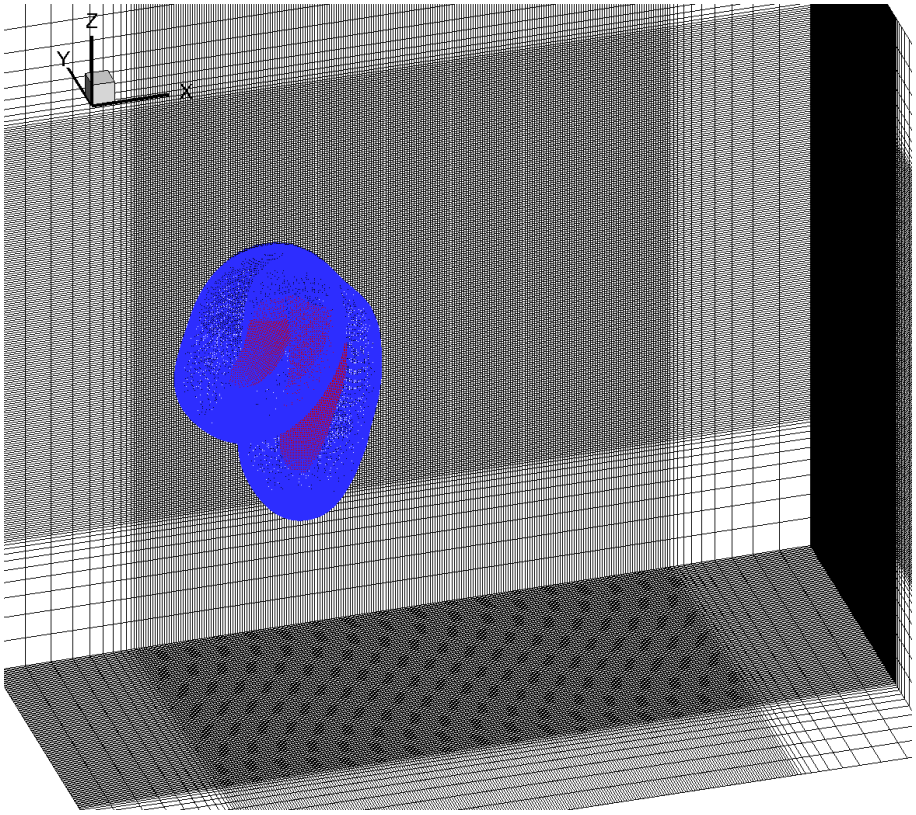

Figure 2.5: An example of two wing meshes and background mesh. The wing surfaces are shown in red while the outer boundary of the wing meshes are shown in blue.

Lee and modified by Lakshminarayan [67] to handle the overlapping meshes.

In order to determine the level of mesh refinement needed to obtain accurate flow solutions, three different wing and background mesh pairs were created and run with the wing flapping in a horizontal stroke plane. The Z force coefficient data for one flapping cycle is shown in figure 2.6. The wing meshes ranged from 1.1 million points in mesh 1 to 4.5 million points in mesh 3 with background meshes of comparable refinement used with each wing mesh. From these results mesh 2 was selected since there is very good agreement between mesh 2 and mesh 3

and, because mesh 2 has fewer points, the solver runs more quickly with mesh 2. The resulting number of points along each dimension of the meshes used in this study are: $185 \times 201 \times 86$ for the forewing and $205 \times 221 \times 89$ for the hindwing in the spanwise, chordwise (which wraps around the wing), and surface normal directions. The meshes for both wings have cells clustered near the leading and trailing edges as well as near the wing base and wing tip, as seen in figure 2.7. This clustering helps resolve the shear layer that forms on the leading and trailing edges of the wing. Two Cartesian background meshes were generated for the use in isolated and tandem wing simulations: the single wing background mesh was $224 \times 120 \times 216$, and the corresponding tandem wing mesh was $283 \times 166 \times 216$ in the x, y, and z directions respectively. The background meshes extended from the plane at which the center of the dragonfly body would lie (note that the body was absent in all computations) out to at least 1 wingspan away from the wing in all directions and at least two wingspans in the downstream direction. The centerline of the dragonfly body is a symmetry plane for all of the solutions.

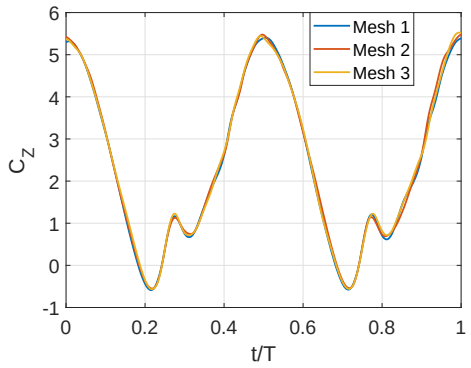

Figure 2.6: Z force coefficients from one flapping cycle for the dragonfly forewing mesh refinement study.

2.2.1 Dragonfly Kinematics

In order to model the wing kinematics of the dragonflies in a variety of flight conditions, two piecewise functions were created: the first to model the flap angle and the second to model the pitch angle. Piecewise functions were chosen because of the need to include a variable upstroke-to-downstroke ratio in the model and the desire to do so without employing lengthy Fourier series. The UDR was incorporated in the time normalization scheme. The normalized time variable was defined as $\tau = tf - \text{floor}(tf)$, where t is the current time and f is the flapping frequency. The downstroke fraction can then be described by the UDR, $\tau_D = \frac{1}{1+UDR}$, and the upstroke fraction is the remainder of the stroke, $\tau_U = 1 - \tau_D$. The model for the flap angle is defined as

$$\phi = \begin{cases} \frac{\Phi}{2}\cos(\pi\frac{\tau}{\tau_D}) + \Phi_{off} & \tau < \tau_D, \\ \frac{\Phi}{2}\cos\left[\pi(1+\frac{\tau-\tau_D}{\tau_U})\right] + \Phi_{off} & \tau \geq \tau_D \end{cases} \tag{2.2}$$

where the flap amplitude Φ and flap angle offset Φ_{off} are prescribed from the experimental results.

For the pitch angle, a regular sinusoidal function would not accurately capture the trends that were observed. Therefore, to enable a better fit of the experimental data while ensuring a continous derivative, a hyperbolic tangent function was employed in conjunction with a cosine function as:

$$\psi = \begin{cases} \frac{\Psi}{2}\frac{\tanh\left(1.5\cos(\pi\frac{\tau}{\tau_D})\right)}{\tanh(1.5)} + \Psi_{off} & \tau < \tau_D \\ \frac{\Psi}{2}\frac{\tanh\left(1.5\cos\left[\pi(1+\frac{\tau-\tau_D}{\tau_U})\right]\right)}{\tanh(1.5)} + \Psi_{off} & \tau \geq \tau_D \end{cases} \tag{2.3}$$

Here, Ψ is the pitching amplitude and Ψ_{off} is the average pitch angle. Since the flapping and pitching motion are frequently offset by some phase angle, the timing variable need not be the same between the two functions and τ can include a phase offset.

2.2.2 Wing Deformation

In order to simulate the deformation of the dragonfly wing, a method for deforming the wing mesh was developed and implimented in OVERTURNS. This method uses some of the same principles as when OVERTURNS is coupled with a structural dynamics model [68], but the prescribed deformations required a different framework. Any changes in wing surface area would adversely affect the accuracy of the calculated forces, thus the deformation method needed to maintain surface area as close to constant as possible. A four step process was therefore implemented to deform the wing surface and that process is described here and shown in figure 2.8. First, a reference mesh was generated in the wing-coordinate system and the z values given by the deformation function (equation 2.1) were calculated for each point in the mesh. This mesh was then flattened, starting at the approximate center of the wing, and each point on the wing surface is matched with the closest point on the flattened mesh. Linear interpolation is then used to

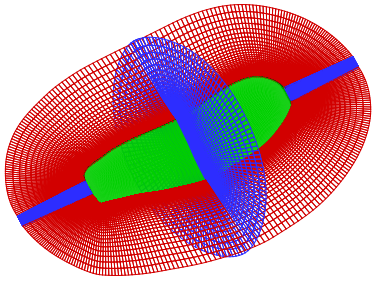

Figure 2.7: An example wing mesh.

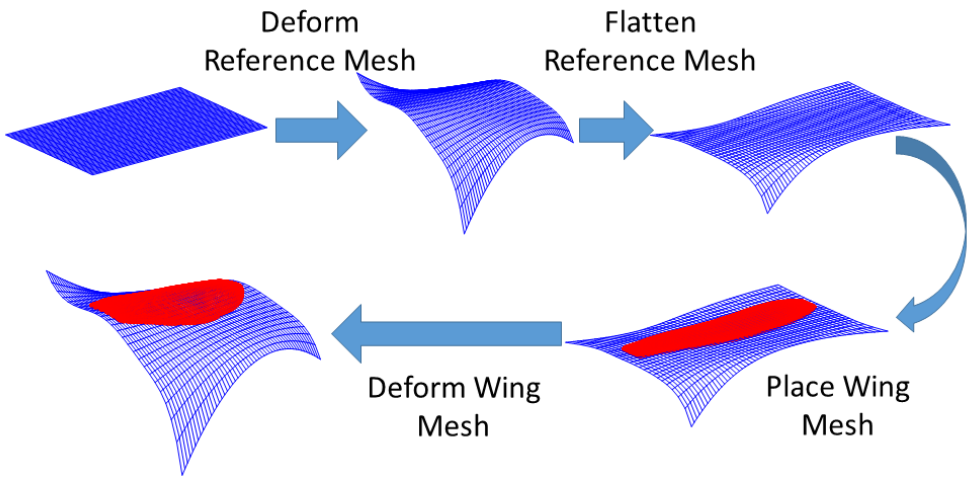

Figure 2.8: The process for deforming the wing surface mesh.

determine the location on the deformed surface of each corresponding wing-surface point. The deformations were propagated out into the rest of the mesh along mesh lines (lines of constant spanwise and chordwise wraparound position). Close to the wing surface, the change in the local surface-normal vector is taken into account to ensure that cells maintain a positive volume. For the points at the wing tip and wing base, seen in blue in figure 2.7, an additional check was performed to ensure that there was no crossing between cell faces. This process resulted in surface area variation of $< 1\%$ for all of the deformations used in this study.

Since the wing deformations are distances off of the wing plane, the wing root and wing tip locations can be displaced due to deformation. As the flap angle determines the location of the root to tip line which may not lie in the wing plane after deformation, a correction was introduced. At the beginning of the deformation process the locations of the wing root and wing tip on the deformed surface were calculated. Then the new root location was subtracted from each point, ensuring

that the wing root stayed at the origin of the wing fixed frame. Finally the wing was rotated so that the root-to-tip line remained on the spanwise axis. These two corrections introduced small discontinuities in the wing velocity, which creates some oscillations in the resulting forcing and fluid flow, but these effects are small and do not change the trends that are the focus of this study.

Chapter 3: Experimental Results

This chapter presents and discusses the results from experiments that were conducted with free flying dragonflies during the summer of 2016. During the experimental campaign, dragonflies were recorded performing several different maneuvers and flying in different orientations. In this chapter the focus is on three different types of flight: straight upright, straight inverted, and gust encounter (where the first two are in a quiescent environment). For additional information about the various maneuvers recorded during this study, the reader is referred to Mateusz Gabryszuk's Master's thesis [64]. First, the body motion and bulk wing kinematics from the three flight types are presented in sections 3.1-3.3, then those kinematics are compared both to prior studies of dragonflies and across flight types to determine any significant changes in wing kinematics with changing flight conditions in section 3.4. Finally the measured wing deformations are presented and discussed in section 3.5.

3.1 Basic Flight Data

The wing kinematics presented here derive from seven individual flights, with two full wingbeats analyzed from each. The flight type, dragonfly orientation, mass,

average speed, and average acceleration are presented in table 3.1 with flight path and speed information in figure 3.1. For all tabulated data in this chapter the results are presented as the average value ± one standard deviation. The velocity data presented in table 3.1 and figure 3.1c were calculated by taking the first derivative of a third order spline fit to the position data. The acceleration data in table 3.1 are based on the second derivative of a fourth order polynomial fit to the dragonfly position data, and the values presented are based only on the magnitude of the acceleration. Though there are some differences in the z position data between flights the main difference between different flight categories is seen in the speed and acceleration data, with the difference shown in figure 3.1c. The upright flights are at a lower speed with a higher acceleration than the other flights, and this must be remembered when comparing between upright and inverted flights.

There are two comparisons between these three different categories of flights that are presented in this work. The first is the difference between upright and inverted flight and the second is the difference between flights with and without a gust encounter (but inverted in both cases). In order to compare multiple different flights, the flight paths (as presented in figure 3.1) must be sufficiently similar. The criteria that were used to identify straight flights were: the trajectory in the x-y plane had a linear fit R^2 value of 0.9 or higher, and the z position change was less than 15 mm during the wingstrokes analyzed. The heading and elevation variation (see figure 2.3 for explanation of these variables) for these five flights were less than 25° and 30° respectively. For the gust response flights, the constraints for straightness and orientation were relaxed ($R^2 > 0.8$ and elevation variation $< 45°$),

Table 3.1: Dragonfly masses and data describing the flights used in this study.

Flight Number	Flight Type	Orientation	Mass (mg)	Speed (m/s)	Acceleration (m/s^2)
1	Straight	Inverted	153	1.7 ± 0.1	5.5 ± 4.1
2	Straight	Inverted	220	1.7 ± 0.1	9.6 ± 8.2
3	Straight	Inverted	153	2.0 ± 0.1	5.7 ± 2.5
4	Straight	Upright	231	1.2 ± 0.1	14.6 ± 8.5
5	Straight	Upright	159	1.1 ± 0.1	8.3 ± 1.8
6	Gust	Inverted	237	1.8 ± 0.1	7.3 ± 1.9
7	Gust	Inverted	251	1.9 ± 0.1	8.7 ± 4.1

but the flight paths chosen were subjectively similar to the straight inverted flights.

3.2 Undisturbed Straight Flights

The straight flights provide the baseline data for determining how a dragonfly alters its wing kinematics when encountering a lateral wind gust. The straight upright flights are closer to normal dragonfly flight, so the kinematics from those flights are used as the baseline case for the CFD simulations. Since the gust encounter flights are both inverted, the kinematic comparison is between those and the straight inverted flights.

The wing kinematics are all presented in a body reference frame, so up- and downstrokes are body relative and for the inverted flights they are not in the global

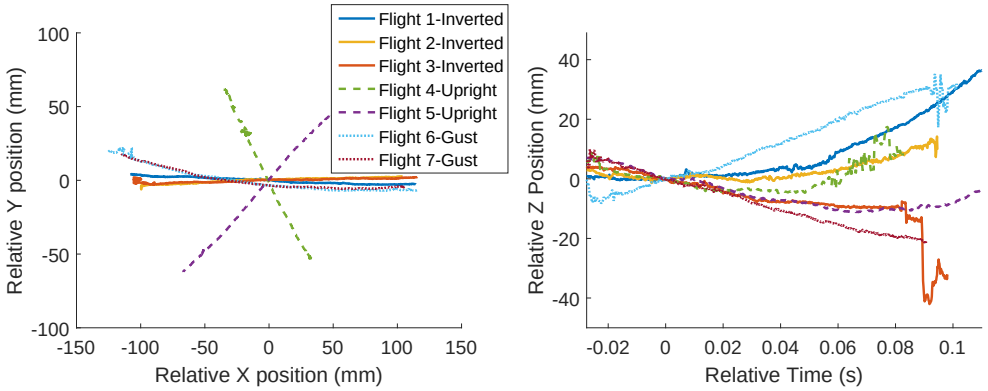

(a) (b)

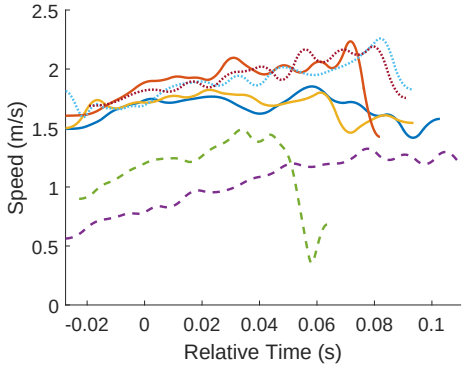

(c)

Figure 3.1: The flight paths and speeds for the seven flights presented in this work.

up and down directions. The upstrokes are defined as the portion of the wingstroke during which the flap angle is increasing (the wing is moving up in the body reference frame), and the downstroke is the portion of the wingstroke during which the flap angle is decreasing (the wing is moving down in the body reference frame). Stroke reversal points correspond to local extrema of the flap angle for the particular wing. The time used in the plots of the wing kinematics is relative to the beginning of the first downstroke for the left forewing and the phase of all wings is presented relative to the left forewing.

3.2.1 Upright Flights

The wing kinematics for the two upright flights are presented in figure 3.2 and tabulated in table 3.2. There are several general features of the kinematics that are worthy of note. First, the flap angle follows a sinusoidal pattern, whereas the pitch angle has a more plateau-like shape, meaning the pitch angle is roughly constant during the stroke and changes rapidly either symmetrically around or slightly leading stroke reversal. Comparing the forewing and hindwing data in figure 3.2, it is clear that the hindwing leads the forewing and that the flap amplitude of both forewing and hindwing is similar, but there are some difference in pitch angle. The left- and right-wing kinematics are primarily symmetric in these two flights.

Looking at the kinematic variables in table 3.2, the large variation in the flap offset angle, Φ_{off}, stands out. This variation is because of the dependence of the flap offset angle on the roll angle of the dragonfly which, as has already been

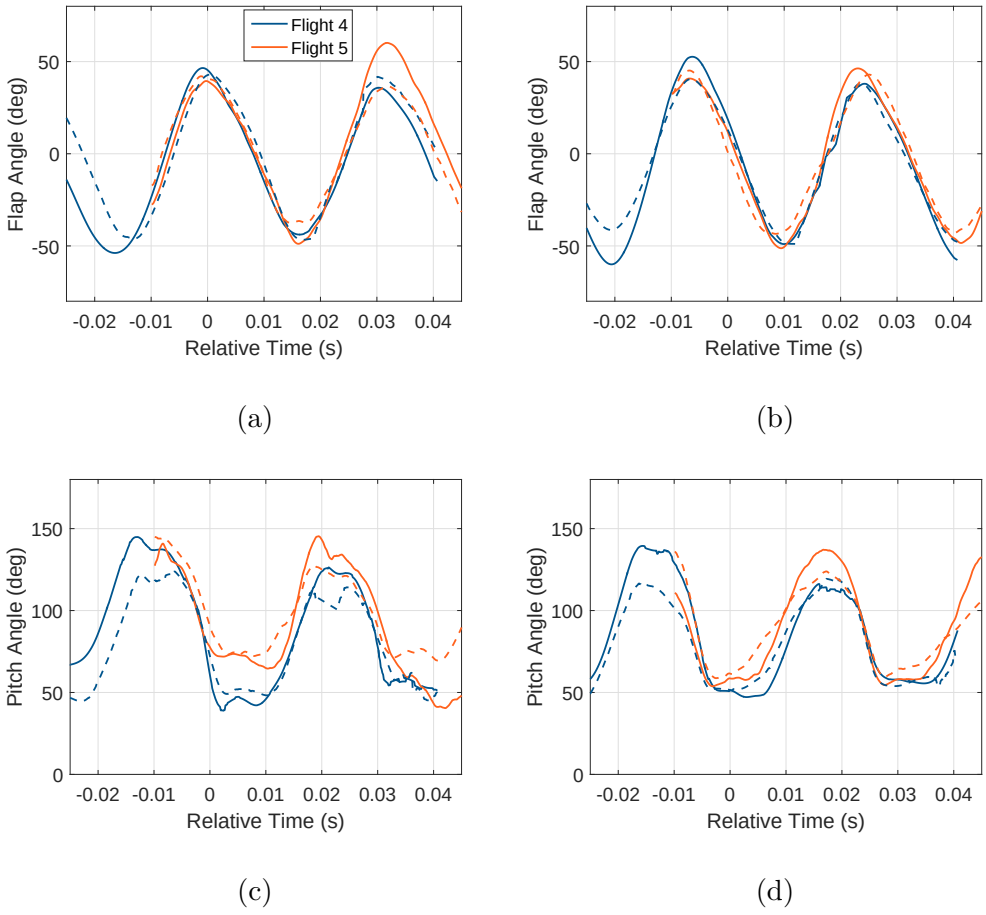

Figure 3.2: Wing kinematics from the two upright flights. Left wing kinematics are shown with solid lines and right wing kinematics are shown with dashed lines. The forewing flap and pitch are shown in (a) and (c) with the hindwing flap and pitch appear in (b) and (d).

Table 3.2: Kinematic parameters for straight, upright flight.

	Φ (°)	Φ_{off} (°)	Ψ (°)	Ψ_{off} (°)	f (Hz)	UDR	Phase (°)
Left Forewing	93 ± 10	17 ± 29	92 ± 12	90 ± 10	31.3 ± 2.2	0.8 ± 0.1	N/A
Left Hindwing	85 ± 5	18 ± 30	78 ± 11	91 ± 6	32.2 ± 0.6	0.9 ± 0.1	-72 ± 6
Right Forewing	82 ± 8	-15 ± 32	67 ± 10	92 ± 9	31.5 ± 0.9	0.9 ± 0.1	-11 ± 29
Right Hindwing	85 ± 5	-12 ± 30	65 ± 3	88 ± 3	32.0 ± 1.3	0.9 ± 0.1	-64 ± 5

noted in section 2.1.2, has high error due to fact that the dragonfly body is mostly axisymmetric. Since the uncertainty for the flap offset values is so high, they are set to 0 in all simulations and they are not analyzed further (though they are presented for all flight types). The tabulated values also indicate that there is some asymmetry in pitch amplitude, particularly for the forewings, but otherwise the kinematics have minimal differences between left and right wings (as was noted of figure 3.2). The other notable feature of the upright flight kinematics is that the UDR is uniformly less than unity, meaning that the downstroke is longer than the upstroke.

To compare the measured wing kinematics with the models presented in section 2.2.1 for use in the CFD simulations (which assume left-right symmetry), the forewing data for both the left and right wings were combined together. Figure 3.3

shows how well the two models match the shape of the measured kinematics. The flap model follows the average flap angle quite accurately; the pitch angle model captures the plateau-like variation of the pitch angle, but does less well matching the exact values. This is because the pitch angle of the dragonfly's wings need not be perfectly cyclic, whereas the model is. From this comparison it was determined that the pitch angle model should lead the flap-angle model by a phase angle of 108° (or $\tau = 0.3$).

3.2.2 Inverted Flights

The average wing kinematics for the inverted flights are shown in figure 3.4 together with the average upright kinematics for reference. The general patterns that were noted for the upright flights are still present for the inverted flights, though the inverted forewing pitch in figure 3.4c has less of the plateau-like shape than the upright forewings or the hindwings from both flight types. Two additional differences can be seen in figure 3.4: the pitch angle for all of the inverted wings differs from that of the equivalent upright wings during the downstroke, and the inverted hindwings have a larger phase lead than the upright hindwings do.

The tabulated inverted wing kinematic parameters, given in table 3.3, clarify some of the observed differences. The pitch amplitudes for the inverted forewings are slightly higher than those for the upright flights, while the pitch offset is lower. The hindwings also have a lower pitch offset, but the pitch amplitude is similar to that of the upright hindwings. The flapping frequencies are slightly lower than

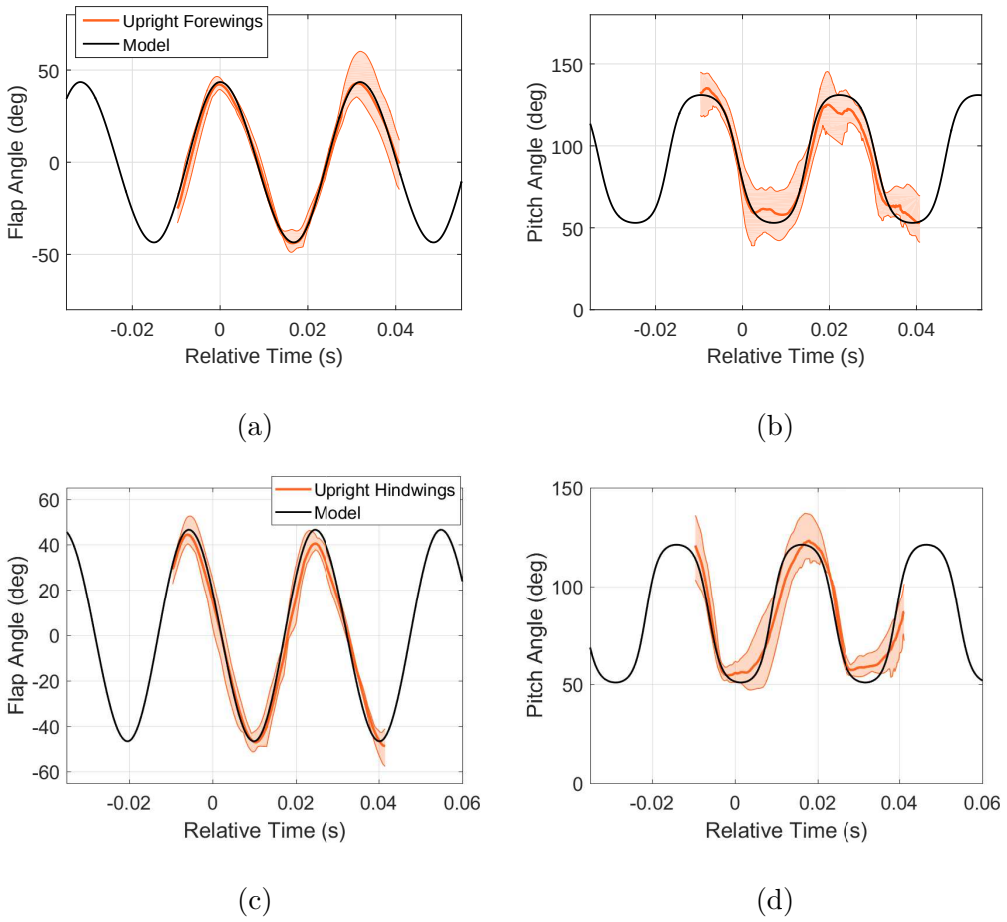

Figure 3.3: Comparison between the upright forewing kinematics and the model. The thick blue lines are the average values for the flap (a) and (c) and pitch (b) and (d) and the shaded region indicates the range of the data. The mean value can only be calculated when there is data available from both flights, so it is a shorter time segment than the data presented in figure 3.2.

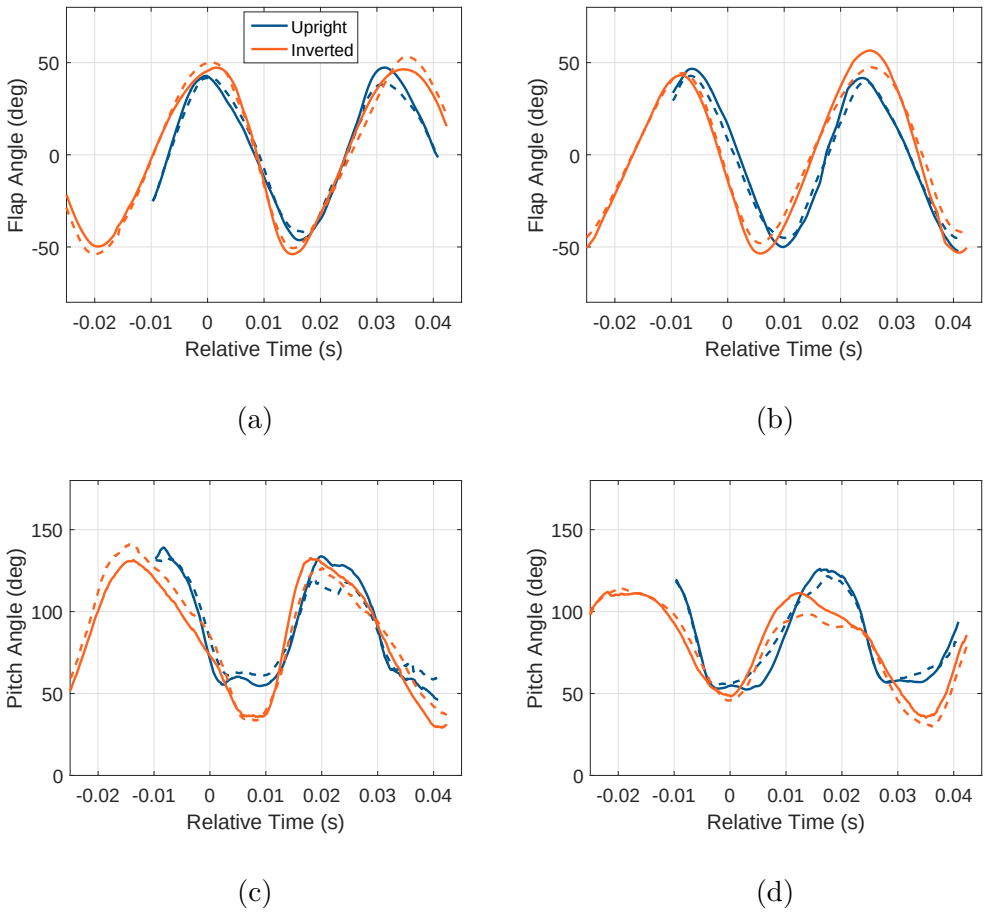

Figure 3.4: Average wing kinematics for upright and inverted flights. The subfigures and line types are as in figure 3.2.

Table 3.3: Kinematic parameters for straight, inverted flight with phase defined relative to the left forewing.

	Φ (°)	Φ_{off} (°)	Ψ (°)	Ψ_{off} (°)	f (Hz)	UDR	Phase (°)
Left Forewing	100 ± 10	6 ± 33	99 ± 32	78 ± 11	28.7 ± 1.8	1.2 ± 0.2	N/A
Left Hindwing	110 ± 12	0 ± 34	71 ± 18	77 ± 13	30.5 ± 2.1	1.2 ± 0.2	-95 ± 13
Right Forewing	101 ± 18	10 ± 31	105 ± 14	86 ± 7	28.6 ± 2.6	1.4 ± 0.3	25 ± 30
Right Hindwing	98 ± 16	-2 ± 35	65 ± 11	72 ± 12	30.8 ± 3.0	1.2 ± 0.1	-94 ± 6

those for the upright flights, but the most significant timing difference is the UDR. For the inverted flights, the UDR is uniformly greater than unity which means that the upstroke is always longer than the downstroke. This is the opposite of what was observed for the upright flights. There are also some differences in the amount of variation in the flap and pitch amplitudes between left and right wings, which may be caused by dragonflies initiating roll maneuvers during the second wingstroke within the test volume in two of the flights.

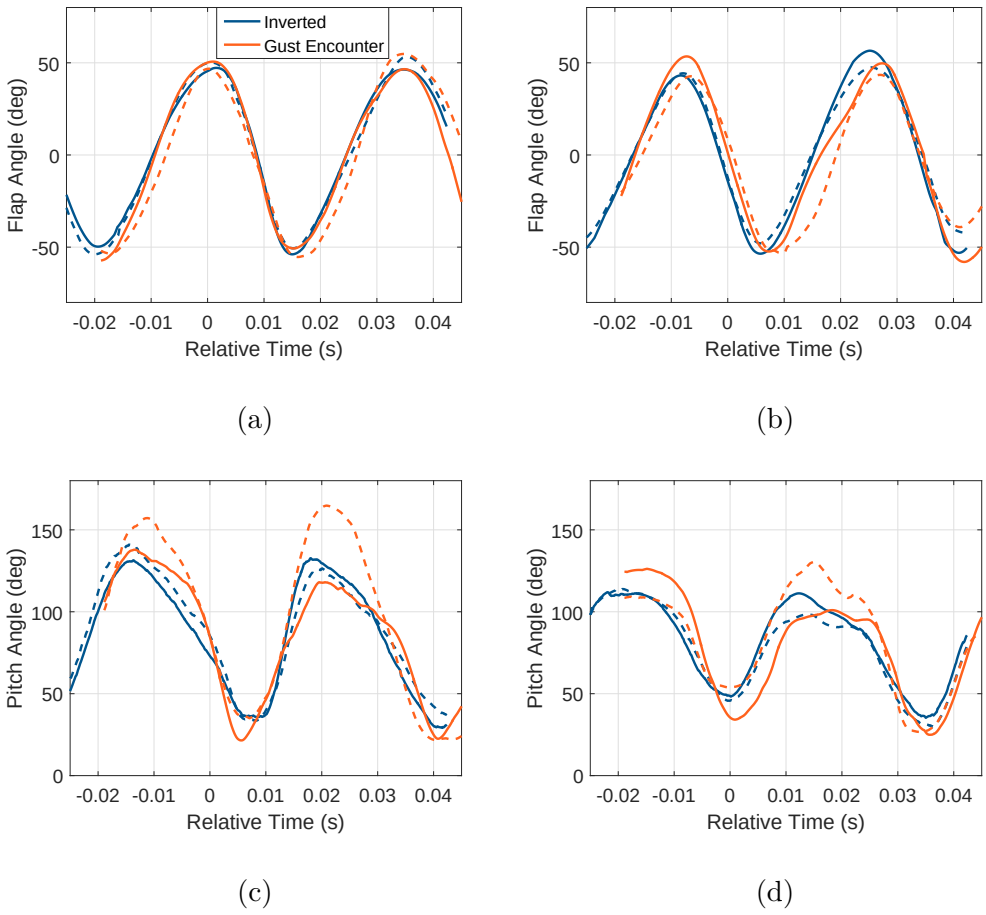

Figure 3.5: Average wing kinematics for gust free and gust encounter inverted flights. The subfigures and line styles are as in figure 3.2.

3.3 Gust Encounters

The wing kinematics for the inverted gust-encounter flights are shown with those for the gust free inverted flights in figure 3.5. There is surprisingly little variation between the two sets of kinematics, with the only noticeable difference being the significantly larger pitch amplitude for the right wing, which is the windward wing for the gust-encounter flights.

Table 3.4: Kinematic parameters for gust encounters.

	Φ (°)	Φ_{off} (°)	Ψ (°)	Ψ_{off} (°)	f (Hz)	UDR	Phase (°)
Left Forewing	103 ± 6	18 ± 18	104 ± 20	73 ± 8	29 ± 0.9	1.2 ± 0.1	N/A
Left Hindwing	110 ± 11	8 ± 27	80 ± 14	68 ± 9	28.8 ± 0.6	1.2 ± 0.1	-84 ± 7
Right Forewing	106 ± 7	-6 ± 29	137 ± 20	100 ± 10	28.9 ± 1.5	1.1 ± 0.1	13 ± 15
Right Hindwing	91 ± 10	-17 ± 34	86 ± 25	83 ± 10	30.3 ± 1.2	1.1 ± 0.1	-70 ± 8

The tabulated kinematic variables for the gust flights, shown in table 3.4, confirm what was observed in figure 3.5. The pitch amplitude of the right forewing is significantly larger than that of the left forewing, though the difference between the left and right hindwings is less significant.

The stroke-plane orientation angles for all three sets of flights are presented in table 3.5. Though the variation in the orientation angles is high, due in part to uncertainty in the roll angle, there are still several noteworthy features. First, the ρ angle for all of the wings is positive for all three flight types, meaning that the stroke plane vectors point above the $\overleftarrow{P} - \overleftarrow{S}$ plane in the body reference frame. Second, the forewing stroke planes point inward toward the body centerline, with left wings having negative θ angles and right wings having positive θ angles. Third,

Table 3.5: Stroke plane orientation angles for straight and gust encounter flights

	Straight-Upright		Straight-Inverted		Gust Encounter	
	θ	ρ	θ	ρ	θ	ρ
Left Forewing	-35 ± 17	22 ± 21	-21 ± 27	24 ± 22	-42 ± 16	19 ± 16
Left Hindwing	-6 ± 17	27 ± 10	-2 ± 23	24 ± 10	-10 ± 24	28 ± 8
Right Forewing	16 ± 36	33 ± 10	23 ± 22	21 ± 16	25 ± 27	37 ± 14
Right Hindwing	-2 ± 26	30 ± 8	-2 ± 23	26 ± 7	-6 ± 29	40 ± 15

the hindwings have θ values very close to aero. Lastly, there is minimal left-right asymmetry (aside from the sign of the forewing θ values) in both the upright and the inverted flights, with the most significant asymmetry appearing between the left and right upright forewings, but this difference is still within the large uncertainty in the θ value. There is notable asymmetry in both θ and ρ angles for the gust encounter flights, but it is difficult to determine the significance of this asymmetry because of the high variation.

Since the most important relationship in the simulations is that between the incoming velocity and the wing, a different reference frame was used to determine the stroke plane orientation for the two undisturbed flight types which are the basis for the CFD simulations (here we will denote a new reference frame with $'$

notation). The θ' angle was calculated relative to the dragonfly velocity in the global x-y plane, with ρ' the angle between the x-y plane and the stroke-plane vector. Since the simulations assume left-right symmetry, these results combine left and right wings. As for the tabulated data these values are presented as mean $\pm$ one standard deviation For the upright flights, the forewing stroke plane vector had $\theta' = 26^o \pm 9^o$ in towards the body and $\rho' = 23^o \pm 11^o$ above the horizontal, with $\theta' = 1^o \pm 7^o$ and $\rho' = 20^o \pm 11^o$ for the hindwings. For the inverted flights, $\theta' = 19^o \pm 25^o$ and $\rho' = 14^o \pm 23^o$ for the forewing, and $\theta' = 0^o \pm 24^o$ and $\rho' = 18^o \pm 19^o$ for the hindwing. With the exception of the upright hindwing θ', which was set to 0^o to simplify the analysis by eliminating any yaw from the hindwing stroke planes, the average values of the orientation angles were used in the respective simulations.

3.4 Kinematic Variations

To put these results into context and to ascertain how well they match with the existing knowledge about dragonflies, in this section these data are compared to prior studies of dragonflies then to each other. The comparison to prior results will establish how closely the measured wing kinematics represent normal flight while the comparison between flight types indicate how dragonflies change their wing kinematics to account for different flight conditions.

3.4.1 Comparison with Prior Studies

In order to better understand the wing kinematic data presented herein, a comparison with wing kinematics measured in prior studies is needed. To simplify the presentation of the various results, this discussion will address each kinematic parameter separately (where there are available data in the literature).

Rüppell, in his study of dragonfly flight in nature, reported that the flapping frequency of dragonflies is dependent on the size of the dragonfly and their wing loading, with flapping frequencies for dragonflies of three species of comparable size to the Blue Dasher having values from 32 to 43 Hz [28]. Other studies of dragonflies in the same size range measured flapping frequencies varying from 29 to 44 Hz [31, 32, 33]. All of the flapping frequencies measured in these experiments were on the low end of this range, with the highest being the upright flights with flapping frequencies of 31 to 32 Hz. The likely reason for these lower values is the relatively low temperature in the laboratory in which the experiments were conducted. Since the performance of insect flight muscles is temperature dependent [69], dragonflies may not be able to achieve normal flapping frequencies until they have been active for some time. As the upright flight sequences were all captured after the dragonfly had done some flying around the test volume, it is likely that their flight muscles were warmer than directly after the dragonflies had exited the staging tube, which is when the two other flight conditions were recorded.

Flapping amplitudes for dragonflies of similar size and mass to those tested in this study range from 50° to 110°, with most reported results in the 80° to

110° range [31, 32, 33, 34]. Wakeling and Ellington noted a slight increase in flapping amplitude with velocity [31]. In the present results, the higher flapping amplitudes of the inverted flights, for which the dragonfly velocity is almost twice that of the upright flights, are consistent with this observation. Overall the flap amplitudes measured in the present experiments fall within the range of previously reported data.

The upstroke-to-downstroke ratio, or a similar measure of relative upstroke and downstroke timing, has been reported in a few studies. Rüppell reported longer or equal duration downstrokes for all of the dragonflies observed in the field. Wakeling and Ellington reported UDRs of 0.93 to 0.98 for dragonflies flying freely in a greenhouse. Only one study reports a UDR greater than 1; Bode-Oke et al. [38] noted this when observing a dragonfly flying backwards and oriented close to vertically. This indicates that dragonflies generally operate with a UDR less than 1, but they are capable of varying that ratio, as was observed in the present experiments. Therefore it is likely that dragonflies consistently have their wings move in the global down direction longer than in the global up direction, though the benefits of this condition are unclear [70].

Dragonflies are known to use a variety of phase differences between forewings and hindwings depending on the conditions and their current flight path. Rüppell observed that the phase differs between species, with larger species generally using lower phase differences during normal flight. He also indicated that lower phase differences, and particularly in-phase flapping, corresponded to flights for which high accelerations were needed or males were carrying females while mating [28]. Studies

of free-flying dragonflies with similar mass to those examined here have recorded phase differences of 50° to 100° [32, 30, 33]. The phase differences measured for all three flight types falls within the range of previously reported data and the significance of the variation between flight conditions will be discussed further in the next section.

The stroke-plane orientation has been reported primarily through the tracking of dragonfly wing tips [30, 31, 32]. Based on prior work and their own measurements, Wakeling and Ellington conclude that the stroke planes of dragonfly wings have little variation relative to the body's longitudinal axis [31]. This conclusion is consistent with the consistency of the stroke-plane orientations, across the different flight conditions, in the body frame measured in this research. Azuma and Watanabe found that the forewing stroke-plane vectors point in toward the body centerline and that the hindwings stroke-plane vectors (following the convention used in this study) generally point away from the centerline [30]. The data from the straight flights presented in this work supports their former conclusion, but the hindwing data does not indicate that the stroke-plane vectors point outward. Since stroke-plane orientation is an important component of wing orientation, this is an area in need of further elucidation.

Wing pitch data are reported in a few studies, though only at particular spanwise locations along the wing. The range of pitch amplitudes is from 70° to 120° for the forewings and 50° to 105° for the hindwings [30, 32, 33, 34]. All of these studies report wing pitch of a position in the outboard half of the wing. Azuma and Watanabe [30] measured the pitch angle at 25%, 50%, and 75% span and found that

the pitching amplitude increases further outboard. In all but one case, namely the experiments of Wang et al. [33], the hindwing pitch amplitude is smaller than that of the forewing at the same spanwise location. The wing-pitch angle measurements in the present study are based on a least squares plane fit to the marker locations, which gives an average pitch angle for the whole wing. Our pitch angles match well with the measured wing pitch from 50% to 75% span [30, 33, 34] and the data from 25% span [30] and the wingtip [32] are lower and higher, respectively. There is also a consistent pattern of the hindwing having an equal or smaller pitch amplitude compared to the forewing in all of the flights analyzed in the present study.

Overall, we thus conclude that the wing kinematics presented herein match well with those of dragonflies observed in nature and in other enclosed environments (with the possible exception of flapping frequency, discussed at the beginning of this section).

3.4.2 Forewing-Hindwing Differences

Within our dataset, we note three significant differences between the kinematics of the forewings and the hindwings: the hindwings lead the forewings by a phase angle of $60-100^\circ$, and the forewings and hindwings have different pitching amplitudes and different θs. The phase difference is the most frequently remarked upon difference between the forewings and hindwings, and is generally thought to be tied to force production [28]. The upright flights, which have a higher acceleration, have a smaller phase difference (72° for the left and 64° for the right hindwing), whereas the

inverted flights, which have minimal acceleration, have a larger phase difference (95° for the left and 94° for the right hindwing). Though this is not conclusive, as there are other kinematic differences between upright and inverted flight that will be discussed in the next section, this trend of decreasing phase difference with increasing acceleration supports the claim that lower wing phase difference leads to increased force production.

Another notable difference observed between in all three flight types in this study is the variation in pitching amplitude. With the exception of the right wings for the upright flights where the difference is much less than the uncertainty associated with pitch amplitude, the hindwings have a consistently lower pitch amplitude than the forewings. This is even seen when there is left-right asymmetry, as in the gust-response flights; here the pitch amplitude of the right hindwing is still lower than that of both forewings. From such experiments alone it is impossible to determine if the pitching amplitude difference is for aerodynamic reasons or related to the physical capabilities of the flight muscles operating the hindwings.

The last significant difference that was noted in these experiments is that in the stroke plane orientation, specifically in the θ value. This difference is most likely due to the physical constraints imposed by the wing spacing, meaning that at most one wing can have a θ angle close to zero. It is also noteworthy that the ρ angles, i.e., the angle between the stroke plane vector and the $\overleftarrow{P} - \overleftarrow{S}$ plane, are remarkably consistent for all wings. It is possible that this lack of variation in ρ between forewing and hindwing is also related to the need to avoid wing-wing collisions, as a larger angle for the forewing than the hindwing could lead to intersecting stroke planes.

3.4.3 Kinematic Differences Between Flight Types

There are two relevant direct comparisons between different flight types that can be made with the experimental data discussed here: comparing undisturbed upright versus inverted flight and gust-free inverted versus gust encounter flight. For these comparisons, this study treats the upright flight kinematics as the baseline case for the simulations, since inverted flight is not a typical flight mode seen in nature.

Figure 3.4 and tables 3.2 and 3.3 reveal a few differences between the upright and inverted flights. As already noted, the upright flights have a higher flapping frequency than the inverted flights. This is likely due to the fact that the upright flight sequences were all recorded after the dragonfly had flown around the test volume for a short period of time, whereas the inverted flights were right as the dragonfly exited the staging tube and flew directly across the test section. The difference in flapping frequency is offset by the difference in flapping amplitude between the two flight types. The inverted dragonflies have a larger flapping amplitude than the upright dragonflies, and therefore have a slightly higher average rotation rate, even though their flapping frequency is lower (upright forewings $2750^o/s$, inverted forewings $2880^o/s$). The UDR is the other major timing difference between upright and inverted flight. The inverted dragonflies have a UDR greater than unity while the upright dragonflies have a UDR less than unity. This means that dragonfly wings are always spending more time moving in the global down direction than in the global up direction, regardless of specimen orientation.

There is also a notable difference in the pitching of the upright and inverted

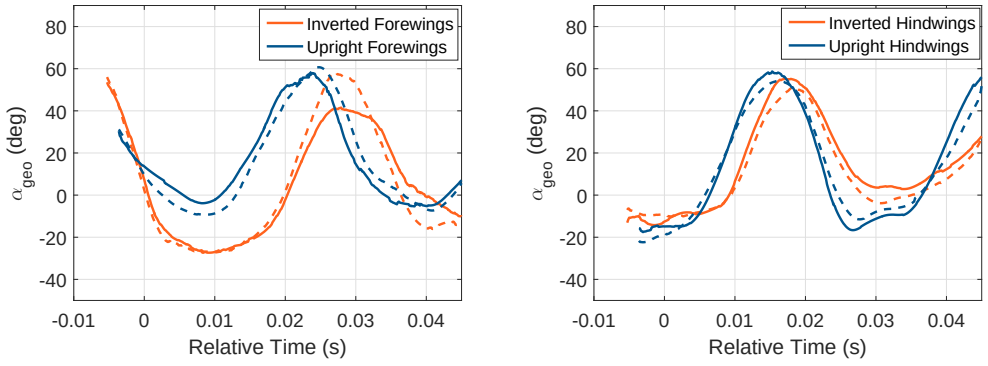

(a) (b)

Figure 3.6: Average geometric angle of attack (α_{geo}) for the upright and inverted flights. Relative time 0 is when the wings first start moving down in the global reference frame (upright downstroke, inverted upstroke).

wings. The inverted flights have a lower mean pitch angle and comparable or larger (depending on which wing) pitching amplitudes than the upright flights. The inverted flights also do not exhibit a relatively constant pitch angle during the upstroke, as the upright flights do. In order to better understand how the difference in pitch may impact the aerodynamics, the geometric angle of attack, α_{geo}, was calculated for the average upright and inverted kinematics and is shown in figure 3.6. The geometric angle of attack is the angle between the wing plane and the average velocity of the dragonfly during the flight.

There is a consistent pattern seen for all wings, where the wing has a negative α_{geo} during the global downstroke — this is small for all but the inverted forewings — and a large positive α_{geo} during the global upstroke. The similarity between the α_{geo} of the hindwings in the two flight types indicates that the dragonflies are

not only modify their wingstroke such that they spend more time moving their wings in the global down direction, but that they also manipulate the orientation of their wings. This manipulation is not done only through the pitch angle, but also through the dragonfly body orientation, shown in figure 3.7. Since the stroke plane orientation is relatively constant with respect to the dragonfly orientation, the dragonflies reorient their bodies to obtain global stroke-plane orientations which will result in the proper wing α_{geo}.

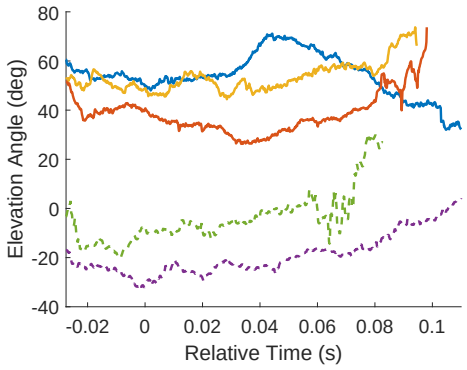

Figure 3.7: Elevation angles for the upright (dashed lines) and inverted (solid lines) flights.

Comparing now the gust-free inverted and gust-encounter flights, we note three significant differences. The first, and most notable, is the pitch asymmetry seen in the gust response flight. The asymmetry comes about as the windward wings increase both the average pitch angle and the pitching amplitude with the forewings exhibiting a larger asymmetry than the hindwings. This change in pitch indicates that dragonflies can actively manipulate the pitching of their wings, and use this ability to respond to low-speed disturbances. The other two kinematic differences between gust-free and gust-response flights are a slight difference in hindwing phase, and differences in stroke plane orientation θ values. The difference in hindwing phase, namely that the gust-response flights have a lower phase lead than the gust-free flights, may be linked to the slightly higher accelerations during the gust encounter flights. The difference in θ values is more difficult to

relate directly to a difference between the flights because of the high variation and the dependence of θ on the roll angle. Nonetheless, this difference appears to show that the stroke planes in the gust-response flights are turned slightly into the gust rather than being symmetric as in both the upright and inverted gust-free flights.

3.5 Wing Deformations

In this section, the deformation results from four different wings are presented and discussed in detail: a fore- and hindwing from flight 4 (upright), and a fore- and hindwing from flight 3 (inverted). The deformation coefficients from these four wings are used in the deforming wing simulations, and these deformations are representative of those experienced by the fore- and hindwings of their particular flight type (wing deformations were extracted from flights 2-5). Overall, the wing deformations for both the forewing and the hindwing follow the pattern observed in the prior studies of dragonfly wing deformation [33, 49].

In both figures 3.8 (forewing) and 3.9 (hindwing), where deformed wing surfaces generated by linearly interpolating between the reconstructed marker locations are compared with surfaces generated using the model presented in section 2.1.4, the wing exhibits a generally cambered shape at the top of the downstroke and in the middle of the downstroke (first and second rows). When the wing is in the middle of the upstroke (fourth row) however, it is twisted, and it is here that the most substantial deformation is observed. Figures 3.8 and 3.9 also show that the model presented in section 2.1.4 accurately reflects the wing shape given by interpolating

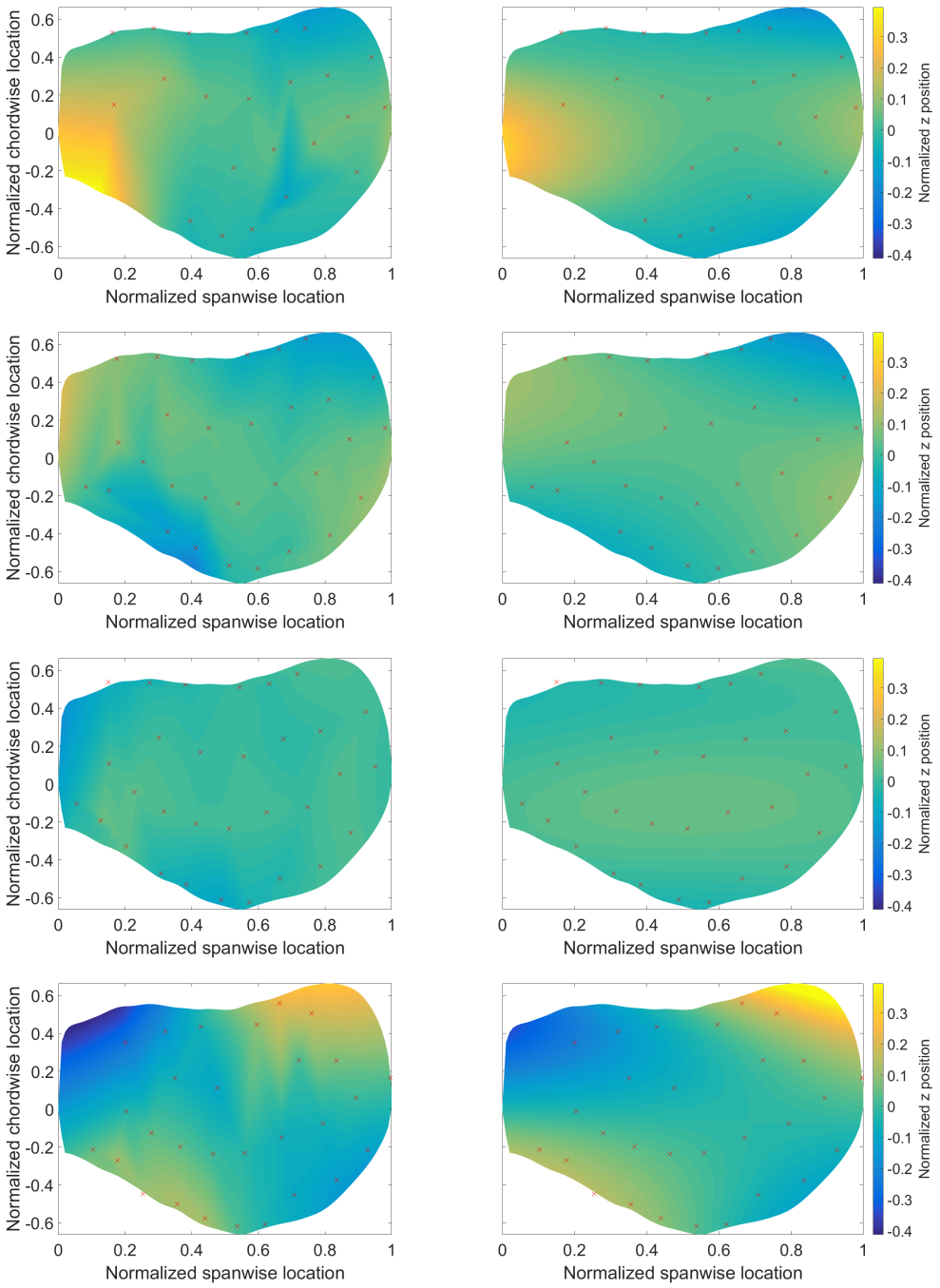

Figure 3.8: Comparison of linear interpolation between wing points (left) and the functional fit for the deformed wing surface (right) at different points during the upright forewing wingstroke: (top) start of the downstroke; (second row) middle of the downstroke; (third row) stroke reversal; (bottom row) middle of the upstroke

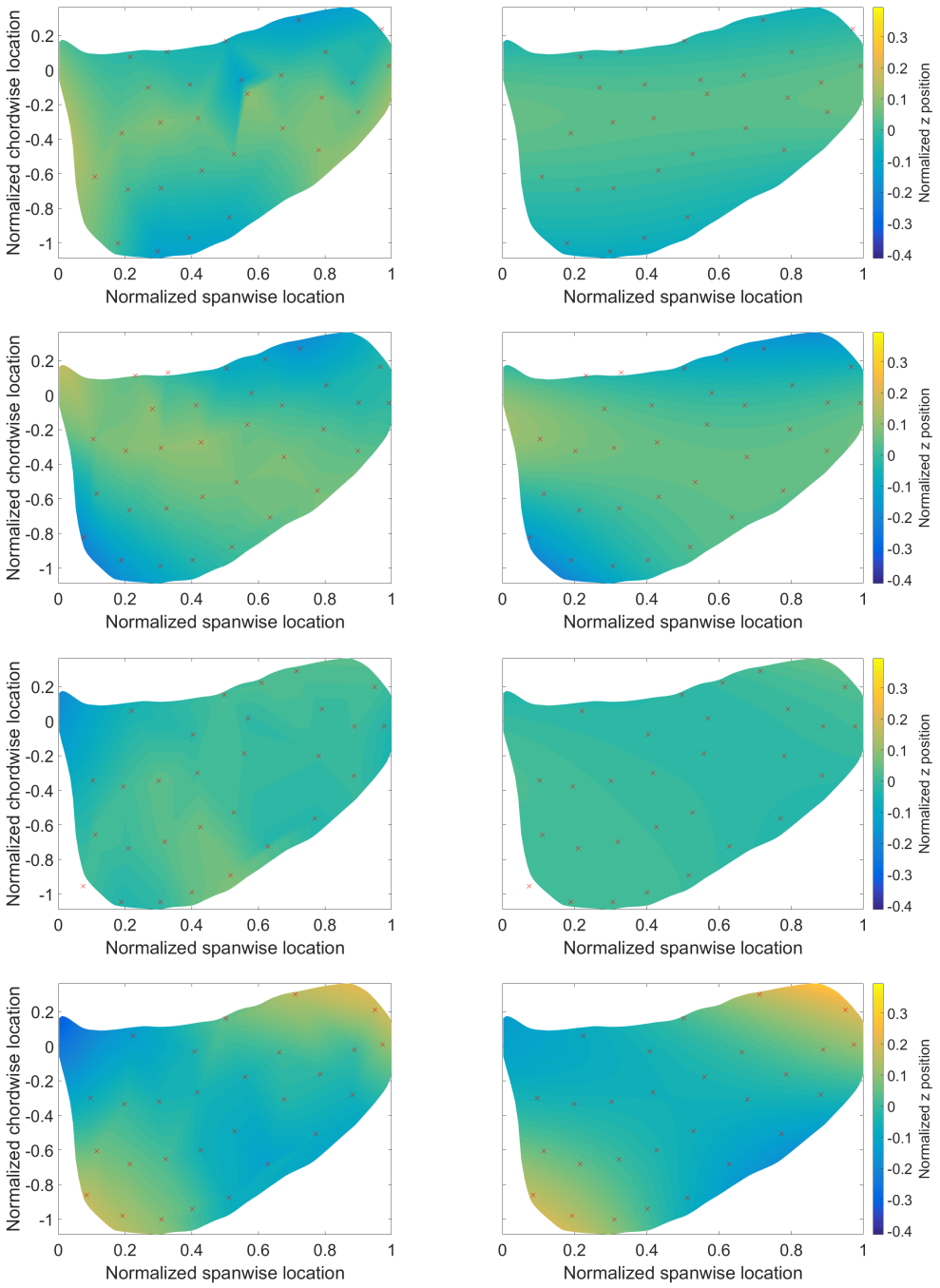

Figure 3.9: Comparison of linear interpolation between wing points (left) and the functional fit for the deformed wing surface (right) at different points during the upright hindwing wingstroke: (top) start of the downstroke; (second row) middle of the downstroke; (third row) stroke reversal; (bottom row) middle of the upstroke

between the measured points.

To further quantify the accuracy of the deformation model, the model error was compared with the error when modeling the wing with a flat plane (as seen in figures 3.10 and 3.11). The error, both mean and maximum, is determined by calculating the distance between wing marker locations and the surface fit. In figure 3.11 the results are shown in terms of the normalized error (i.e., the model-fitted error divided by the plane-fit error) for the four wings that are used to provide deformation coefficients to the simulation. In all cases the model reduces the error by over 50% when compared to the plane fit during the wingstrokes, but doesn't significantly reduce the error around stroke reversal. This is unsurprising, as the wing deformation around stroke reversal is very small particularly at supination (downstroke to upstroke transition) where the mean out-of-plane distance approaches the accuracy of the photogrammetric measurement system (0.1 mm), as seen in figure 3.10. The one area where the model has high error is the second upright hindwing upstroke (figure 3.11c, relative time $\sim$ 0.0175 to 0.03 seconds) where the normalized errors are close to 1. This is due to an error in properly orienting the wing points in the wing frame during the first step in fitting the deformation model, so all further results for the upright hindwing will use the data from the first upstroke (relative time ~ -0.015 to 0 seconds). For all other wings, the defor-

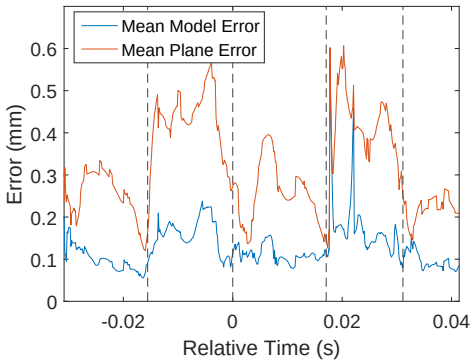

Figure 3.10: Mean error for the upright forewing from flight 4 for both the deformation model and a plane fit.

mation data presented in the remainder of this section and used in the simulations is from the first full downstroke and the following upstroke.

To gain a better understanding of how the wings are deforming, two terms are used to describe the deformation at a particular spanwise section: the are twist and camber, as illustrated in figure 3.12. The twist is the angle between the wing plane and the chord line at the particular spanwise station. The camber is the maximum distance — positive if above the wing, negative if below — between the wing surface and the chord line. These two values are calculated from the wing surface fit.

The wing twist is shown in figure 3.13 for the four wings. During the downstroke the wing has less twist than during the upstroke in both upright and inverted flights. The degree to which the twist increases is different for each wing, but the general pattern of wing twist is consistent across all four.

The maximum camber data, shown in figure 3.14, does not show the same consistency across wings as the twist does. For each wing the camber has less variation in the spanwise direction than the wing twist has, with the whole wing generally having either positive or negative camber. The only consistent pattern across all four wings is that they are positively cambered during the downstroke and negatively cambered during the upstroke. The specifics of that pattern, as well as the magnitude of the camber, vary significantly between both fore- and hindwings as well as upright and inverted flights.

The wing deformations measured here reinforce the conclusions of prior studies that dragonfly wings are primarily cambered during the downstroke and primarily twisted during the upstroke [33, 49]. The camber data presented here show less

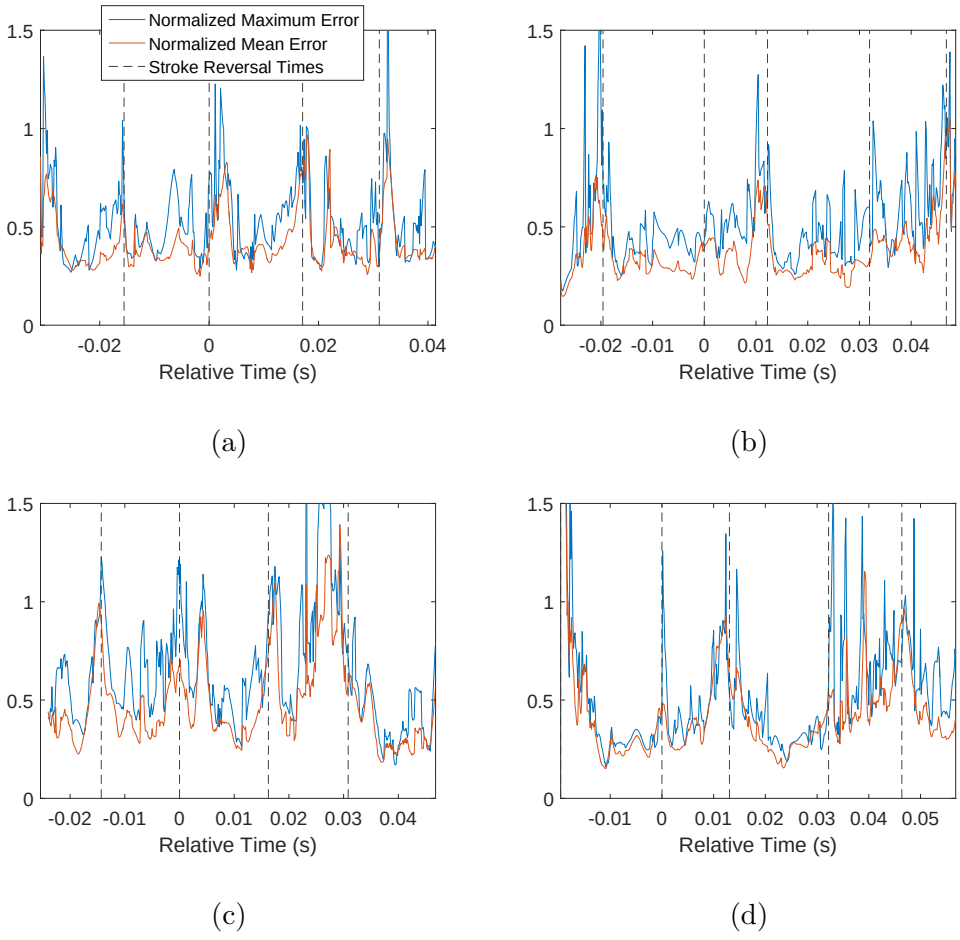

Figure 3.11: Error plots for the four wings used for the simulations: (a) upright forewing, (b) inverted forewing, (c) upright hindwing, and (d) inverted hindwing. Errors are the maximum/mean distance of wing-marker points to the deformation model surface normalized by the maximum/mean distance of wing-marker points to a planar fit of the wing. Relative time 0 is the beginning of the first recorded full downstroke of the wing.

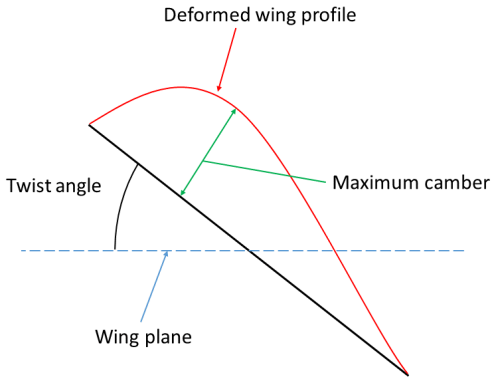

Figure 3.12: A diagram describing how maximum camber and twist angle are determined.

variation across the wing span than presented in one of the prior studies [49], but the general trend of positive camber during the downstroke and negative camber during the upstroke is consistent; this trend has also been observed in several other insects [71, 72].

The most striking feature of the deformation results for these two dragonflies is the similarity between them despite their opposite orientations. Though the exact magnitudes differ between the upright and inverted wings, the trends are very much consistent. This is in spite of the fact that the aerodynamic loading on the inverted wings is opposite that seen in normal upright flight. Though determining the cause of these deformations is beyond the scope of the present work, this similarity supports the claim of Appel et al. [47] that the microstructures within dragonfly wings are key elements constraining the wing deformation.

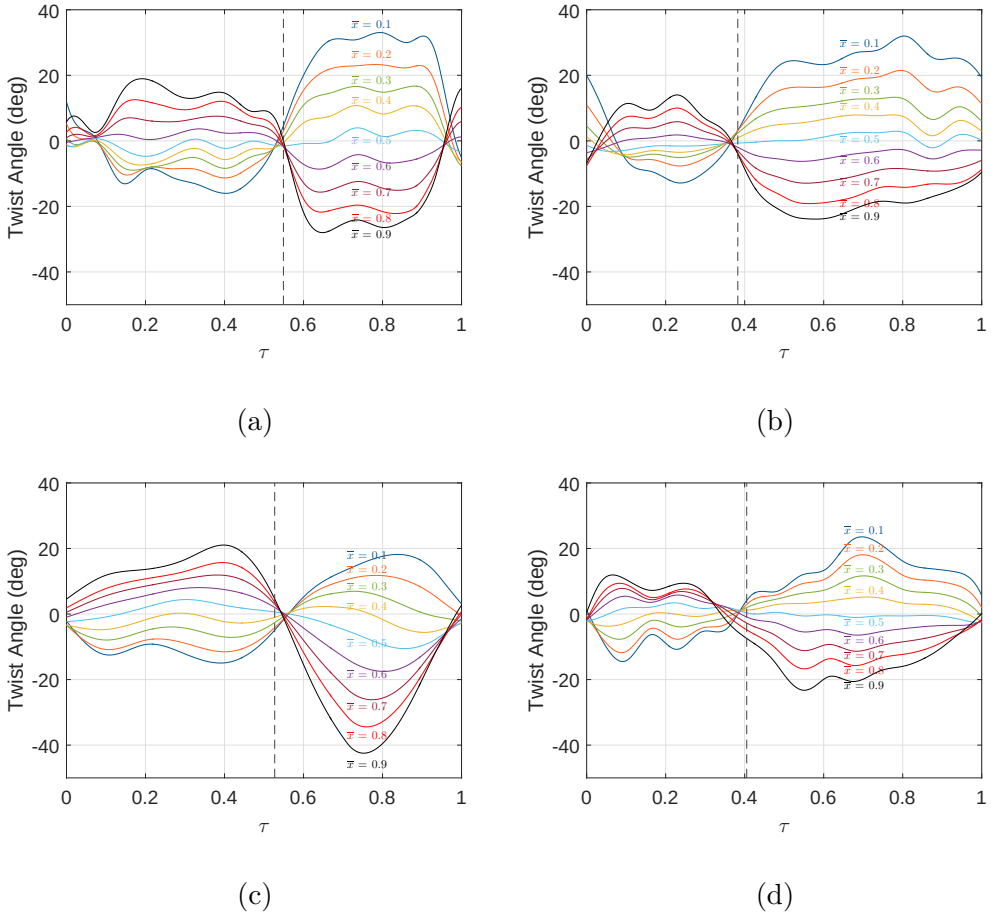

Figure 3.13: Twist angle at various spanwise stations throughout one wingstroke for the four wings used in the deforming wing simulations: (a) upright forewing; (b) inverted forewing; (c) upright hindwing; and (d) inverted hindwing. Each line color corresponds to a particular normalized spanwise location ($\overline{x} = \frac{x}{b}$) and the stroke reversal point is indicated by the dashed line.

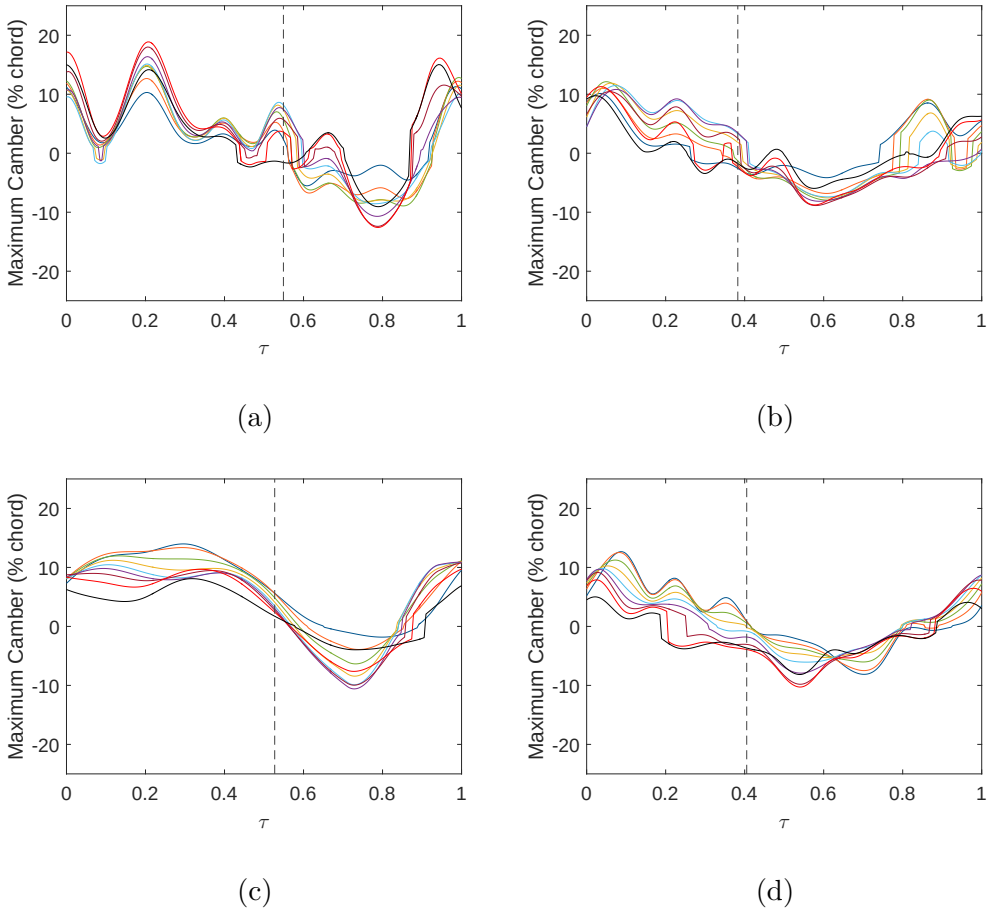

Figure 3.14: Maximum camber at various spanwise stations throughout one wingstroke for the four wings used in the deforming wing simulations: (a) upright forewing; (b) inverted forewing; (c) upright hindwing; and (d) inverted hindwing. Each line color corresponds to a particular normalized spanwise location ($\overline{x} = \frac{x}{b}$) and the stroke reversal point is indicated by the dashed line.

3.6 Highlights of Experimental Results

- When encountering a lateral gust while flying a similar flight path to undisturbed flights dragonflies employ asymmetric wing pitch, with the windward wings having a higher pitch amplitude and mean pitch angle than the leeward wings.

- Wing pitch is the kinematic parameter with the most variation between flights and between flight types.

- Dragonflies use different upstroke-to-downstroke ratios to ensure that their wings are always moving down in the global reference frame for longer than they move up in the global reference frame.

- Dragonflies reorient their wings and body so that their wings have a similar orientation relative to the flight velocity regardless of whether the dragonfly is inverted or upright.

- The general pattern of dragonfly wing deformation (low twist with positive camber during the downstroke and high twist with negative camber during the upstroke) is consistent in the body-relative frame regardless of the dragonfly orientation.

Chapter 4: Simulation Results

This chapter focuses on the results from the OVERTURNS simulations. For all simulations, force coefficients for the lift C_L, thrust C_T, and magnitude of the total force $|C_F|$ for the full wingstroke are the primary data for comparison between different simulations. The forcing in steady flight is periodic, so the simulations have been run until the cycle to cycle variation in forces is $< 1\%$. Average values for these coefficients, along with the average efficiency $\eta = \frac{M(\overline{C_L}+\overline{C_T})}{\overline{C_P}}$ (where M is the average tip Mach number) over a wingstroke, are tabulated throughout this section. The force coefficients for rigid and deforming wings are presented together to facilitate the comparison for all of the simulations. Flowfield visualizations are also shown to highlight important flow features and how they vary between different simulations. The wing kinematics used for these simulations are shown in table 4.1, with the isolated wing simulations using the same kinematics as the upright tandem simulation.

The wing motion for these simulations is prescribed using the models for flap and pitch angle and the stroke plane orientation defined by θ' and ρ' with the addition of prescribed wing deformation when needed (for more detail on the models and method of deformation see chapter 2). For tandem wing simulations the spacing

Table 4.1: Wing kinematics used for OVERTURNS simulations

		Φ (°)	Phase (°)	Ψ (°)	Ψ_M (°)	UDR	θ' (°)	ρ' (°)	V_∞ (m/s)
Upright	Forewing	87	0	78	92	0.8962	26	23	1.19
	Hindwing	91	68	72	90	0.8962	0	20	1.19
Inverted	Forewing	101	0	102	82	1.228	19	14	1.8
	Hindwing	104	94	68	75	1.228	0	18	1.8

between the attachment point between the two wings was calculated based on the mean size of the dragonfly bodies, quantified through the scale parameter in figure 2.3, and the observation that the distance between the wing bases was approximately half the length of the top of the thorax, again the scale parameter in figure 2.3.

4.1 Isolated Wing Simulations

Four simulations of isolated wings — a rigid forewing, a deforming forewing, a rigid hindwing, and a deforming hindwing — are first highlighted to analyze the impact of wing deformations on the aerodynamics in a less complex environment than tandem wings, and for comparison with tandem-wing simulations to identify the role/influence of wing-wing interactions.

4.1.1 Isolated Forewing

The force coefficients for the isolated forewing simulations are shown in figure 4.1. There are a few general features seen here that will apply to all of the results. First, figure 4.1a shows a large lift peak during the downstroke and a small negative lift peak during the upstroke. Second, there is positive thrust produced during both the upstroke and the downstroke (figure 4.1b). Lastly, from figure 4.1c we see that the total force produced during the downstroke is much larger than that produced during the upstroke. The combination of positive thrust and negative lift during the upstroke points to an important relationship between the wing orientation and the direction of the aerodynamic force. Since the majority of the force on these wings is due to pressure differences between the top and bottom surfaces, the direction of the total force is very closely aligned with the wing surface normal vector. Throughout the downstroke the wing surface is close to horizontal, so the force is primarily vertical. The pitch angle of the wing is much higher during the upstroke, so the wing surface is closer to vertical and the majority of the force is directed horizontally.

Figure 4.1 also shows the difference between the rigid and deforming forewings. During the downstroke, the deforming forewing produces more force, which translates to significantly more lift and slightly more thrust. During the upstroke, the deforming wing produces less force, so there is less thrust but also less negative lift. Figures 4.2a and 4.2b show part of the rigid and deforming wing flowfields at $\tau = 0.21$, when the deforming wing is producing more lift than the rigid wing. On the top side of both wings (figure 4.2a) the leading edge vortex (LEV) is a key flow

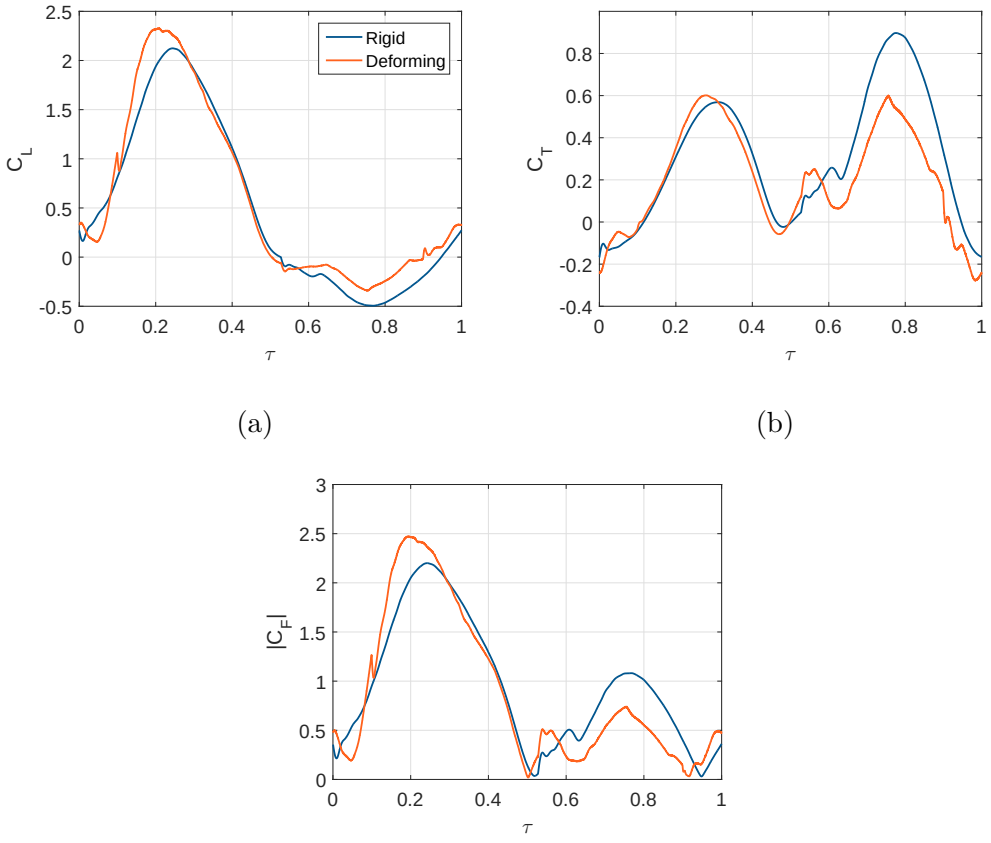

Figure 4.1: Force coefficients for the rigid and deforming isolated forewing simulations over one wingstroke.

feature that significantly enhances the force produced by the wing. The LEV, which is visualized by isosurfaces of Q criterion [73], is larger at the wing tip than over the inboard section of the wing for these two wings. Comparing the LEVs in the two different cases, the deforming wing LEV covers a larger portion of the wing surface than that on the rigid wing. Under this vortex are regions of low pressure on the top wing surface, meaning that the low pressure region on the deforming wing is larger than that on the rigid wing. On the underside of the wings (figure 4.2b) there is a high pressure region concentrated near the wing tip. This region is larger on the deforming wing than on the rigid wing which, when combined with the larger extent of the low pressure region on the top surface, shows how the deforming wing is producing more force than the rigid wing.

During the upstroke, shown in figures 4.2c and 4.2d, the flow features are reversed, with the high pressure region on the top surface of the wing and the flow separation and LEV on the bottom of the wing. The twist of the deforming wing during the upstroke creates a variation in the effective angle of attack, i.e. the local angle between the wing and the incoming flow in the wing-fixed frame, along the span. The twist reduces the effective angle of attack of the outboard section of the wing and increases it on the inboard section. This leads to reduced flow separation on the outboard portion of the wing, and no LEV is formed on the underside of the wing until the end of the upstroke. The lack of a LEV during the upstroke for the deforming wing results in higher pressure on the underside of the wing, which produces a lower pressure difference between the top and bottom, and therefore a lower force on the wing. Because the deforming forewing produces less force during

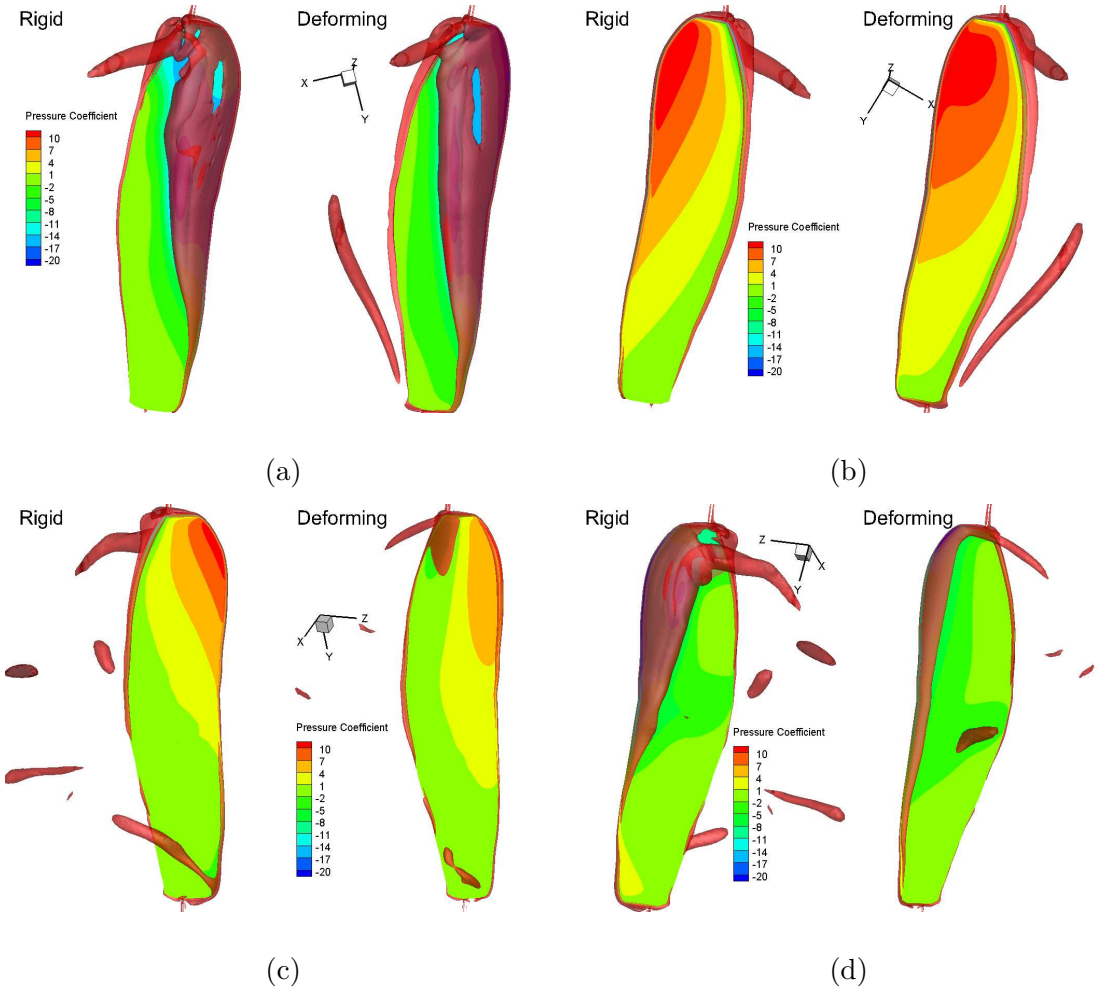

Figure 4.2: Comparison between the flowfield around a rigid and deforming forewing at (a & b) $\tau = 0.21$, and (c & d) $\tau = 0.75$, with the top surface shown in (a) and (c) and the bottom surface in (b) and (d). Isosurfaces of Q criterion are displayed in red and pressure coefficient contours are shown on the wing surface.

Table 4.2: Average forces and efficiencies for the isolated wings.

	Rigid Forewing	Deforming Forewing	Rigid Hindwing	Deforming Hindwing
$\overline{C_L}$	0.49	0.59	0.54	0.59
$\overline{C_T}$	0.30	0.21	0.40	0.40
$\overline{\lvert C_F \rvert}$	0.94	0.88	1.27	1.14
η	1.24	1.57	1.10	1.60

the upstroke, the average lift is increased and the average thrust decreases. Table 4.2 shows that the gain in average lift over the entire wingstroke is slightly larger than the loss in average thrust and that the efficiency of the deforming wing is 26% higher than that for the rigid wing.

4.1.2 Isolated Hindwing

The hindwing forces, shown in figure 4.3, follow the same general pattern as those of the forewings. During the downstroke, starting at $\tau = 0.81$ and ending at $\tau = 0.34$, there is a large positive lift peak with some thrust produced; whereas during the upstroke, there is a negative lift peak with more thrust than during the downstroke. The average force produced by the hindwing is larger than that produced by the forewing, as the hindwing maintains large forces for a longer duration than the forewing.

From figure 4.3 it appears that the only significant differences that the hindwing deformation makes is the reorientation of a slightly lower force during the

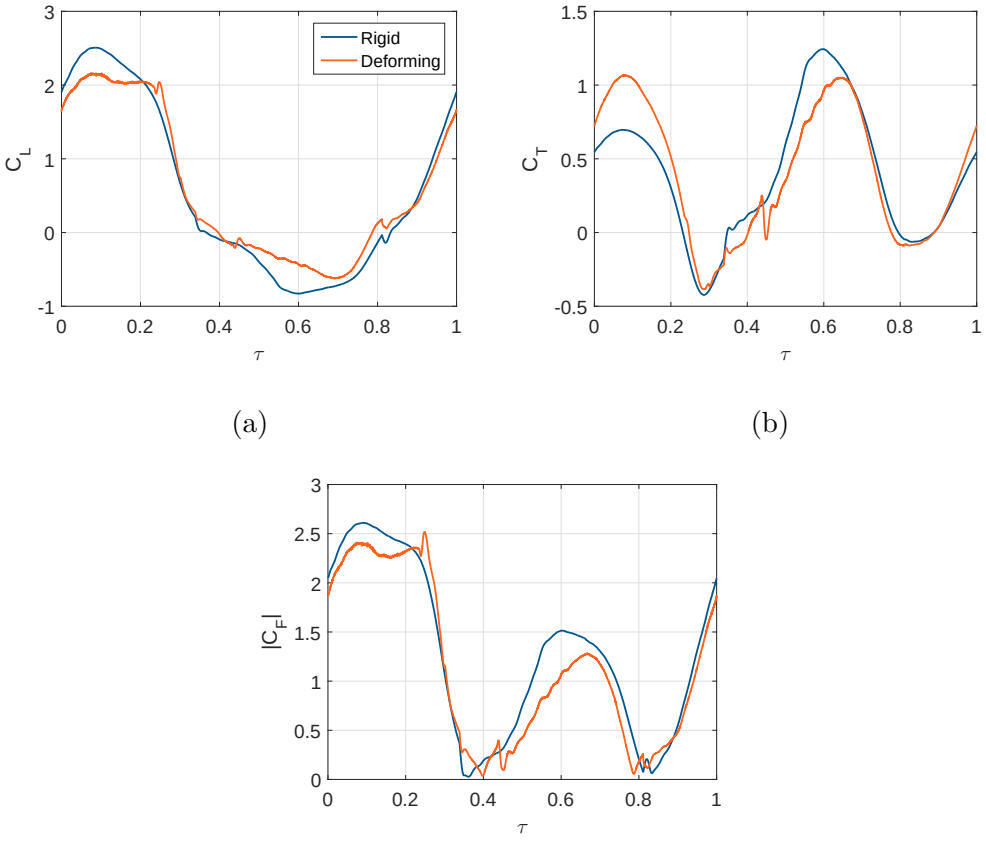

Figure 4.3: Force coefficients for the rigid and deforming isolated hindwing simulations over one wingstroke.

downstroke and a slight decrease in force during the upstroke. The difference during the downstroke is somewhat unexpected, as the deformation pattern for both fore- and hindwings is similar, but the effect is not similar. Looking at the flowfield around the wing at mid-downstroke and mid-upstroke in figure 4.4 helps clarify this result. During the downstroke, in figures 4.4a and 4.4c, the deforming wing has a smaller LEV covering less of the top surface of the wing, but the high-pressure region on the underside of the wing is larger than on the rigid wing. The smaller area covered by the LEV on the deforming hindwing contrasts with what was observed for the deforming forewing, but the larger high pressure region is consistent with the results seen in figure 4.2b. During the upstroke, in figures 4.4b and 4.4d, we observe similar phenomena to those of the deforming forewing. The deforming hindwing has less separation on the outboard section of the wing, meaning that the LEV forms on the underside of the wing much later and the pressure on the underside of the wing is higher.

The changes in average forces produced by deformation of the hindwings are different from those seen for the forewings. The deforming hindwing produces both more lift and more thrust on average, though both these changes are small, with an increase in efficiency of 45%. The contrast between the small increase in average forcing, a 5% increase for $\overline{C_L}+\overline{C_T}$, and the significant increase in efficiency indicates that the power required for the motion of the deforming hindwing is significantly lower than that for the rigid hindwing.

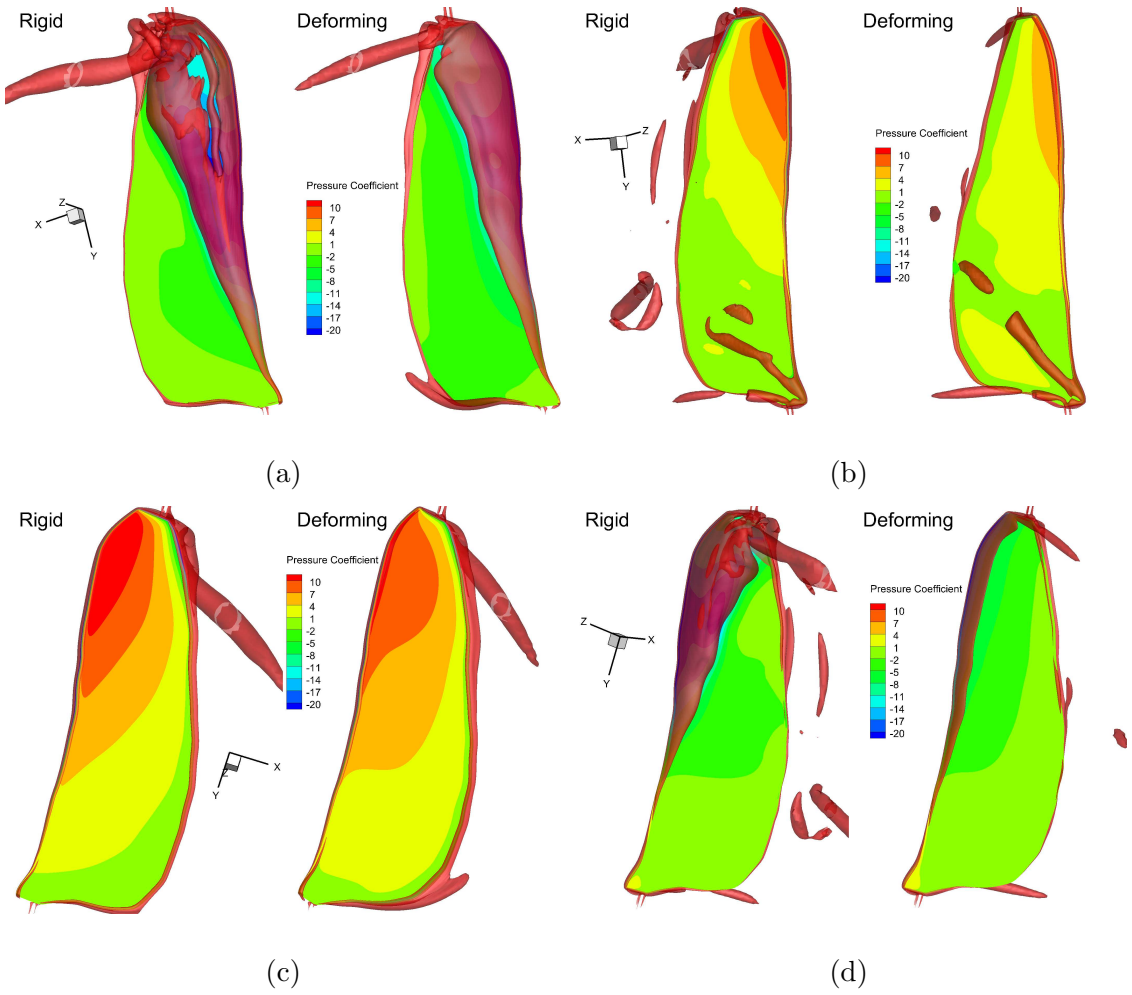

Figure 4.4: Comparisons between the flowfields around rigid and deforming hindwings at $\tau = 0.08$, (a) top and (c) bottom, and $\tau = 0.58$, (b) top and (d) bottom. Isosurfaces of Q criterion are displayed in red and pressure coefficient contours are shown on the wing surface.

4.1.3 Discussion of Isolated Wing Results

The four simulations of isolated dragonfly wings provide a simplified scenario for determining the impact of deformation on the aerodynamics of flapping dragonfly wings. Both fore- and hindwings had a LEV formed during the downstroke, which increases the force produced during the downstroke. Several studies that analyzed the airflow around free flying dragonflies, both in experiments and simulations, have observed a LEV on the forewing [34, 35, 36, 39, 38]. In contrast, for the hindwing, the two experiments with free flying dragonflies in a wind tunnel, and simulations of dragonfly wings at a variety of advance ratios, show attached flow over the hindwing rather than separated flow [35, 36, 39]. Since the deforming hindwing had a much smaller LEV, it is reasonable to say there was very little flow separation in the deforming case which matches the observations from the experiments. The likely reason for the difference between the previously reported CFD results [39] and the current study is the pitch angle of the hindwing, where the pitch angle in their simulations is much lower than that the present study, since LEV formation is known to depend on the angle of attack of the wing [23, 74] (the impact of wing-wing interactions, which were also present in the simulations of Wang and Sun's work [39] will be discussed in the next section). Simulations of a turn and backwards flight have shown that there is flow separation over the hindwing in those cases [34, 38]; this is similar to the observations of the present study.

In addition to significantly impacting the flow features, the wing orientation also determines the direction of the total force. Though this is not a surprising state-

ment, it is important to remember when analyzing the details of force production by flapping wings. The difference in wing orientation between up- and downstroke not only changes the flow features on the wings, as the rigid wings have a much smaller LEV during the upstroke due to the reduced effective angle of attack, but also orients the force more horizontally than vertically. This means that the force produced during the upstroke is primarily thrust with some negative lift.

The comparison between the rigid and deforming wing simulations provides an opportunity to better understand how dragonfly wing deformations affect the forces and flow features produced during flight. During the forewing downstroke, the deformation increases the total force production making it tempting to say that the increase in wing camber is the cause, as increased camber increases the lift for a thin airfoil [75] and prior work on a rotating rigid fruit-fly-like wing with fixed camber demonstrated that positive camber increases lift production and lift to drag ratio while changing the LEV shape [56]. Unfortunately, the hindwing downstroke shows that, for flapping wings, the situation is not so simple. Both wings follow a similar, though not identical, pattern of camber during the downstroke, but the hindwing does not experience the same increase in total force production; this makes it difficult to determine exactly how the addition of camber affects the aerodynamics. Figure 4.5 shows side views of the LEV on the rigid and deforming isolated wings. In both figures 4.5a (forewing) and 4.5b (hindwing) the deforming wing LEV doesn't extend as far away from the wing surface as the LEV on the rigid wing. Though the LEV on the deforming forewing covers a larger area of the wing surface, it does not extend as far away from the wing. This complicates the determination of how

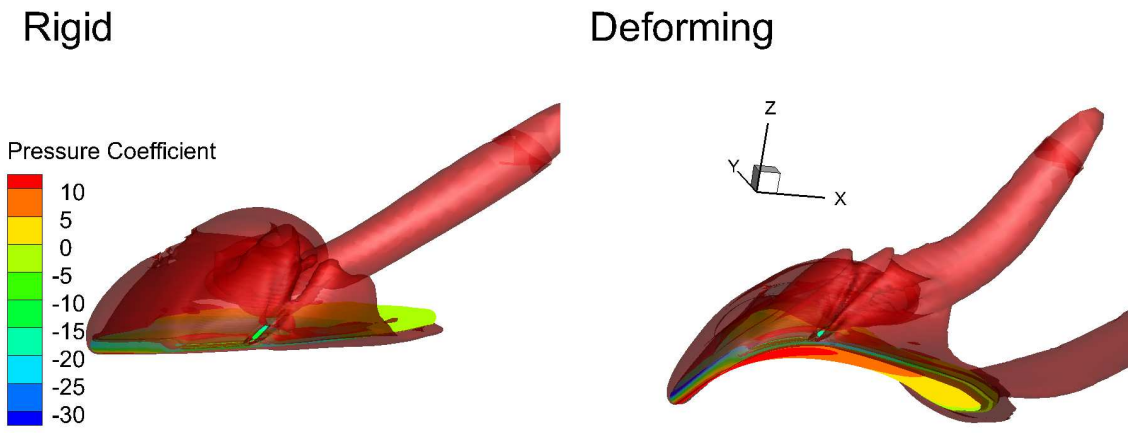

(a)

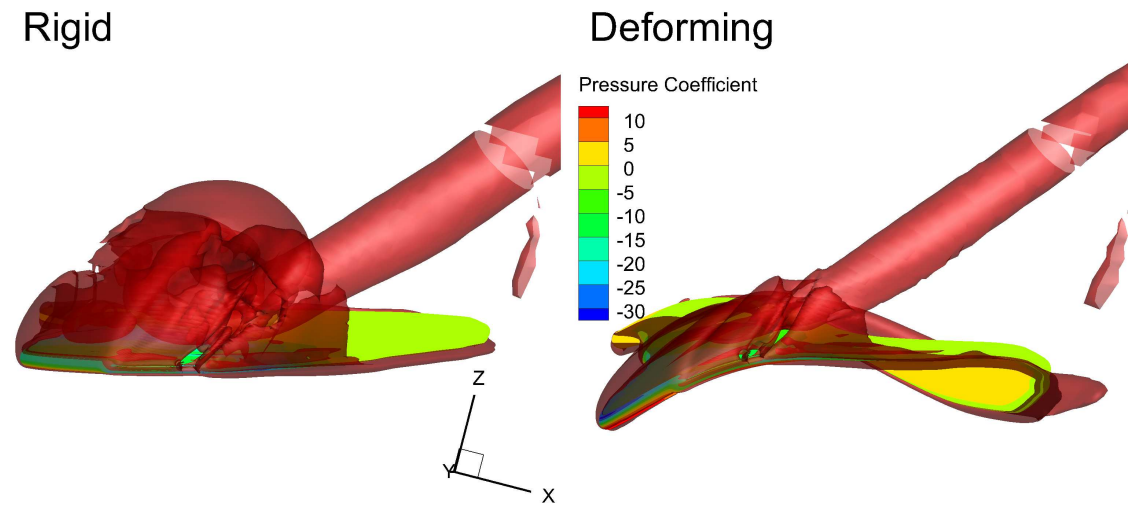

(b)

Figure 4.5: Side views of the LEV, shown with isosurfaces of Q criterion, on both rigid and deforming (a) forewings at $\tau = 0.21$ and (b) hindwings at $\tau = 0.08$ during mid downstroke.

wing deformations impact the forces and flow features in dragonfly flight. For both the forewing and the hindwing, deformations modify the shape of the LEV which reduces its volume; the later of which in low speed unsteady flight with an attached LEV is usually associated with less force production [15]. The impact on force production, however, is mixed and the loss of force production for the hindwing is smaller than would be expected based on the difference in the LEV shown in figure 4.5b. This hints that the increase in camber increases the bound circulation of the wing, as the flow at the trailing edge appears to be attached in both the rigid and deforming cases, which is similar to predictions of thin airfoil theory and the results of prior experiments [57]. The net result on the force produced by the wing is then a balance between the increase in the bound circulation of the wing and the loss of circulation in the LEV. This balance is affected by specific wing kinematics and may also be affected by wing shape as the net effect is different on the two wings.

To determine if changing the bulk wing kinematics changes the impact of camber deformations, three simulations were run with a forewing following upright-hindwing bulk kinematics: one rigid, one using forewing deformation coefficients, and one using hindwing deformation coefficients. The total force coefficient data from these three simulations are shown in figure 4.6. The difference between the rigid forewing and the one using forewing deformation coefficients is similar to that seen between the rigid and deforming hindwing. In both cases the maximum force produced by the rigid wing is larger, though the wing following forewing deformations reaches its maximum lift coefficient sooner and remains at a higher level longer. As this result is significantly different than that observed for the same wings follow-

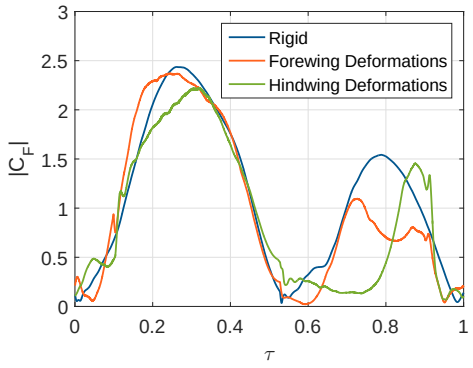

Figure 4.6: Total force coefficients for simulations of a forewing using hindwing bulk kinematics.

ing the forewing bulk kinematics, we can conclude that the specific wing kinematics do change the impact of the camber deformation. The results from the forewing following both hindwing kinematics and deformations demonstrate that there is also a dependence on wing shape, as the decrease in force from the rigid wing is much larger than that seen by the hindwing in figure 4.3c.

The impact of deformation during the upstroke is much more consistent between the fore- and hindwings than that during the downstroke. In both cases the wing twist results in a reduction in flow separation on the underside of the wing. This reduced separation means that a smaller LEV is formed much later in the upstroke, and thus the pressure difference between the two sides of the wing is smaller than that on the rigid wing. This reduces the total force produced, with the result of less thrust and less negative lift, which is consistent with prior studies of twist for flapping wings [53, 54]. Though the loss of thrust is significant, particularly for the forewing, the benefit of less downward force on the wing during the upstroke is substantial.

The averaged effect of the deformations is seen when comparing average force coefficients and efficiencies (table 4.2). Both wings experience an increase in average lift, due to less negative lift during the upstroke and more lift during the downstroke for the forewing. The thrust trend is less consistent: the thrust for the forewing decreases whereas that for the hindwing increases. The magnitude of these differences is not the same between the two wings, with the forewing experiencing significantly larger changes in average forces. For both wings, the efficiency increases significantly when the deformations are added. This means that, while the deformations in some cases increase the average force production, the one consistent benefit of wing deformations for dragonflies is an increase in aerodynamic efficiency.

4.2 Tandem Wing Simulations

Four simulations of tandem wings are presented here: rigid and deforming upright wings, and rigid and deforming inverted wings. The upright tandem simulation results are compared with the isolated wing simulations to determine how the interaction between wings changes the aerodynamic loads and flow features. The inverted tandem simulation results are examined to determine if there is any difference in the aerodynamic mechanisms used by dragonflies when flying upside-down.

4.2.1 Upright

To better understand how the interactions between fore- and hindwings alter the aerodynamic forces and flow features without the added complication of deforma-

tions, results from simulations of rigid isolated and tandem wings are compared in figures 4.7 and 4.8. The total force coefficient data in figure 4.7c show a significant increase in force production for the hindwing during both the downstroke and the upstroke, which is mirrored in the lift and thrust coefficients (figures 4.7a and 4.7b), whereas the forewing sees only minor changes in forcing during the downstroke. The increase in force production during the forewing downstroke is due to the upwash created by the LEV and bound circulation of the hindwing. The small impact on the forewing and large impact on the hindwing is expected as the hindwing is operating directly in the wake of the forewing, and thus sees a significantly different incoming flow than the isolated hindwing.

In order to gain further understanding of the mechanisms that increase the force produced by the hindwing in tandem flight, flow fields from mid-downstroke ($\tau = 0.08$) and mid-upstroke ($\tau = 0.54$) are shown in figure 4.8. During the downstroke (figures 4.8a and 4.8b) the LEV on the top of the tandem hindwing is larger, with a corresponding larger region of low pressure on the top surface of the wing, and the high pressure region on the bottom surface of the wing is larger. This wake in which the tandem hindwing is operating has positive vertical velocity that increases the effective angle of attack for the hindwing, leading to higher pressure on the underside of the wing and a larger LEV. During the hindwing upstroke, a similar phenomenon occurs. The tandem hindwing has a larger high-pressure region on the top surface of the wing and a larger LEV on the bottom surface of the wing. In addition to the larger extent of these features, the outboard section of the hindwing crosses through the tip vortex produced by the forewing. This interaction

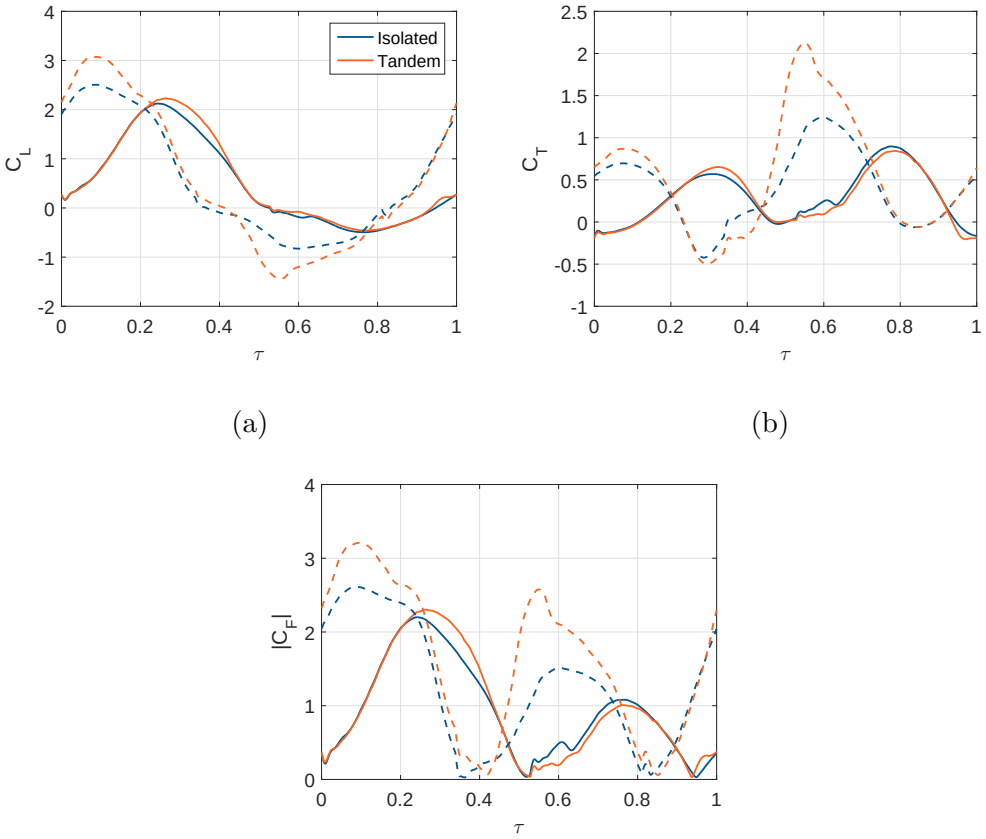

Figure 4.7: Force coefficients for rigid isolated and tandem wings; coefficients for the forewings are shown in solid lines and the hindwings in dashed lines.

further extends the high pressure region on the top and the low pressure region on the bottom of the hindwing.

Comparing rigid and deforming tandem wings demonstrates how deformations influence the wing-wing interaction. Figure 4.9 shows that the deforming forewing produces more force during the downstroke and less force during the upstroke than the rigid forewing. This is consistent with the results from the isolated wings in section 4.1. The influence of deformation for the tandem hindwing, however, is not the same as that seen for isolated wings, with the deforming tandem hindwing producing significantly less force than the rigid tandem hindwing. This hints at how the wing deformation has changed the wing-wing interaction. The hindwing is still passing through the wake of the forewing, but the wake produced by the deforming forewing upstroke is significantly weaker as the wing twist reduces the force produced by the wing. During the hindwing upstroke, the twist of the hindwing reduces the impact of crossing through the vortices shed by the forewing.

The differences in average forces for the tandem wings are similar to those of the isolated wings. The main difference from the isolated wings is that the deforming hindwing produces slightly less thrust than the rigid wing, since there is significantly less force produced during the upstroke. The deforming wings are both significantly more efficient than their rigid counterparts: taken together, the tandem deforming wings are 35% more efficient than the tandem rigid wings (Rigid $\eta = 1.08$, Deforming $\eta = 1.46$).

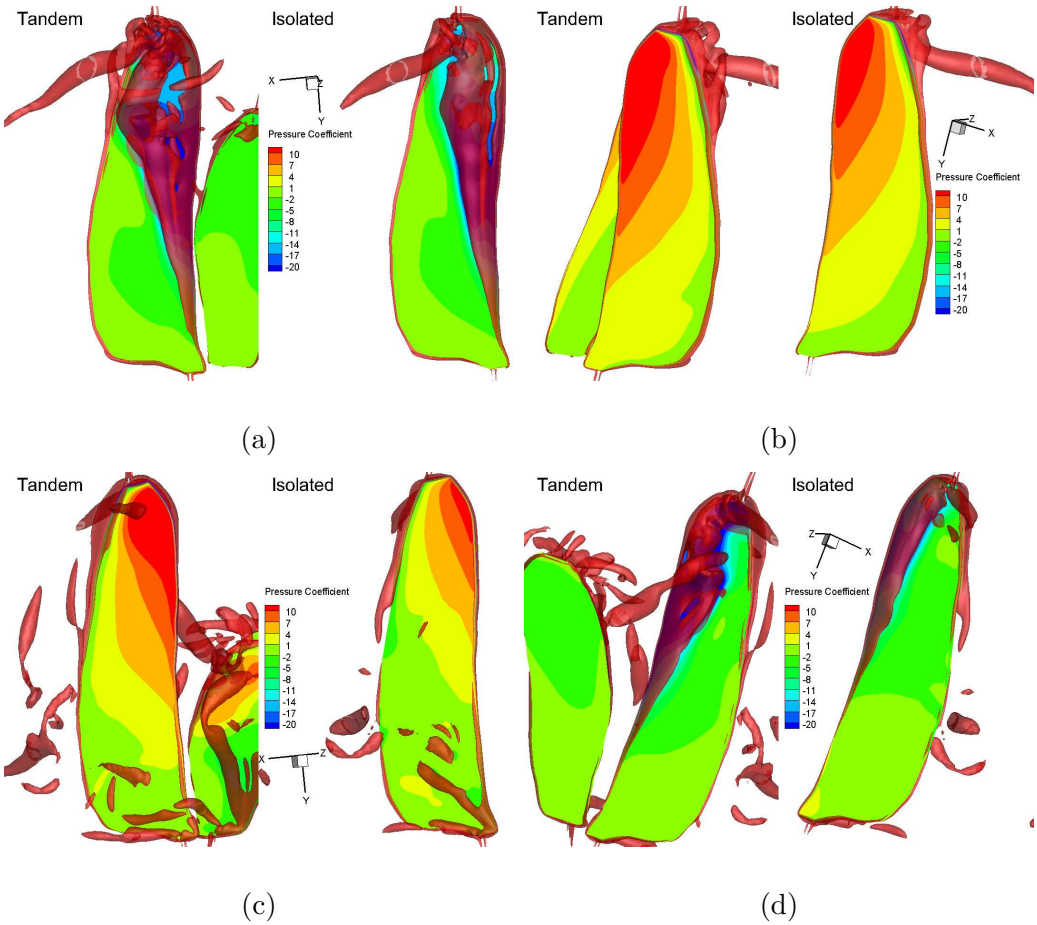

Figure 4.8: Rigid tandem and isolated hindwing simulation results with pressure coefficient contours on the wing surface and iso-surfaces of constant Q criterion: (a) and (b) are the top and bottom views at $\tau = 0.08$; (c) and (d) are the top and bottom views at $\tau = 0.54$.

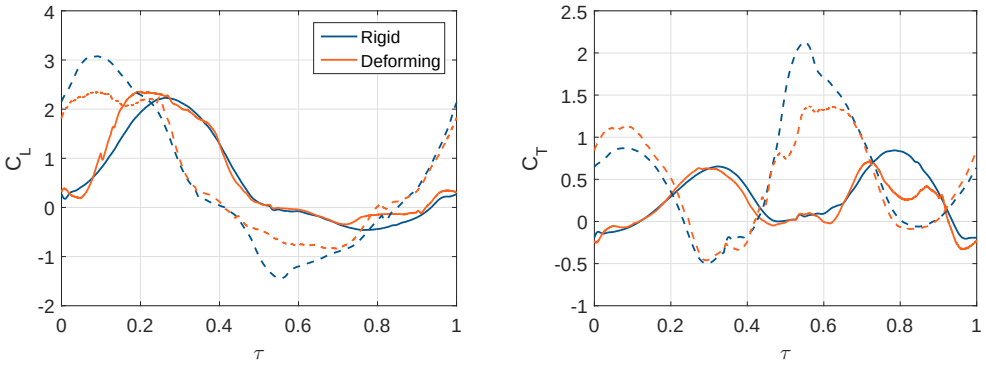

(a)

(b)

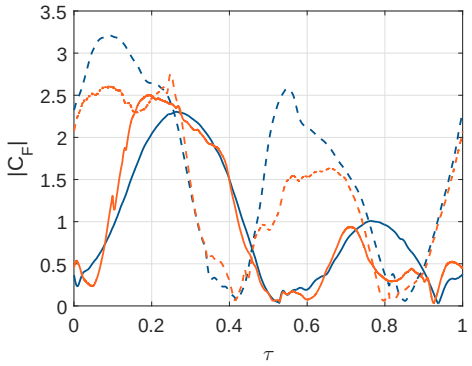

(c)

Figure 4.9: Force coefficients for the rigid and deforming tandem upright wings. Coefficients for the forewings are shown in solid lines and the hindwings in dashed lines.

Table 4.3: Average force coefficients and efficiency for upright tandem rigid and deforming wings.

	Rigid Forewing	Rigid Hindwing	Deforming Forewing	Deforming Hindwing
$\overline{C_L}$	0.55	0.54	0.65	0.57
$\overline{C_T}$	0.29	0.56	0.21	0.50
$\overline{\lvert C_F \rvert}$	0.95	1.62	0.94	1.36
η	1.31	0.99	1.60	1.46

4.2.2 Inverted

For the inverted dragonfly wings, the resultant forces follow a similar pattern as for the upright wings. To make comparisons simpler the results from the inverted wing simulations are shifted so that $\tau = 0$ is the beginning of the downstroke of the forewing in the global frame, the body-relative upstroke, and the use of down- and upstroke in this section refer to the global convention. The majority of the force is produced during the downstroke, when the wing is moving down in the global frame (forewing: $\tau = 0$ to $\tau = 0.56$, hindwing: $\tau = 0.74$ to $\tau = 0.29$). There is very little force produced during the upstroke, which differs from the upright wings. This is because of the larger pitching amplitude and lower mean pitch values, which result in wing planes that are closer to vertical during the global upstroke than those of the upright wings. This results in significantly lower thrust production, which is consistent with the difference in the acceleration observed between the upright and inverted flights.

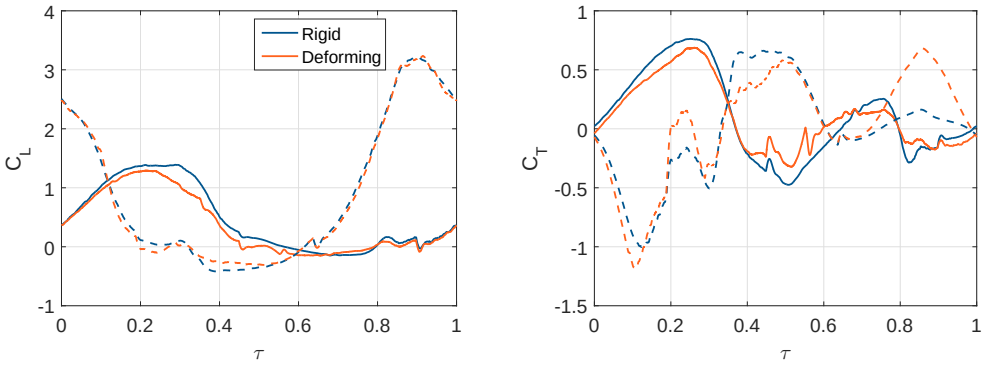

(a)

(b)

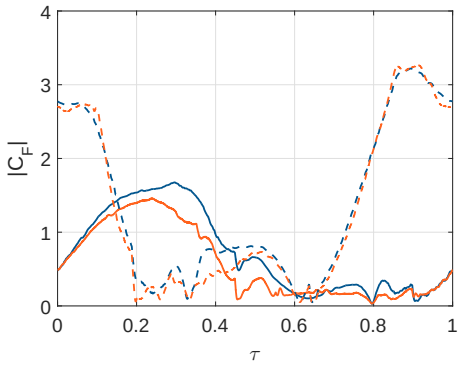

(c)

Figure 4.10: Force coefficients for the rigid and deforming tandem inverted wings. Coefficients for the forewings are shown in solid lines and the hindwings in dashed lines.

Since the wing deformations follow a consistent pattern with respect to the body relative down- and upstroke, the benefits seen for the deforming upright wings are not expected to apply in the inverted case. Indeed the force data indicate that there is little change between the rigid and deforming wings, with the only significant difference being the loss of lift and thrust during the downstroke of the forewing. The fact that the forces produced by the deforming wings during their respective downstrokes are so similar to those produced by the rigid wings is somewhat surprising, given that both deforming wings are twisted. As was seen for the upright wings, twist reduces the flow separation on the outboard section of the wing and leads to a smaller LEV. In the case of the inverted forewing, highlighted in figures 4.11a and 4.11b, very little flow separation occurs over the outboard portion of the wing, but there is notable flow separation over the inboard section of the wing, with a small vortex structure forming over that section. The flow features on the deforming hindwing differ slightly from those around the rigid hindwing, as the deformations appear to reduce flow separation at the leading edge, but these differences do not result in a significant variation in force production.

The most significant differences between the rigid and deforming inverted wings are seen in table 4.4. There is a notable decrease in average lift, and a slight increase in average thrust, but the most significant difference is in the increased efficiency. This demonstrates that even though the wing deformations for the inverted wings result in a net loss of lift and thrust, the decrease in power required to produce these forces is larger than the decrease in force itself.

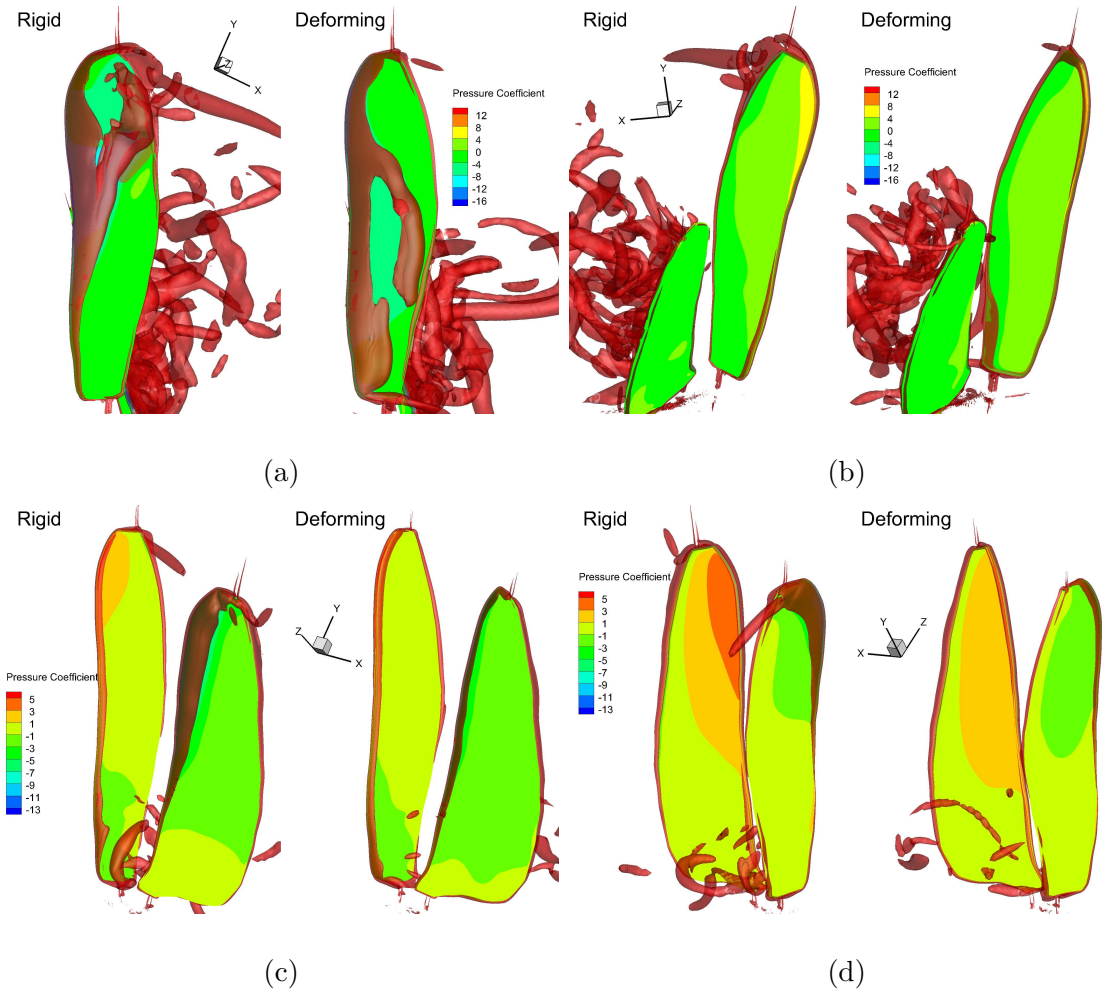

Figure 4.11: Inverted wings at $\tau = 0.20$ during the global downstroke, when the wing is twisted (a, top surface, and b, bottom surface); and at $\tau = 0.74$ during the global upstroke, when the wing is cambered (c, top surface, and d, bottom surface). Both rigid and deforming simulations results are shown with red isosurfaces of Q criterion and pressure coefficient contours on the wing surface.

Table 4.4: Average force coefficients and efficiency for tandem rigid and deforming inverted wings.

	Rigid Forewing	Rigid Hindwing	Deforming Forewing	Deforming Hindwing
$\overline{C_L}$	0.47	0.88	0.38	0.87
$\overline{C_T}$	0.10	-0.02	0.11	0.04
$\overline{\lvert C_F \rvert}$	0.72	1.37	0.58	1.30
η	1.46	1.01	1.68	1.22

4.3 Discussion of Tandem Wing Results

There are two new comparisons that depend on the tandem wing results and will be the focus of this section: that between isolated wings and tandem wings, and that between inverted and upright wings. The comparison between rigid and deforming tandem wings also allows us to investigate how wing deformations change the wing-wing interaction. In the following subsections, the discussion of upright wings highlights the impact of the wing-wing interactions as well as how deformations change those interactions; and the discussion of the inverted wings focuses on the differences between the aerodynamics of the upright and inverted wings and how the wing deformations impact the operation of inverted wings.

4.3.1 Upright

When comparing the isolated and tandem upright wings, the difference experienced by the hindwings are much more significant than that seen by the forewings. The forewings produce slightly more force during the downstroke and slightly less force during the upstroke. The increase in force during the downstroke is due to upwash generated by the LEV on the hindwing during its downstroke, which increases the effective angle of attack of the forewing. The decrease during the upstroke is not directly relatable to any particular flow feature, but it is likely due to differences in how the vortex on the forewing bursts and sheds, since it is larger on the tandem than the isolated forewing. Though these differences are notable, they are much smaller than those experienced by the hindwing as it operates in the wake of the forewing.

In the present simulations the tandem wings produce more lift and thrust (combined) than their isolated counterparts. There have been several prior studies of tandem wings, with a variety of results [76], so the focus here will be comparing with other 3D simulations of dragonfly wings. An earlier study, looking at a variety of phase angles and advance ratios, indicated that wing-wing interactions are detrimental to the force production of dragonfly wings [39], but more recent work has indicated that there is an increase in force production caused by the interaction [34, 38, 77]. Based on the findings about how the wing-wing interaction works, we believe that all of these results are correct in their determination of the impact of wing-wing interactions, but that the impact of the wing-wing interaction is highly

dependent on the wing kinematics, particularly the phase difference and advance ratio. Though Wang and Sun [39] studied a variety of phase angles and advance ratios, they were using kinematics derived from hovering flight when they concluded that wing-wing interactions are detremental to force production, and these kinematics are unlikely to be representative of forward flight wing kinematics. Thus, we conclude that the interaction between the fore- and hindwing of the dragonfly is beneficial to the force production when using the proper wing kinematics.

The addition of wing deformation to the tandem wings changes the force production and therefore wing-wing interaction. The forewing changes are the same as they were for isolated wings, with more force produced during the downstroke and less force produced during the upstroke. The change in forces between the rigid and deforming tandem hindwing is significantly different from that seen by the isolated hindwings, where the total force produced was comparable during the downstroke. The deforming tandem hindwing decrease in force production during both the downstroke and the upstroke is more significant than that for the isolated hindwing, indicating that the wing-wing interaction is not increasing the force on the tandem deforming hindwing as significantly as on its rigid counterpart. The general trend in aerodynamic forces between isolated and tandem deforming wings is nevertheless the same as that for the rigid wings, so the general pattern of the interaction, in which the hindwing produces more force during both upstroke and downstroke and the forewing produces more force during the downstroke, remains unchanged. This means that the hindwing is receiving the same benefit from passing through the forewing wake, but the magnitude of that benefit is lessened.

This reduced benefit experienced by the deforming tandem hindwing is related to the forces and flow structures produced by the deforming forewing. The deforming forewing produces less force during the upstroke than the rigid forewing, meaning that the upwash in the region of the wake generated during the upstroke is less than that produced by a rigid wing. Since the benefit the hindwing receives during its downstroke is due to the upwash generated by the forewing, this is reduced and the additional force produced by the hindwing during the downstroke is lessened. During the hindwing upstroke, there are two factors that change the results of the wing-wing interaction. First, the hindwing does not have a LEV on the underside of the wing with which vortical structures shed by the forewing can interact. Second, the forewing sheds multiple streamwise vortices during the downstroke, rather than a single coherent tip vortex. Both of these factors reduce the increase in force on the tandem deforming hindwing.

Even though there are significant differences in how the wings interact when they are deforming, the changes in average force produced are relatively small. The deforming wings produce less thrust than the rigid wings, which is primarily a result of the effects of twist discussed above and the lessening of the wing-wing interaction. The average lift for the deforming wings is higher than that for the rigid wings because less negative lift is produced during the upstrokes. This results in a very similar average combined lift and thrust ($\overline{C_L} + \overline{C_T}$) for both wings. The significant increase in efficiency then results from reduction in the aerodynamic power required for the deforming wings.

4.3.2 Inverted

The simulations of inverted wings in straight flight provide insight into how dragonflies are able to fly upside-down and how the wing deformations impact the aerodynamics in off-design flight conditions. When comparing the force coefficients of inverted and upright flight it is important to remember that the average tip speed, which is used to calculate force coefficients, is higher for the inverted wings, meaning that an equal force will have a lower corresponding force coefficient. That being said, the inverted forewing produces roughly the same amount of lift and less thrust than the upright forewing. The inverted hindwing produces significantly more lift than the upright hindwing, but generates almost no thrust. The ability of the wings to produce comparable forces to the upright flights is related to the similarity of the wing orientation in the global frame. This results in a similar LEV during the downstroke, which produces the large force coefficients. During the upstroke, the inverted wings are oriented closer to vertical and have a lower effective angle of attack than the upright wings, meaning that there is less flow separation and therefore no LEV on the underside of the wing. This lack of an LEV results in very low forces during the upstroke; as a result, the average thrust for the both wings combined is nearly zero, whereas the upright wings had significant positive thrust. This difference is consistent with the variation in acceleration between the upright and inverted flights, in particular that the upright flights exhibited much higher accelerations than the inverted flights.

For the inverted flights, the body-relative wing deformations were found to be

qualitatively the same as in upright flight, whereas the body-relative directions do not correspond to the global directions (up and down); because of this, the wings are twisted during the downstroke and cambered during the upstroke (in the global frame). Given what has already been learned about the impacts of deformation on dragonfly flight, one might expect this to be significantly detrimental to the force production. However, the simulation results indicate that there is much less difference between rigid and deforming inverted wings than there is between rigid and deforming upright wings. Since the wings are cambered during the global upstroke, when the rigid wings produce little force, it is not surprising that there is minimal change during this period of the stroke. What is surprising is that the wing twist during the global downstroke does not significantly impact the aerodynamic forces produced, as it did during the upstroke for the upright wings. For the hindwing this is because the wing is very close to horizontal so, though the twist does reduce the angle of attack for the outboard sections of the wing, the angle of attack is still high enough that the flow separates and there is a shear layer to feed the LEV. For the forewing, the twist inhibits flow separation at the wing tip, but separation persists near the wing root. This results in a vortex forming over the inboard section of the wing, with the associated low pressure region. Though this is not as effective at increasing the force produced by the wing as the LEV on the rigid wing, it does provide a similar effect. In summary, these results demonstrate that wing deformations, though they may not always lead to increased force production, consistently reduce the power required to produce similar aerodynamic forces even in off-design conditions.

4.4 Highlights of Simulation Results

- The impact of the camber deformation during the downstroke is dependent on the wing kinematics and the specific wing planform.

- The wing twist reduces the flow separation on the outboard sections of the wing, but can also increase flow separation on the inboard section of the wing, resulting in significantly different LEV structures (inverted wings) or a much slower development of a LEV (upright wings).

- The interaction between fore- and hindwings increases the force produced by both wings, with more significant differences for the hindwing as it passes through the wake of the forewing. The details of the interaction are different for rigid vs. deforming wings, but the general impact remains the same.

Chapter 5: Conclusions

The primary objectives of this research were: (1) to identify the aerodynamic impact of the deformation of dragonfly wings; and (2) to determine how dragonflies mitigate the effects of a lateral gust. Experiments with free flying dragonflies provided kinematic data for specimens both in an undisturbed environment and when encountering a lateral wind gust. Because of how the dragonflies were originally placed in the testing environment, the dragonfly was inverted during the majority of the straight flights and therefore comparing upright and inverted wing kinematics and deformations became part of this research. Because of the time required to extract wing motions and deformations, the kinematic and deformation data are extracted from a relatively small number of wingstrokes (a total of 14 wingstrokes are used to generate the kinematic data presented here). Thus the differences between different flight conditions highlighted herein suggests ways which dragonflies alter there kinematics in response to their condition, but there is no guarantee that these responses are typical in nature.

In order to understand how wing deformations affect the aerodynamics of dragonflies in free flight, computational fluid dynamic simulations of both rigid and deforming wings were run. A total of eight simulations provided the bulk of the

data for this study. Four of those simulations were of rigid wings following the bulk kinematics derived from the experiments and the other four included the deformations while following the same bulk kinematics. Within each set there were two simulations of isolated wings (one fore- and one hindwing), one simulation of tandem wings following upright flight kinematics, and one simulation of tandem wings following inverted flight kinematics. This provided data to determine how the wing deformations impact the aerodynamic performance, whether the interactions between fore- and hindwing are beneficial for straight flight, and how the aerodynamics differ between upright and inverted flight. The primary data used for these comparisons were the instantaneous force coefficients and visualizations of vortex structures within the flow.

In this chapter we detail the main conclusions from these experiments and simulations. The first section highlights the findings from the free-flight experiments, addressing both bulk kinematics and wing deformations. The second section details the important conclusions drawn from the CFD simulations of dragonfly wings. Lastly, several future directions for research are recommended for further understanding both dragonfly flight as well as the general aerodynamic phenomena involved in flapping-wing flight.

5.1 Dragonfly Kinematics and Deformations

In the analysis of the three different flight types there were several notable differences in wing kinematics, and these differences highlight particular kinematic parameters

that dragonflies vary to achieve similar flight paths under a variety of conditions. There were two kinematic parameters that varied significantly between flight types: the upstroke-to-downstroke ratio (UDR) and the wing pitch angle. The UDR describes the relative length of the upstroke and downstroke (in the body reference frame), so significant variation of the UDR indicates that dragonflies are able to control the amount of time that the wing spends moving in a particular direction. The UDR for the upright flights was consistently less than unity while the UDR for the inverted flights was consistently greater than unity. This means that the dragonflies in these flights were modifying their wingstrokes such that their wing spend more time moving in the global down direction than the global up direction.

The second kinematic parameter that varied significantly was the wing pitch angle. This parameter showed the highest left-right asymmetry in both disturbed and undisturbed flight. In undisturbed flight, the asymmetry was generally correlated with the initiation of a roll. For dragonflies encountering a lateral gust, there was a significant increase in the pitch angle of the windward wings during the global downstroke (body-relative upstroke) when compared to the undisturbed flights. Despite the presence of the disturbance, the dragonflies maintained the same flight path and orientation as undisturbed flights, indicating that this pitch asymmetry helped to counter the effects of the wind gust.

Though deformation coefficients from only four wings were presented and used in the CFD simulations, they are representative of the deformations observed in other flights. The deformation patterns measured confirmed earlier reports of the general shape of flapping dragonfly wings, with positive camber and small amounts

of twist during the downstroke, and negative camber and large twist during the upstroke. The new information found in the present study is that this pattern is consistent even when the dragonfly is inverted. The fact that this pattern holds even when the aerodynamic load is reversed indicates that the wing deformation is constrained by structures within the wing, which is a hypothesis that has been proposed by researchers studying the structure of dragonfly wings.

5.1.1 Summary List of Kinematics and Deformation Conclusions

- Dragonflies use asymmetric wing pitch when encountering a lateral wind gust to maintain a similar flight path to flights without the gust encounter.
- Wing pitch is the kinematic parameter with the most variation both between individual flights and different flight types.
- Dragonflies vary the upstroke-to-downstroke ratio based on their orientation (upright or inverted) so that the global downstroke is always longer than the global upstroke.
- The general deformation pattern was consistent (low twist with positive camber during the downstroke and high twist with negative camber during the upstroke) regardless of dragonfly orientation.

5.2 Dragonfly Wing Aerodynamics

The CFD simulations yielded data that provides a deeper understanding of on the impact of wing deformations and forewing-hindwing interactions. As was mentioned in chapter 1, the benefits and/or costs of the interaction between the fore- and hindwing of a dragonfly are not well understood; previous studies have produced a variety of results with no clear, general conclusion. Though the present work focuses on a specific flight condition, the results indicate how dragonflies can benefit from wing-wing interactions. Similarly, previous research on wing deformations has indicated that there can be benefits, though there are competing claims as to whether those benefits are an increase in force production or an increase in efficiency. To improve our understanding of these benefits, the present study provides insight into the benefits that dragonflies derive from their wing deformations.

Comparing the results from the isolated wings with the tandem-wing simulations shows that the wing-wing interaction increases the force production on both wings. The forewing experiences a more minor change, associated with the circulation produced by the hindwing. The hindwing, in contrast, operates directly in the wake of the forewing; the forces on the tandem hindwing are much greater than those on the isolated hindwing because the phase difference and flight speed combine to create a favorable environment for force production. In particular, each hindwing half-stroke passes through the wake generated by the opposite forewing half-stroke. Generally, the wake from the forewing adds some upwash (for the hindwing downstroke) or downwash (for the hindwing upstroke), but during the hindwing upstroke

there is the additional interaction with the tip vortex from the forewing, which creates a sharp spike in force. The same pattern is seen for the deforming wings, though with a smaller increase in force than the rigid wings experience. The increase in force production from wing-wing interactions comes with a small loss of efficiency, but these results nevertheless indicate that closely spaced tandem wings can produce more force than the same wings in isolation.

The comparisons between rigid and deforming wings demonstrate the benefits that specific wing deformations can provide. For all cases the wing deformations increased the aerodynamic efficiency of the wings, even for inverted dragonflies. This is particularly surprising; the deformations were not expected to benefit the inverted specimens since the pattern of deformation was consistent in the body-relative frame and not the global reference frame. The twist had a consistent impact on the aerodynamic forces and flow features during the body-relative upstroke (downstroke for inverted wings). The wing twist decreases the effective angle of attack of the outboard sections of the wing, resulting in less flow separation. On the inverted wings an increase in flow separation on the inboard section of the wings enabled them to produce similar forces to their rigid counterparts, whereas the upright wings produced significantly less force. The impact of wing camber on the forces and flow features produced by flapping dragonfly wings during the downstroke was difficult to determine; though the camber resulted in increased force production on the upright forewing, it decreased the force produced by the hindwing. Further study of this discrepancy indicated that the specific bulk wing kinematics and wing shape changed the impact of the wing camber.

5.2.1 Summary List of Aerodynamic Conclusions

- The deformations of dragonfly wings increase the aerodynamic efficiency regardless of the dragonfly orientation when compared to rigid wings undergoing the same bulk motion.

- The impact of camber on a flapping dragonfly wing is dependent on the specific bulk kinematics and can either increase or decrease the amount of force produced.

- The interaction between fore- and hindwings of a dragonfly in straight flight increases the forces produced when compared to wings operating in isolation, with a slight decrease in efficiency.

5.3 Future Work

Though this study provides insights into steady, straight dragonfly flight, more work is necessary to better understand why dragonflies manipulate particular kinematic parameters for maneuvering. In the flights examined here, the wing pitch angle was varied when dragonflies were inducing a roll maneuver or encountering a lateral gust. In order to better understand how and why dragonflies manipulate their wing pitch, additional data about wing pitch during flight is needed; acquiring detailed wing kinematics from additional straight flights, as well as various maneuvers, would enable researchers to determine the purpose of wing-pitch variations and how controlled those variations are. As the experiments described herein resulted in videos

of almost 300 undisturbed flights, there may already be enough experimental data available for this task.

These experiments showed that the dragonflies use asymmetric wing pitch angles to remain on the same flight path when encountering a lateral wind gust. To understand the aerodynamic mechanisms that this change in kinematics employs simulations with four wings and a full body of a dragonfly are necessary. This is because the symmetry assumption used in this research is no longer valid and the leeward wings will encounter the wake produced by the body. A better understanding of the aerodynamic mechanisms utilized during dragonfly gust response will facilitate the process of applying these techniques or similar techniques to micro aerial vehicles.

In addition to varying the wing pitch angle, dragonflies changed their upstroke-to-downstroke ratio depending on their orientation. We surmise that this is because the global downstroke (time when the wing is moving in the global down direction) is the only time when positive lift is produced, therefore dragonflies would benefit aerodynamically from the downstroke being longer than the upstroke. This leads to two questions: why do dragonflies, and most other insects, use a UDR close to unity, and what aerodynamic benefits come from a UDR different than unity? The answer to the first question lies in further study of dragonfly behavior and physiology focusing on the capabilities of dragonfly flight muscles and when they very UDR. The second question requires aerodynamic simulations with varying UDR for a flapping wing following consistent bulk wing kinematics to determine if there is some optimal UDR or what the costs and benefits are for increasing or decreasing this value.

This work focused on one particular species of dragonfly, with minimal variation in size between specimens. To understand how these observations apply to dragonflies generally and could be used on MAVs of different sizes, further study of different species of different sizes is necessary. As there is already evidence that wing kinematics vary with size, further quantification of how significant those differences are and if there are different mechanisms that are used for maneuvering is necessary.

Of the two types of wing deformation observed in this research, the impact of deformation induced camber is the least clear. In analyzing the differences between the impact of camber on forewings and hindwings it was found that the change in forces due to camber is dependent on wing kinematics and may also be dependent on wing planform. Since prior research into wing camber indicates that there are aerodynamic advantages, it is important to understand which cases will benefit most. Therefore, additional studies should be conducted to explore the impact of camber deformations on revolving or flapping wings to determine the kinematics and wing geometry where camber is beneficial.

Finally, the ultimate goal of studying dragonflies in this context is to improve micro aerial vehicle design and performance. The work presented here has contributed to the understanding of unsteady low-speed aerodynamics of flapping wings and there are two elements of these findings that could benefit MAVs. The first is how dragonflies make use of their control of the wing pitch angle. This suggests that there are advantages to having control of the wing pitch angle throughout the wingstroke and therefore, for the design of flapping wing MAVs, it is important to understand the costs and benefits of adding pitch angle control. The second

area, improved wing performance with deformations, could apply to MAVs generally as the use of specific wing deformations could improve the flight efficiency. In order to implement wing structures that leverage specific deformations, materials and structural configurations that allow for such deformations would need to be created. Though the use of nanostructures like those seen on dragonfly wings is a possibility, it is unlikely to be economical for MAVs in the near future, it is possible that currently available materials could be leveraged to produce similar effects.

5.4 Final Summary

The combined experimental-computational approach of the present work has led to several new findings and developments. The experimental work produced a new testing environment and methodology for obtaining video of a large number of dragonfly flights as well as a new piecewise model of insect wing kinematics. The wing kinematics observed in the experiments provided basic insight into how dragonflies both fly while inverted and mitigate the impact of a lateral gust. The simulations demonstrated the aerodynamic benefits of specific wing deformations and closely spaced tandem wings operating with the proper kinematics. Though there are further steps that are required before micro aerial vehicles employing wings with variable deformation patterns and pitch control are in general use, the findings of this research contribute to our understanding of the aerodynamics of flapping wings and provide a guide for improving the aerodynamic efficiency of flapping-wing vehicles.

Appendix A: Wake Analysis

In order to strengthen the conclusion that the wing deformation was the primary factor in producing different flowfields and forces on the wings, additional simulations were run to determine how the differences in the wakes produced by the different wing motions affect the flow around the wing. Since the most significant differences, in terms of forces produced, were seen by the forewing, this analysis was conducted with four additional simulations using the upright isolated forewing. By comparing these four simulations to the simulation results from isolated forewings presented in chapter 4, the impact of the wake on the flow around the wing can be illuminated.

A.1 Methodology

The additional simulations all used the upright forewing kinematics, with different starting wakes and wing deformations. Two simulations only included the deformation during the downstroke, while the other two simulations only included the deformation during the upstroke. One simulation from each pair was started using a rigid wing solution (D1 for the deforming downstroke and U1 for the deforming upstroke), meaning that a fully developed rigid-wing wake was already established.

The other two simulations were started without any prior solution (D2 for the deforming downstroke and U2 for the deforming upstroke), so the wakes include the effects of the half stroke of deformation.

In order to obtain deformation for only one half stroke, the deformation coefficients for the upright forewing were windowed differently than for the fully deforming simulations. Rather than forcing the coefficients to an average value at the beginning or end of the halfstroke, they were forced to zero at each stroke reversal point using at Tukey window and set to zero for the halfstroke where no deformation was present. This means that the deformation for the beginning and end of the halfstroke is slightly different than that for the fully deforming wing, which has an impact on the results. In addition, at the transition from rigid to deforming and vice versa there is a discontinuity in the wing motion, due to the corrections to ensure that the wing root and tip remain along the spanwise axis. This results in a spike in forces at these transition points.

A.2 Results and Discussion

Starting with the results for deformation during the downstroke, which are found in figure A.1. The first noteworthy element is the similarity between the forces for D1 and D2. This indicates that the wake from the previous downstroke does not have as significant of an impact as the wake from the previous upstroke or the difference in wing motion near stroke reversal. That being said, there are notable differences between the D1 and D2 results and the forces on a fully deforming wing.

These differences are most noticeable in the lift coefficient and coefficient of total force, figures A.1a and A.1c respectively, and suggests that the combination of the wake from the rigid upstroke and the different wing motion around stroke reversal reduces the amount of force produced by the wing, though only by a small amount. The notable differences seen at the beginning of the wingstroke are due to the deformation coefficient differences. The resulting variation does have some impact on the leading edge vortex formation, so the difference at the force peak includes some effect due to the difference in the wing motion.

To better understand how the difference in the wakes from the upstrokes impacts the flow around the wing, a further discussion of the difference between the rigid and deforming wing upstroke is needed. As noted in chapter 4, the deforming wing twists significantly during the upstroke and there is not a strong vortex formed on the underside of the wing. The vortex created by the rigid upstroke, which then sheds and convects with the flow, induces downwash on the wing. The induced downwash reduces the effective angle of attack of the wing and therefore reduces the force produced by the wing.

Taking an average of the total force coefficient for D1, D2, and the fully deforming wings, this difference can be quantified. The D1 simulation results in a average total force that is 3% lower than the fully deforming simulation while the D2 simulation has a 2% reduction. Though these are notable differences, they are less than half of the 8% difference between the rigid and deforming wings. This indicates that the difference in the wakes does contribute to the difference in forces on the deforming wing during the downstroke, but the deformation itself is the

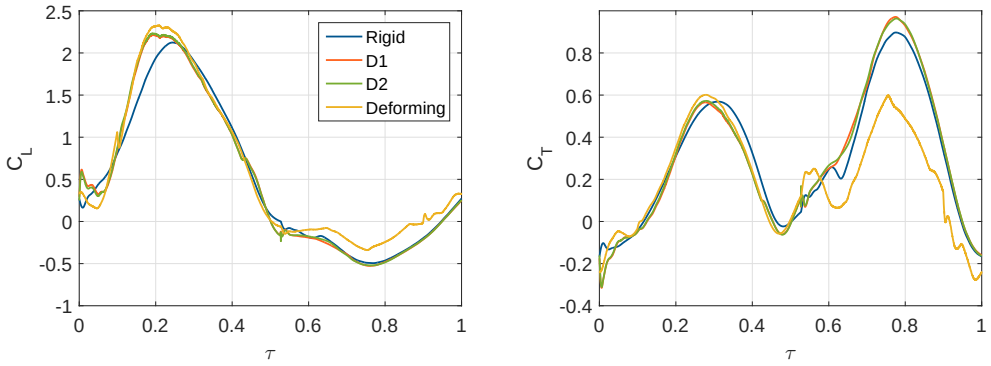

(a) (b)

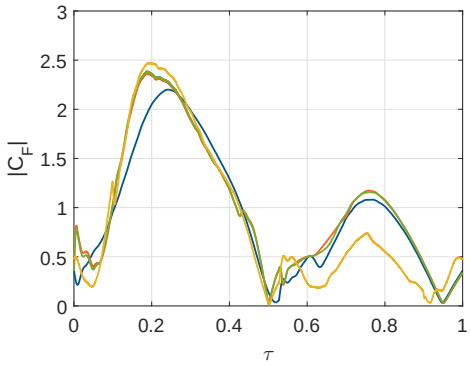

(c)

Figure A.1: Force coefficients for four isolated forewing simulations: fully rigid, deforming during the downstroke with a rigid wing wake (D1), deforming during the downstroke started from scratch (D2), and a fully deforming wing.

dominant influence.

The different conditions experienced by the four different cases presented here result in different leading edge vortex development. This is shown in figure A.2 with isosurfaces of Q criterion used to visualize the LEV. The circled vortex structure in the D1 and D2 flowfields is the main difference between them and the deforming wing flowfield. This vortex structure originated during the wing rotation around stroke reversal and it stays further above the wing than the vortex formed in the fully deforming case. As a result of the presence of this vortex and the impact of the wake, discussed above, the LEV over the outboard section of the wing does not cover as much of the wing surface as it does in the fully deforming case. Thus, there is higher pressure on the upper surface of the wing, decreasing the maximum force during the downstroke.

To better understand the difference in vortex formation on these four wings, and how the vortex structure highlighted in figure A.2 originated, flowfield data are presented in figure A.3 for the beginning of the downstroke. The beginning of LEV formation, and the key differences between the rigid and deforming cases are shown through this figure. In the rigid case, and the D1 and D2 cases, the distribution of vertical velocity at the leading edge of the wing (seen in the slices) is highly nonuniform, with a larger positive vertical velocity at the wing tip (the wing is beginning to move down, so this is not directly induced by current wing motion). On the deforming wing the distribution is much more uniform along the leading edge. This provides an indication of how wake capture impacts the LEV formation at the beginning of the downstroke. During the upstroke for the rigid

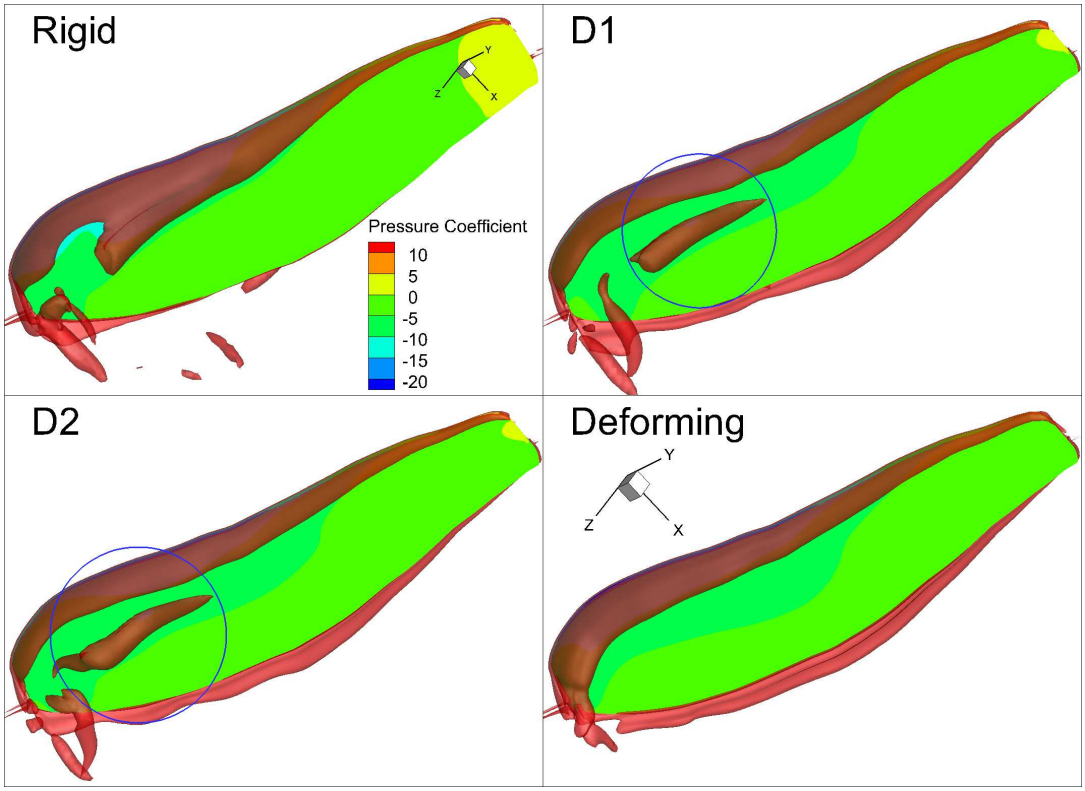

Figure A.2: Pressure contours and isosurfaces of Q criterion for the four different simulations with deformation during the downstroke at $\tau = 0.125$. The vortex structure that formed during stroke reversal in D1 and D2 is circled.

wings the amount of air accelerated in the vertical direction along with the wing is larger than that accelerated by the deforming wing (since the wing is twisted and the negative lift is lower). As the wing tip moves faster than the inboard sections of the wing, the air near the wing tip has a higher velocity, so when that high velocity air encounters the wing at stroke reversal it creates a higher vertical velocity at the wingtip compared to further inboard. This is a phenomenon known as "wake capture" (the wing encountering the wake from the previous halfstroke) and is quite common in hovering wings, but rarely noted in analysis of forward flight. The increase in vertical velocity increases the strength of the shear layer on the outboard edge of the wing, causing faster growth of the LEV. In the case of the deforming wing, the twist during the upstroke results in a smaller amount of air being accelerated near the wing tip and a larger amount at the wing root. This difference in quantity compensates for the difference in velocity, resulting in a shear layer with significantly less spanwise variation. This results in a slower development of the LEV on the outboard section of the wing when compared to the rigid case.

For the upstroke force coefficients, seen in figure A.4, a similar pattern to that seen in figure A.1 emerges. The impact of the deformation coefficients being forced to 0 is more significant at the end of the upstroke than it was at the beginning of the downstroke for the previous results. Fortunately for this analysis, that does not significantly impact the prior portion of the upstroke, though there is some affect on the downstroke in U2, and therefore the problem can be avoided by only considering the section from $\tau = 0.53$ to $\tau = 0.9$. The difference between the fully deforming wing and the U1 and U2 simulations is larger than what was observed for

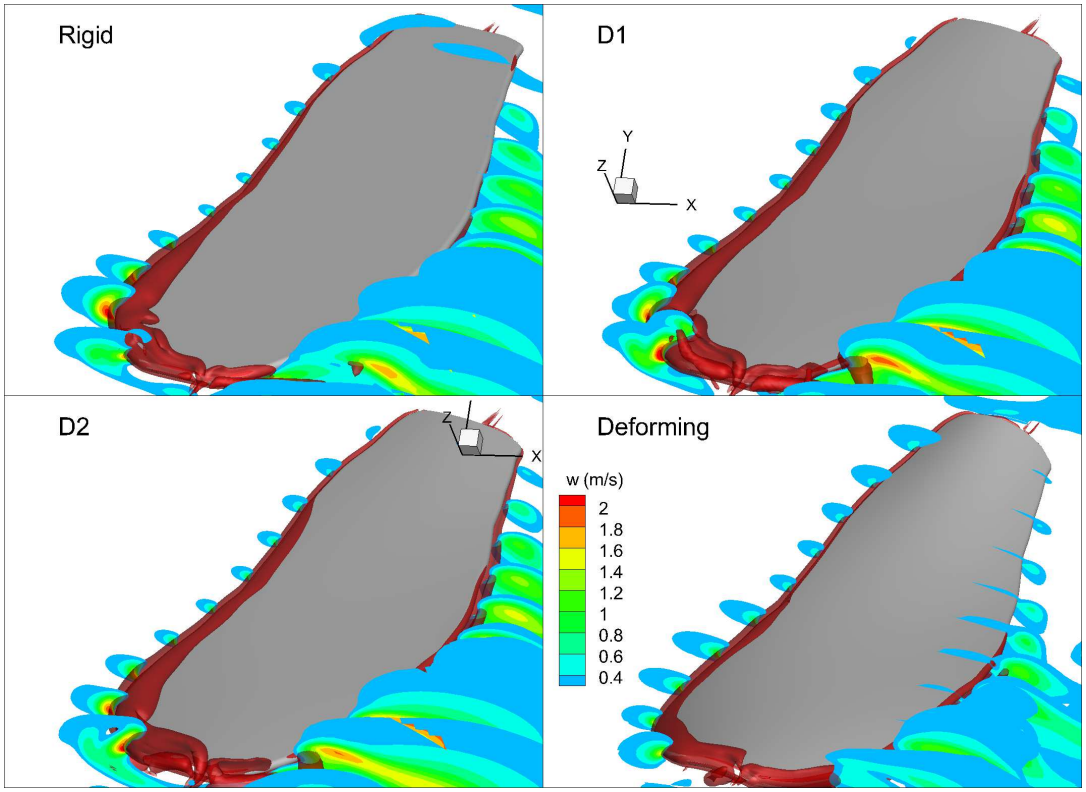

Figure A.3: Slices of vertical velocity and isosurfaces of Q criterion for the four different cases at $\tau = 0.04$.

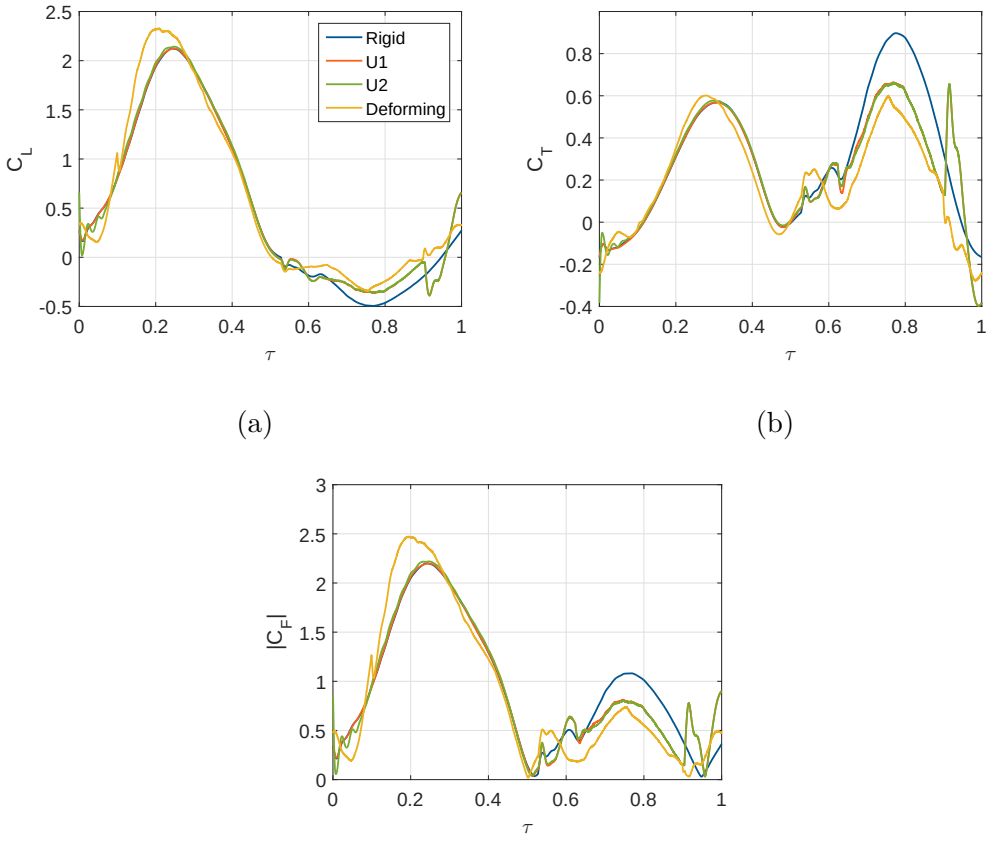

Figure A.4: Force coefficients for four isolated forewing simulations: fully rigid, deforming during the upstroke with a rigid wing wake (U1), deforming during the upstroke started from scratch (U2), and a fully deforming wing.

the downstroke, indicating that the impact of factors beyond the wing deformation are more significant. Nevertheless, average total force coefficients for the indicated period demonstrate that the wing deformation is still the dominant factor, with the average force produced by the rigid wing being 164% of that produced by the deforming wing, whereas the U1 and U2 simulations produce only 124% of the deforming wing force.

Though the majority of the difference in forcing between rigid and deforming wings is due to the wing deformation, it is important to understand how the wake from the downstroke contributes to the forces produced by the wing. As was noted previously, the fact that there is minimal difference between the U1 and U2 simulations indicates that the wake from the previous upstroke has almost no effect on the wing. Therefore, the difference between the U1 and U2 results and the deforming wing results must be due to the wake produced during the downstroke and the differences in wing motion at the reversal from downstroke to upstroke. The impact of the wake can be understood through a discussion of the vorticity shed during the downstroke. Since the deforming wing is producing a larger force during the downstroke, more vorticity is shed before stroke reversal. This shed vorticity then induces upwash on the wing, as the vorticity was in the tip to root direction in the wing reference frame. This upwash reduces the effective angle of attack for the wing through the upstroke, leading to lower force production.

The difference in wing motion and wake capture at the beginning of the upstroke results in the flow feature circled in figure A.5. This feature reduces the pressure on the underside of the rigid, U1, and U2 wings, resulting in a higher total force on the wing during the upstroke. At the end of the downstroke both the rigid and deforming wings shed several vortex structures which interact with the flow around the wing as it begins the upstroke. Since the forcing in the two cases is different, there is some difference in how the vortex structures are shed, particularly at the wing tip, where the LEV has burst by the end of the wingstroke. Again, there is a wake capture effect as the wing slows and reverses direction while the air that

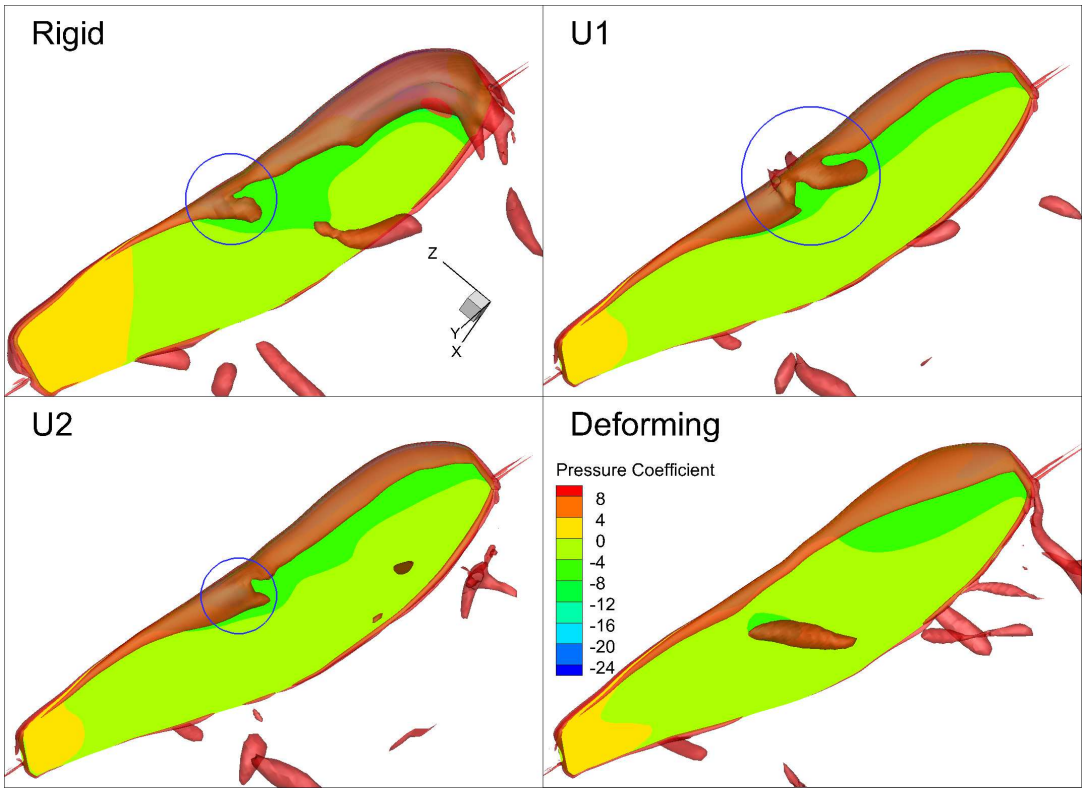

Figure A.5: Pressure contours and isosurfaces of Q criterion for the four simulations at $\tau = 0.71$. The vortex structure resulting from the interaction between a shed vortex and the leading edge shear layer is circled in the three cases where it appears.

accelerated with it during the downstroke does not immediately slow and impacts the wing.

To better understand the development of the flow feature seen in figure A.5, which has a significant influence on the force on the wing, figure A.6 shows how this vortical structure develops on rigid and deforming wings. On the deforming wing, the rotation of the outboard section of the wing produces a vortex that interacts with the shed vortices, but grows quickly and begins to break away from the wing by $\tau = 0.59$. In the rigid case there is a similar vortex that develops, but its development is slower and it interacts with a vortex structure at midspan that then becomes the feature noted in figure A.5. The primary difference between these two flowfields is how quickly the newly formed vortex develops and how its orientation changes relative to the wing. In the rigid case the new vortex, and the structure at midspan that interacts with it, are generally aligned with the leading edge throughout the motion. This is in contrast with the deforming case, where the section of the vortex closest to the wing is no longer aligned with the leading edge by $\tau = 0.59$. The difference in the rate at which these vortices form also sheds light on the difference in the timing of the force peaks at stroke reversal, where the deforming wing has a force peak at $\tau \sim 0.55$ and the rigid wing has a force peak at $\tau = 0.6$. Figure A.6 shows that the vortex forming on the deforming wing reaches its maximum size around $\tau = 0.56$ and by $\tau = 0.6$ it has broken away from the wing. The vortex forming on the rigid wing does not reach its maximum size until $\tau = 0.6$ and it does not break away from the wing surface as quickly as the vortex on the deforming wing does.

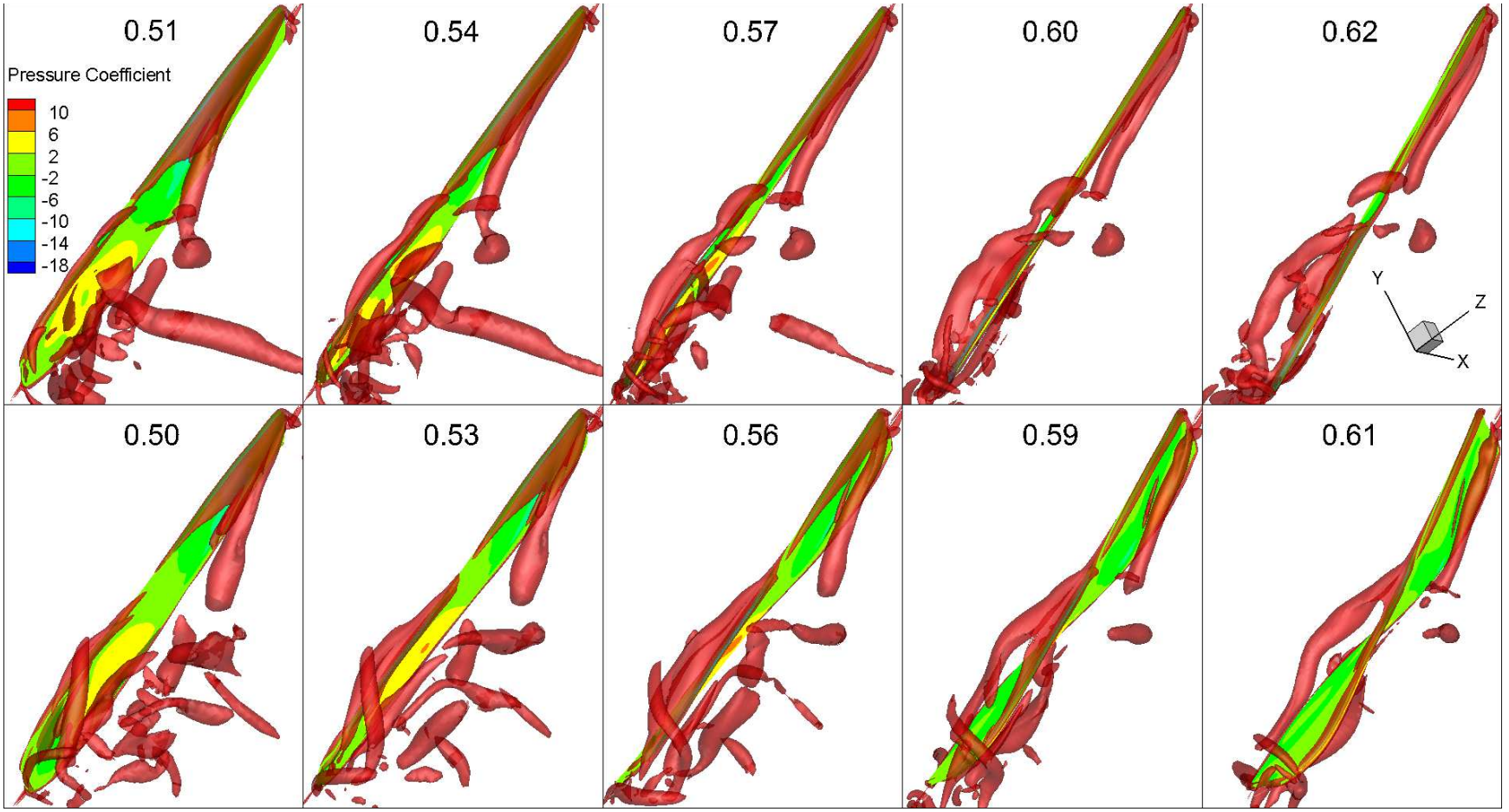

Figure A.6: Isosurfaces of q criterion for the rigid wing (top row) and deforming wing (bottom row) showing how the wing interacts with the shed vortex structures at the beginning of the upstroke.

From this analysis there are two points worth emphasizing. First, the wing deformations are responsible for the majority of the difference in force when comparing rigid and deforming wing aerodynamics. Second, there is a notable impact of the wake, particularly the wake capture effects, on the wing and the specific wing deformations seen in dragonflies appear to take advantage of that impact. This further highlights the benefits that could be obtained through the use of a specific pattern of deformations in a wing operating in an unsteady, low Reynolds number flow.

Bibliography

[1] Wei Shyy, Hikaru Aono, Satish Kumar Chimakurthi, P Trizila, C-K Kang, Carlos ES Cesnik, and Hao Liu. Recent progress in flapping wing aerodynamics and aeroelasticity. *Progress in Aerospace Sciences*, 46(7):284–327, 2010.

[2] M James and CMSF McMichael. Micro air vehicles—toward a new dimension in flight. *US DAPPA/TTO Report*, 1997.

[3] Luca Petricca, Per Ohlckers, and Christopher Grinde. Micro-and nano-air vehicles: State of the art. *International journal of aerospace engineering*, 2011, 2011.

[4] Matthew Keennon, Karl Klingebiel, and Henry Won. Development of the nano hummingbird: A tailless flapping wing micro air vehicle. In *50th AIAA aerospace sciences meeting including the new horizons forum and aerospace exposition*, page 588, 2012.

[5] Robert J Wood. The first takeoff of a biologically inspired at-scale robotic insect. *IEEE transactions on robotics*, 24(2):341–347, 2008.

[6] Shuanghou Deng, Mustafa Percin, and Bas van Oudheusden. Experimental investigation of aerodynamics of flapping-wing micro-air-vehicle by force and flow-field measurements. *AIAA Journal*, pages 1–15, 2015.

[7] Robert Wood, Radhika Nagpal, and Gu-Yeon Wei. Flight of the robobees. *Scientific American*, 308(3):60–65, 2013.

[8] Fritz-Olaf Lehmann. The mechanisms of lift enhancement in insect flight. *Naturwissenschaften*, 91(3):101–122, 2004.

[9] Alex Fisher, Sridhar Ravi, Simon Watkins, Jon Watmuff, Chun Wang, Hao Liu, and Phred Petersen. The gust-mitigating potential of flapping wings. *Bioinspiration & biomimetics*, 11(4):046010, 2016.

[10] JT Vance, I Faruque, and JS Humbert. Kinematic strategies for mitigating gust perturbations in insects. *Bioinspiration & biomimetics*, 8(1):016004, 2013.

[11] Rajeev Kumar and Sergey Shkarayev. Kinematic and aerodynamic response of locusts in sideslip. *International Journal of Micro Air Vehicles*, 7(2):159–180, 2015.

[12] Roberto Albertani, Matthew Goettl, and Tyler Wilson. A wind tunnel investigation of lepidopterae flight in cross-wind conditions. In *51st AIAA Aerospace Sciences Meeting and Exhibit*, pages 7–10, 2013.

[13] Wei Shyy, Hikaru Aono, Chang-kwon Kang, and Hao Liu. *An introduction to flapping wing aerodynamics*, volume 37. Cambridge University Press, 2013.

[14] David Lentink and Michael H Dickinson. Biofluiddynamic scaling of flapping, spinning and translating fins and wings. *Journal of Experimental Biology*, 212(16):2691–2704, 2009.

[15] Jeff D Eldredge and Anya R Jones. Leading-edge vortices: Mechanics and modeling. *Annual Review of Fluid Mechanics*, (51), 2019.

[16] Max F Platzer, Kevin D Jones, John Young, and JC S. Lai. Flapping wing aerodynamics: progress and challenges. *AIAA journal*, 46(9):2136–2149, 2008.

[17] James M Birch and Michael H Dickinson. Spanwise flow and the attachment of the leading-edge vortex on insect wings. *Nature*, 412(6848):729, 2001.

[18] Field Manar, Peter Mancini, David Mayo, and Anya R Jones. Comparison of rotating and translating wings: force production and vortex characteristics. *AIAA Journal*, 2015.

[19] Field Manar. *Measurements and modeling of the unsteady flow around a thin wing*. PhD thesis, University of Maryland, College Park, 2018.

[20] Albert Medina and Anya R Jones. Leading-edge vortex burst on a low-aspect-ratio rotating flat plate. *Physical Review Fluids*, 1(4):044501, 2016.

[21] Peter Mancini, Field Manar, Kenneth Granlund, Michael V Ol, and Anya R Jones. Unsteady aerodynamic characteristics of a translating rigid wing at low reynolds number. *Physics of Fluids*, 27(12):123102, 2015.

[22] Zakery R Carr, Adam C DeVoria, and Matthew J Ringuette. Aspect-ratio effects on rotating wings: circulation and forces. *Journal of Fluid Mechanics*, 767:497–525, 2015.

[23] Peter Mancini, Anya R Jones, Michael V Ol, and Kenneth Granlund. Parameter studies on translating rigid and flexible wings. In *52nd Aerospace Sciences Meeting*, page 0073, 2014.

[24] Anya R Jones, Albert Medina, Hannah Spooner, and Karen Mulleners. Characterizing a burst leading-edge vortex on a rotating flat plate wing. *Experiments in Fluids*, 57(4):52, 2016.

[25] RJ Wootton, J Kukalová-Peck, DJS Newman, and J Muzón. Smart engineering in the mid-carboniferous: How well could palaeozoic dragonflies fly? *Science*, 282(5389):749–751, 1998.

[26] Michael L May. Dragonfly flight: power requirements at high speed and acceleration. *Journal of Experimental Biology*, 158(1):325–342, 1991.

[27] Mark A. Reavis and Marvin W. Luttges. Aerodynamic forces produced by a dragonfly. *AIAA Aerospace Sciences Meeting*, January 1988. AIAA Paper 88-0330.

[28] G Rüppell. Kinematic analysis of symmetrical flight manoeuvres of odonata. *Journal of Experimental Biology*, 144(1):13–42, 1989.

[29] Chris Somps and Marvin Luttges. Dragonfly flight: novel uses of unsteady separated flows. *Science*, 228(4705):1326–1329, 1985.

[30] Akira Azuma and Tadaaki Watanabe. Flight performance of a dragonfly. *Journal of Experimental Biology*, 137(1):221–252, 1988.

[31] JM Wakeling and CP Ellington. Dragonfly flight. ii. velocities, accelerations and kinematics of flapping flight. *Journal of Experimental Biology*, 200(3):557–582, 1997.

[32] Akira Azuma, Soichi Azuma, Isao Watanabe, and Toyohiko Furuta. Flight mechanics of a dragonfly. *Journal of Experimental Biology*, 116(1):79–107, 1985.

[33] Hao Wang, Lijiang Zeng, Hao Liu, and Chunyong Yin. Measuring wing kinematics, flight trajectory and body attitude during forward flight and turning maneuvers in dragonflies. *Journal of Experimental Biology*, 206(4):745–757, 2003.

[34] Chengyu Li and Haibo Dong. Wing kinematics measurement and aerodynamics of a dragonfly in turning flight. *Bioinspiration & Biomimetics*, 2017.

[35] Adrian LR Thomas, Graham K Taylor, Robert B Srygley, Robert L Nudds, and Richard J Bomphrey. Dragonfly flight: free-flight and tethered flow visualizations reveal a diverse array of unsteady lift-generating mechanisms, controlled primarily via angle of attack. *Journal of Experimental Biology*, 207(24):4299–4323, 2004.

[36] Richard J Bomphrey, Toshiyuki Nakata, Per Henningsson, and Huai-Ti Lin. Flight of the dragonflies and damselflies. *Philosophical Transactions of the Royal Society b*, 371(1704):20150389, 2016.

[37] Mao Sun and Shi Long Lan. A computational study of the aerodynamic forces and power requirements of dragonfly (aeschna juncea) hovering. *Journal of Experimental Biology*, 207(11):1887–1901, 2004.

[38] Ayodeji T Bode-Oke, Samane Zeyghami, and Haibo Dong. Flying in reverse: kinematics and aerodynamics of a dragonfly in backward free flight. *Journal of The Royal Society Interface*, 15(143):20180102, 2018.

[39] Ji Kang Wang and Mao Sun. A computational study of the aerodynamics and forewing-hindwing interaction of a model dragonfly in forward flight. *Journal of Experimental Biology*, 208(19):3785–3804, 2005.

[40] Antonia B Kesel. Aerodynamic characteristics of dragonfly wing sections compared with technical aerofoils. *Journal of Experimental Biology*, 203(20):3125–3135, 2000.

[41] Won-Kap Kim, Jin Hwan Ko, Hoon Cheol Park, and Doyoung Byun. Effects of corrugation of the dragonfly wing on gliding performance. *Journal of Theoretical Biology*, 260(4):523–530, 2009.

[42] Jiyu Sun and Bharat Bhushan. The structure and mechanical properties of dragonfly wings and their role on flyability. *Comptes Rendus Mécanique*, 340(1):3–17, 2012.

[43] James R Usherwood and Fritz-Olaf Lehmann. Phasing of dragonfly wings can improve aerodynamic efficiency by removing swirl. *Journal of The Royal Society Interface*, 5(28):1303–1307, 2008.

[44] Wu Qi Gong, Bo Bo Jia, and Guang Xi. Experimental study on mean thrust of two plunging wings in tandem. *AIAA Journal*, 53(6):1693–1705, 2015.

[45] Z Jane Wang and David Russell. Effect of forewing and hindwing interactions on aerodynamic forces and power in hovering dragonfly flight. *Physical Review Letters*, 99(14):148101, 2007.

[46] SR Jongerius and D Lentink. Structural analysis of a dragonfly wing. *Experimental Mechanics*, 50(9):1323–1334, 2010.

[47] Esther Appel and Stanislav N Gorb. Comparative functional morphology of vein joints in odonata. *Zoologica*, 159:1–104, April 2014.

[48] Seth Donoughe, James D Crall, Rachel A Merz, and Stacey A Combes. Resilin in dragonfly and damselfly wings and its implications for wing flexibility. *Journal of morphology*, 272(12):1409–1421, 2011.

[49] Christopher Koehler, Zongxian Liang, Zachary Gaston, Hui Wan, and Haibo Dong. 3d reconstruction and analysis of wing deformation in free-flying dragonflies. *The Journal of Experimental Biology*, 215(17):3018–3027, 2012.

[50] A Roland Ennos. The importance of torsion in the design of insect wings. *Journal of Experimental Biology*, 140(1):137–160, 1988.

[51] I Gursul, DJ Cleaver, and Z Wang. Control of low reynolds number flows by means of fluid–structure interactions. *Progress in Aerospace Sciences*, 64:17–55, 2014.

[52] Liang Zhao, Qingfeng Huang, Xinyan Deng, and Sanjay P Sane. Aerodynamic effects of flexibility in flapping wings. *Journal of The Royal Society Interface*, 7(44):485–497, 2010.

[53] Hoang Vu Phan, Quang Tri Truong, Thi Kim Loan Au, and Hoon Cheol Park. Optimal flapping wing for maximum vertical aerodynamic force in hover: twisted or flat? *Bioinspiration & biomimetics*, 11(4):046007, 2016.

[54] William Thielicke and Eize J Stamhuis. The effects of wing twist in slow-speed flapping flight of birds: trading brute force against efficiency. *Bioinspiration & biomimetics*, 13(5):056015, 2018.

[55] MA Ashraf, J Young, and JCS Lai. Reynolds number, thickness and camber effects on flapping airfoil propulsion. *Journal of Fluids and structures*, 27(2):145–160, 2011.

[56] RR Harbig, J Sheridan, and MC Thompson. Relationship between aerodynamic forces, flow structures and wing camber for rotating insect wing planforms. *Journal of Fluid Mechanics*, 730:52–75, 2013.

[57] William Thielicke and Eize J Stamhuis. The influence of wing morphology on the three-dimensional flow patterns of a flapping wing at bird scale. *Journal of Fluid Mechanics*, 768:240–260, 2015.

[58] SA Combes and TL Daniel. Flexural stiffness in insect wings i. scaling and the influence of wing venation. *Journal of Experimental Biology*, 206(17):2979–2987, 2003.

[59] Stacey A Combes and Thomas L Daniel. Into thin air: contributions of aerodynamic and inertial-elastic forces to wing bending in the hawkmoth manduca sexta. *Journal of Experimental Biology*, 206(17):2999–3006, 2003.

[60] V Naidu, J Young, and JCS Lai. Effect of wing flexibility on dragonfly hover flight. In *19th Australasian Fluid Mechanics Conference, Melbourne, Australia (December, 2014)*, 2014.

[61] Toshiyuki Nakata and Hao Liu. A fluid–structure interaction model of insect flight with flexible wings. *Journal of Computational Physics*, 231(4):1822–1847, 2012.

[62] John Young, Simon M Walker, Richard J Bomphrey, Graham K Taylor, and Adrian LR Thomas. Details of insect wing design and deformation enhance aerodynamic function and flight efficiency. *Science*, 325(5947):1549–1552, 2009.

[63] Simon M Walker, Adrian LR Thomas, and Graham K Taylor. Photogrammetric reconstruction of high-resolution surface topographies and deformable wing kinematics of tethered locusts and free-flying hoverflies. *Journal of The Royal Society Interface*, 6(33):351–366, 2009.

[64] Mateusz Gabryszuk. Photogrammetric reconstruction of tandem-wing kinematics for free-flying dragonflies undergoing a range of flight maneuvers. Master's thesis, University of Maryland-College Park, 2017.

[65] Camli Badrya. *CFD/Quasi-Steady Coupled Trim Analysis of Diptera-type Flapping Wing MAV in Steady Flight*. PhD thesis, University of Maryland, College Park, 2016.

[66] Bram Van Leer. Towards the ultimate conservative difference scheme. v. a second-order sequel to godunov's method. *Journal of computational Physics*, 32(1):101–136, 1979.

[67] VK Lakshminarayan. *Computational Investigation of Micro-Scale Coaxial Rotor Aerodynamics in Hover*. PhD thesis, University of Maryland, College Park, 2009.

[68] James Lankford. *Experimental And Coupled CFD/CSD Investigation of Flexible MAV-Scale Flapping Wings in Hover*. PhD thesis, University of Maryland, College Park, 2018.

[69] Robert Dudley. *The biomechanics of insect flight: form, function, evolution*. Princeton University Press, 2002.

[70] Nathan Shumway, Mateusz Gabryszuk, and Stuart J Laurence. Flapping tandem-wing aerodynamics: dragonflies in steady forward flight. In *2018 AIAA Aerospace Sciences Meeting*, page 1290, 2018.

[71] CP Ellington. The aerodynamics of hovering insect flight. iii. kinematics. *Phil. Trans. R. Soc. Lond. B*, 305(1122):41–78, 1984.

[72] Simon M Walker, Adrian LR Thomas, and Graham K Taylor. Deformable wing kinematics in free-flying hoverflies. *Journal of the Royal Society Interface*, page rsif20090120, 2009.

[73] Julian CR Hunt, Alan A Wray, and Parviz Moin. Eddies, streams, and convergence zones in turbulent flows. In *Studying Turbulence Using Numerical Simulation Databases, 2. Proceedings of the 1988 Summer Program*, pages 193–208, 1988.

[74] Pradeep Gopalakrishnan and Danesh K Tafti. Effect of rotation kinematics and angle of attack on flapping flight. *AIAA journal*, 47(11):2505–2519, 2009.

[75] John David Anderson Jr. *Fundamentals of aerodynamics*. Tata McGraw-Hill Education, 2010.

[76] Yongsheng Lian, Timothy Broering, Kyle Hord, and Russell Prater. The characterization of tandem and corrugated wings. *Progress in Aerospace Sciences*, 65:41–69, 2014.

[77] Zongxian Liang and Haibo Dong. Computational study of wing-wake interactions between ipsilateral wings of dragonfly in flight. *39th AIAA Fluid Mechanics Conference*, 2009. AIAA Paper 2009-4192.